AD-A170 019 HYPERSTRENGTH CEMENT TESTING(U) FLORIDA UNIV 1/2
GAINESVILLE DEPT OF ENGINEERING SCIENCES
L E MALVERN ET AL. MAR 86 AFESC/ESL-TR-85-47
UNCLASSIFIED F08635-83-C-0136 F/G 13/3 NL

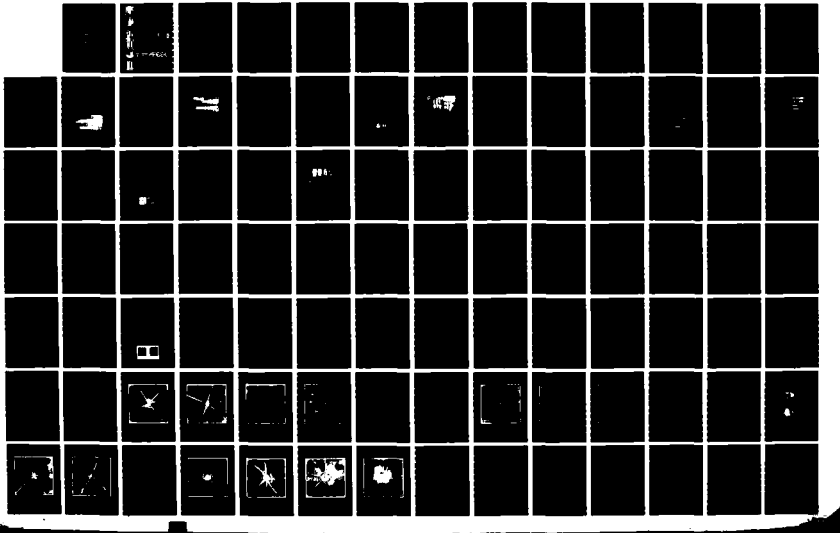

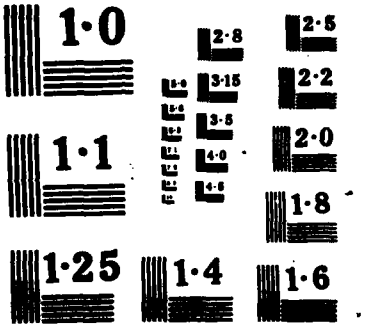
1·0
1·1
1·25
1·4
1·6
1·8
2·0
2·2
2·5
2·8
3·15
3·5
4·0
4·5

ESL-TR-85-47

Hyperstrength Cement Testing

LAWRENCE E. MALVERN
ROBERT L. SIERAKOWSKI

UNIVERSITY OF FLORIDA
DEPARTMENT OF ENGINEERING SCIENCES
GAINESVILLE, FLORIDA 32611

FINAL REPORT

MARCH 1986

JANUARY 1984 - SEPTEMBER 1985

AFESC

ENGINEERING & SERVICES LABORATORY
AIR FORCE ENGINEERING & SERVICES CENTER
TYNDALL AIR FORCE BASE, FLORIDA 32403

NOTICE

PLEASE DO NOT REQUEST COPIES OF THIS REPORT FROM HQ AFESC/RD (ENGINEERING AND SERVICES LABORATORY). ADDITIONAL COPIES MAY BE PURCHASED FROM:

NATIONAL TECHNICAL INFORMATION SERVICE
5285 PORT ROYAL ROAD
SPRINGFIELD, VIRGINIA 22161

FEDERAL GOVERNMENT AGENCIES AND THEIR CONTRACTORS REGISTERED WITH DEFENSE TECHNICAL INFORMATION CENTER SHOULD DIRECT REQUESTS FOR COPIES OF THIS REPORT TO:

DEFENSE TECHNICAL INFORMATION CENTER
CAMERON STATION
ALEXANDRIA, VIRGINIA 22314

UNCLASSIFIED

SECURITY CLASSIFICATION OF THIS PAGE

AD-A170019

REPORT DOCUMENTATION PAGE

1a REPORT SECURITY CLASSIFICATION: UNCLASSIFIED	1b RESTRICTIVE MARKINGS
2a SECURITY CLASSIFICATION AUTHORITY	3 DISTRIBUTION/AVAILABILITY OF REPORT: Approved for Public Release; Distribution Unlimited.
2b DECLASSIFICATION/DOWNGRADING SCHEDULE	
4 PERFORMING ORGANIZATION REPORT NUMBER(S)	5 MONITORING ORGANIZATION REPORT NUMBER(S): ESL-TR-85-47
6a NAME OF PERFORMING ORGANIZATION: DEPARTMENT OF ENGINEERING SCIENCES; 6b OFFICE SYMBOL (If applicable)	7a NAME OF MONITORING ORGANIZATION: Headquarters Air Force Engineering and Services Center
6c ADDRESS (City, State and ZIP Code): UNIVERSITY OF FLORIDA, GAINESVILLE, FLORIDA 32611	7b ADDRESS (City, State and ZIP Code): HQ AFESC/RDCS, TYNDALL AFB FL 32403-6001
8a NAME OF FUNDING/SPONSORING ORGANIZATION: AIR FORCE ENGINEERING & SERVICES CENTER; 8b OFFICE SYMBOL (If applicable): AFESC	9 PROCUREMENT INSTRUMENT IDENTIFICATION NUMBER: [illegible] 84-1, [illegible]-0136
8c ADDRESS (City, State and ZIP Code): TYNDALL AFB FL 32403-6001	10 SOURCE OF FUNDING NOS.

PROGRAM ELEMENT NO.	PROJECT NO.	TASK NO.	WORK UNIT NO.
62601F	2673	00	31

11 TITLE (Include Security Classification): [illegible] CEMENT TESTING (UNCLASSIFIED)

12 PERSONAL AUTHOR(S): MALVERN, LAWRENCE E. and SIERAKOWSKI, ROBERT L.

13a TYPE OF REPORT	13b TIME COVERED	14 DATE OF REPORT (Yr., Mo., Day)	15 PAGE COUNT
FINAL	FROM [illegible] TO [illegible]	[illegible] 1986	111

16 SUPPLEMENTARY NOTATION

Availability of this report is specified on reverse of front cover.

17 COSATI CODES			18 SUBJECT TERMS (Continue on reverse if necessary and identify by block number)
FIELD	GROUP	SUB. GR.	CEMENT, MECHANICAL PROPERTIES, COMPOSITE MATERIALS, FRACTURE TOUGHNESS, ENVIRONMENTAL EFFECTS, DYNAMIC TESTING, [illegible], RATE EFFECTS, BALLISTIC IMPACT, DAMPING

19 ABSTRACT (Continue on reverse if necessary and identify by block number)

[illegible] objective was to measure and evaluate the [illegible] cement matrix [illegible] of a hydraulic cement [illegible]. [illegible] were prepared using a twin-mill operation, [illegible] research and development facility of the [illegible] Imperial Chemical Industries [illegible]. The material has unusually high static [illegible] cementitious material, [illegible] very brittle. The testing program [illegible] flexure tests to determine moduli, elastic [illegible] strength and fracture toughness tests. Effects of moisture and thermal [illegible] high-strain-rate compressive tests [illegible] damping measured by vibration and by wave [illegible] ballistic impact tests are also reported.

20 DISTRIBUTION/AVAILABILITY OF ABSTRACT: [illegible]	21 ABSTRACT SECURITY CLASSIFICATION: UNCLASSIFIED
22a NAME OF RESPONSIBLE INDIVIDUAL: WALTER [illegible]	22b TELEPHONE NUMBER (Include Area Code): (904) 283-6303; 22c OFFICE SYMBOL: HQ AFESC/RDCS

DD FORM 1473, 83 APR — EDITION OF 1 JAN 73 IS OBSOLETE.

UNCLASSIFIED

SECURITY CLASSIFICATION OF THIS PAGE

PREFACE

This report was prepared by the Department of Engineering Sciences, University of Florida, Gainesville, Florida, 32611, under Task Order 84-1 of Contract No. F08635-83-0136, for the Air Force Engineering and Services Center, Engineering and Services Laboratory (AFESC/PDCS), Tyndall AFB, Florida 32403-6001. Portions of the contract was sublet to the Civil Engineering Department, Ohio State University, Columbus, Ohio 43210.

This report summarizes the work done between 26 January 1984 and 30 September 1985. HQ AFESC/RDCS program manager was Walter C. Buchholtz. The principal investigator at the University of Florida was L. E. Malvern, PhD, Department of Engineering Sciences, 231 Aerospace Engineering Building, Gainesville, Florida 32611 and the responsible official at Ohio State University was R. L. Sierakowski, PhD, Chairman, Civil Engineering Department, 407 Hitchcock Hall, Ohio State University, Columbus, Ohio 43210.

This report has been reviewed by the Public Affairs Office (PA) and is releasable to the National Technical Information Service (NTIS). At NTIS, it will be available to the general public, including foreign nations.

This technical report has been reviewed and is approved for publication.

WALTER C. BUCHHOLTZ
Project Officer

ROBERT E. HOYER, Colonel, USAF
Director, Engineering and Services Laboratory

EVERETT L. MABRY, Lt Col, USAF
Chief, Engineering and Research Division

(The reverse of this page is blank.)

TABLE OF CONTENTS

LIST OF FIGURES

LIST OF FIGURES (Continued)

LIST OF FIGURES (Concluded)

LIST OF TABLES

LIST OF TABLES (Concluded)

SECTION I
INTRODUCTION

A. OBJECTIVE

The objective of this investigation was to measure and evaluate the material characteristics of a hyperstrength cement mixture consisting of a hydraulic cement and a water-soluble polymer. The material was produced in the form of flat plates by the Mond Division of Imperial Chemical Industries, PLC, Runcorn, Cheshire, England, designated NIMS 127® (New Inorganic Materials). The samples were made in the Research and Development facility of the Mond Division. A few samples of laminated plates formed with a reinforcing nylon mesh, designated NIMS 127R® were also tested for resistance to ballistic impact, but the main testing program was concerned with unreinforced NIMS 127.

B. BACKGROUND

The NIMS 127 composition consists (by weight) of 100 parts of calcium aluminate cement, 4 - 8 parts of hydrolyzed polyvinyl acetate polymers and 10 - 15 parts of water. The dry components (in particulate form) are mixed with the water and converted to a plastic dough-like material that can be extruded, compression-moulded, or calendared. The plate samples were prepared with a twin-roll mill, followed by cold-pressing one or more layers taken from the mill and then by oven-drying. Although the process is considerably simpler than the forming of laminated plates from fiber-reinforced epoxy preimpregnated tapes, for example, it is a manufacturing operation and not comparable to field pouring of concrete.

The material had been reported to have unusually high strength in tension for a cementitious material. The test and evaluation program was undertaken with the aim of providing information that could be used by the Air Force in deciding whether the material is promising for some kind of structural use.

C. SCOPE

The testing program procedures and results are given in the following three sections. Section II describes standard static tensile, compressive and flexural tests to determine moduli, elastic limits and ultimate strengths, and fracture toughness tests. These tests followed the outlined procedures established within the standards of the American Society of Testing and Materials.

The ASTM Standard Test Methods used are,

1. Tensile Properties of Plastics (D368-82)
2. Compressive Properties of Rigid Plastics (D695-80)
3. Flexural Properties of Unreinforced and Reinforced Plastics and Electrical Insulating Materials (D790-81)
4. Plane Strain Fracture Toughness of Metallic Materials (E399-81)

The test specimens used in all of the tests conducted were made from supplied panels of approximately 5 mm and 10 mm thickness. All tests were performed at room temperature.

Section III is concerned with environmental history effects. The flexural properties were used to judge the effects of two kinds of environmental history - moisture and temperature. Moisture environment was provided by soaking the specimens in distilled water for periods of 1 day and 7 days. Thermal environments from 80°C to 150°C were provided by heating dry in an autoclave at atmospheric pressure for periods from 1 to 30 hours. All testing was performed at room temperature after removal from the environmental exposure.

Section IV reports on dynamic tests. These include high-strain-rate compressive tests with a split Hopkinson's Bar, dynamic modulus measurements by vibration tests and also by wave propagation tests and damping measurements by vibration tests. Ballistic impact tests are also reported. The dynamic tests are not routine tests and do not follow ASTM standards.

Sections V and VI present discussion of results and conclusions. The material does have exceptionally high-static strength in tension and compression, for a cementitious material.

Average static compressive strengths were around 310 MPa [45 kips per square inch (ksi)] for specimens from 5 mm thick plates and 334 MPa (48 ksi) for specimens from 10 mm thick plates. Average static tensile strengths were around 73 MPa (11 ksi) for specimens from 5 mm thick plates and 67 MPa (9.7 ksi) for specimens from 10 mm thick plates. This falls approximately in the range of 70 - 100 MPa tensile strength quoted as typical by the manufacturer and exceeds the range of 200 - 250 MPa compressive strength quoted.

The material is, however, very brittle, which will limit its applications in situations where dynamic loading is expected.

SECTION II
STANDARD STATIC TESTS

A. TENSILE TESTS

The ASTM test standard D638-82 was selected for the testing of the tensile properties of the material. The tensile tests were performed on dumbbell-shaped specimens and are referred to as Type I and Type III for the material thicknesses of 5 mm and 10 mm, respectively. The plan dimensions for these specimens are given in Figure 1. Intact specimens are shown in Figure 2.

Strain gages were applied to each tensile specimen within its gage length. Most of the gages were the single-element type and were precisely aligned in the principal uniaxial loading direction. On some specimens, dual-element type gages were used to obtain Poisson's ratio.

The load-deflection curve of each tested specimen was autographically recorded, with the corresponding strain level superimposed on the readout. The speed of testing was set at 5.0 mm/min for the crosshead on all tests. From the data obtained, reliable stress-strain histories were produced by simple data reduction. Typical forms of the test data and the reduced data are shown in Figure 3. The tensile strength, elastic modulus, and rupture strain have been evaluated for each test. A summary of these results is given in Table 1. In the table, the samples are identified by a four-digit plate number, followed by X or Y to indicate whether parallel (X) or perpendicular to the final rolling direction in the plate fabrication and the sample number (1 to 5) of that group. Locations of the individual specimens in the panels from which they were cut are summarized in Section II.E.

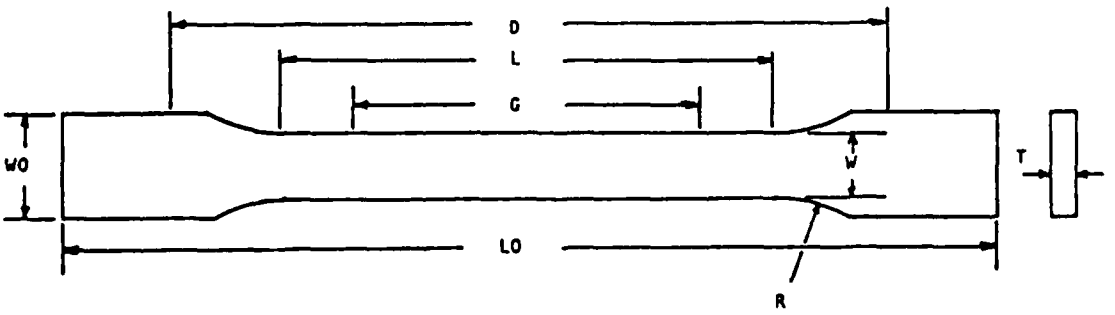

Dimensions, mm	Type I	Type III	Tolerance
T - thickness	5.0	10.0	------
W - width of narrow section	13.0	19.0	± 0.5
L - length of narrow section	57.0	57.0	± 0.5
WO - width overall	19.0	29.0	± 6.0
LO - length overall	165.0	246.0	No Max
G - gage length	50.0	50.0	± 0.25
D - distance between grips	115.0	115.0	± 5.0
R - radius of fillet	76.0	76.0	± 1.0

Figure 1. Planform of Tensile Specimens.

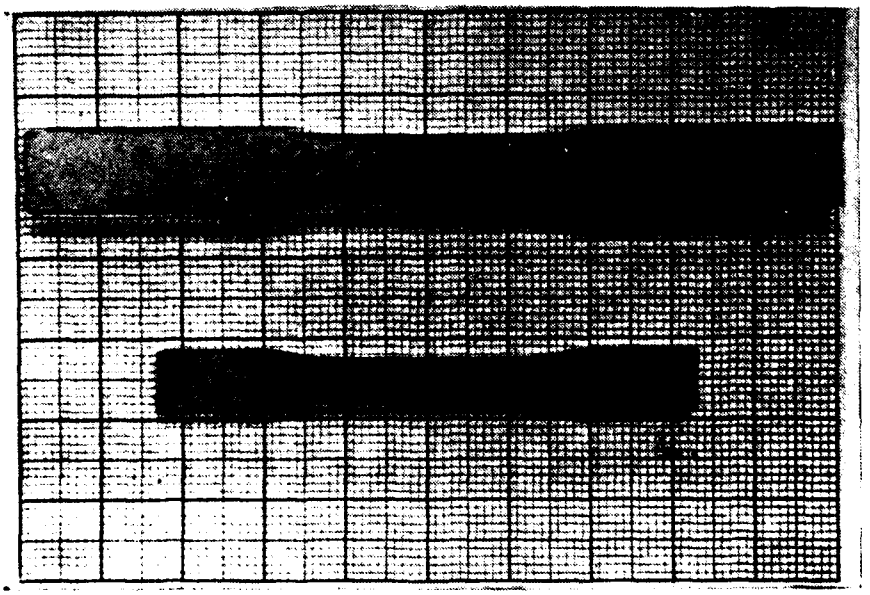

Figure 2. Intact Tensile Specimens.

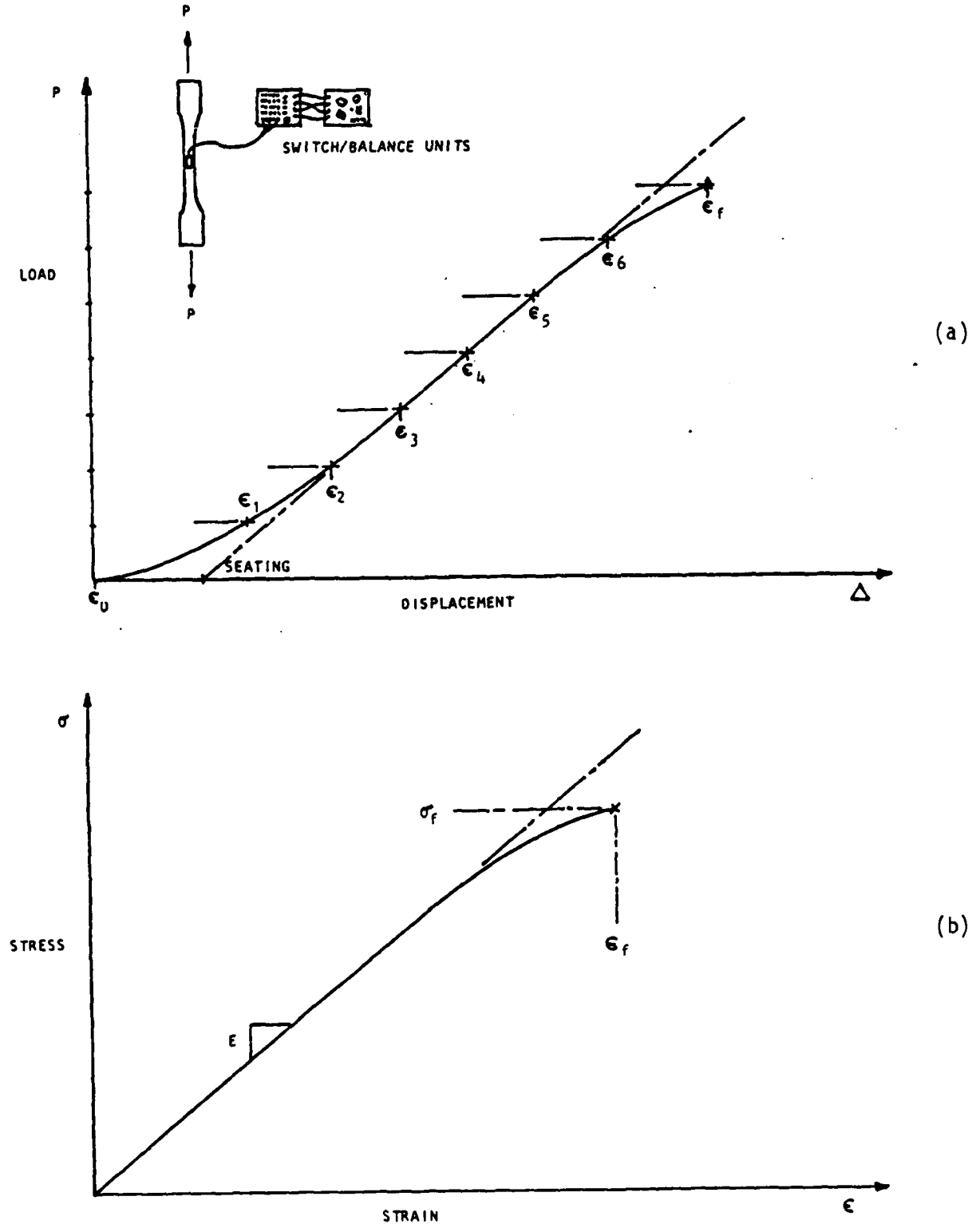

Figure 3. Typical Forms of (a) Test Record and (b) Reduced Record of Tensile Test.

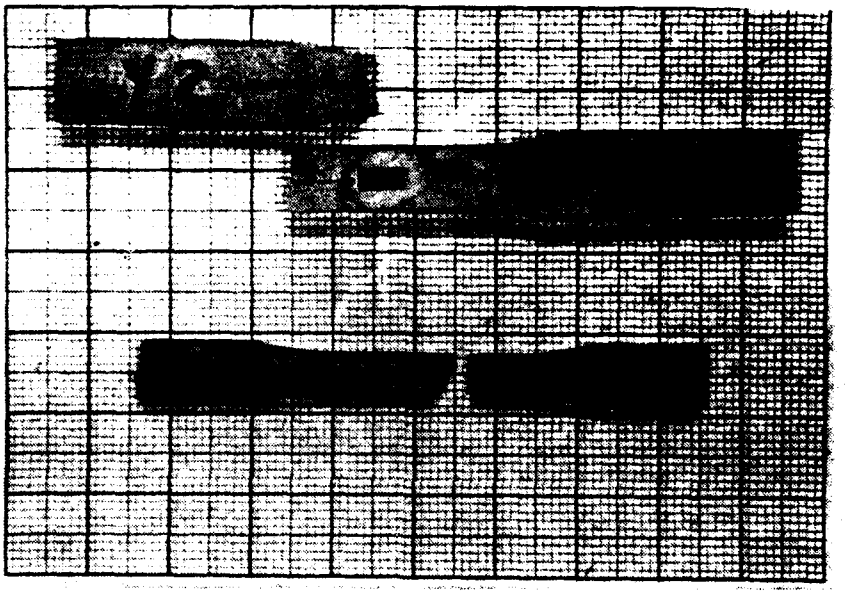

Figure 4. Failed Test Specimens.

TABLE 1. TENSILE TEST RESULTS

5 mm Tensile Tests (ASTM D638-82)

Sample	Elastic Modulus (x 10^6 psi)	Tensile Strength (psi)	Max Strain (in/in)	Poisson's Ratio
1917-X2	6.64	10079	0.002077	
1917-X3	6.47	10784	0.002123	
1917-X4	6.87	9574	0.001990	
1917-X5	7.17	10895	0.001990	
Mean	6.79	10333	0.001974	
St.D.	0.303	621	0.000195	
1917-Y1	6.15	9790	0.001852	0.26
1917-Y2	6.50	11325	0.002227	
1917-Y3	6.96	11753	0.002353	
1917-Y4	6.88	10263	0.001896	
1917-Y5	6.05	10851	0.002127	
Mean	6.51	10796	0.002091	
St.D.	0.41	790	0.000214	

10 mm Tensile Tests (ASTM D638-82)

Sample	Elastic Modulus (x 10^6 psi)	Tensile Strength (psi)	Max Strain (in/in)	Poisson's Ratio
1958-X1	5.39	10645	0.002337	0.27
1958-X2	6.05	10225	0.002393	
1958-X3	5.76	10438	0.002356	
1958-X4	5.70	9019	0.001950	
1958-X5	5.61	9266	0.001988	
Mean	5.70	9919	0.002205	
St.D.	0.24	729	0.000217	
1958-Y1	4.75	8752	0.001896	0.26
1958-Y2	5.56	9303	0.002080	
1958-Y3	6.24	9427	0.001972	
1958-Y4	5.56	10345	0.002400	
Mean	5.53	9457	0.002087	
St.D.	0.61	661	0.000220	

B. COMPRESSIVE TESTS

Compressive properties of the material were evaluated by use of the outlined procedures in the ASTM standard D695-80. (Compression tests using nonstandard size samples have results closer to the manufacturer's tests.) The compression test specimen dimensions follow the prescribed values set in Section 6.7.1 of the standard. These dimensions were 12.7 mm wide by the material thickness and by a length such that the greatest slenderness ratio was between 11:1 and 15:1. These lengths were selected at 18 mm and 36 mm for the 5 mm and 10 mm thick specimens, respectively. Plan dimensions are shown in Figure 5. All cut surfaces were machined to obtain as near perfect right rectangular prismatic sections as possible. Intact specimens are shown in Figure 6.

Testing was accomplished under controlled displacement conditions of the loading crosshead while the load-deformation curves were autographically recorded. The crosshead speed was selected at 1.0 mm/min for all compression tests. From the test data curves, simple data reduction was done to establish the compressive properties. The compressive strength, elastic modulus, and strain at failure have been obtained for each test and are summarized in Table 2. The elastic modulus values of the small specimens are based on the slope of the testing machine load-deflection curves and are lower than expected, possibly because of machine elasticity. Typical forms of the test data and reduced data curves are shown in Figure 8.

Failure of the compression test specimens was accompanied by an explosive separation of the material in a vertical plane. This plane was normally in-plane with respect to the thickness of the material and most likely due to tensile stresses on this plane. Protective shielding was required during testing. Some examples of failed compression specimens are shown in Figure 7.

(a) (b)

Figure 5. Compression Test Specimen Dimensions (a) 10 mm, (b) 5 mm Thickness.

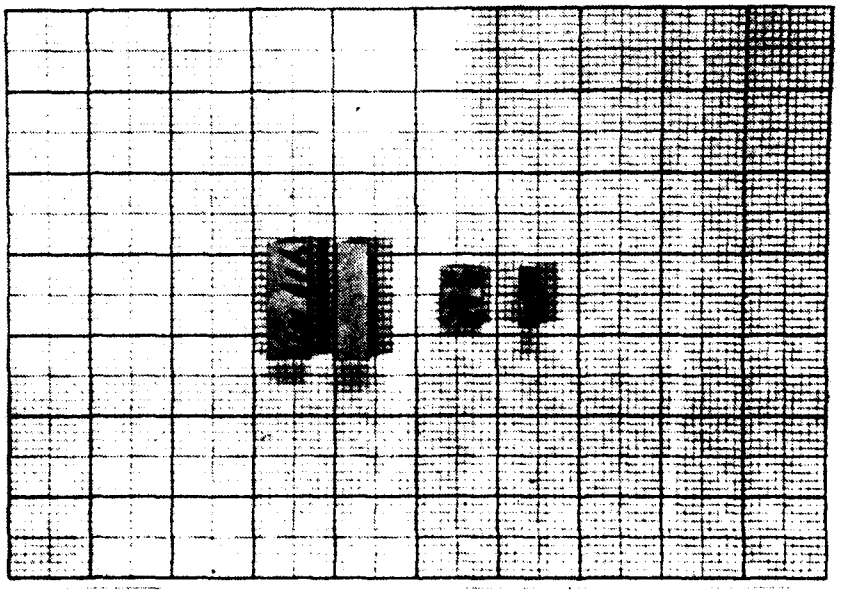

Figure 6. Intact Compression Specimens.

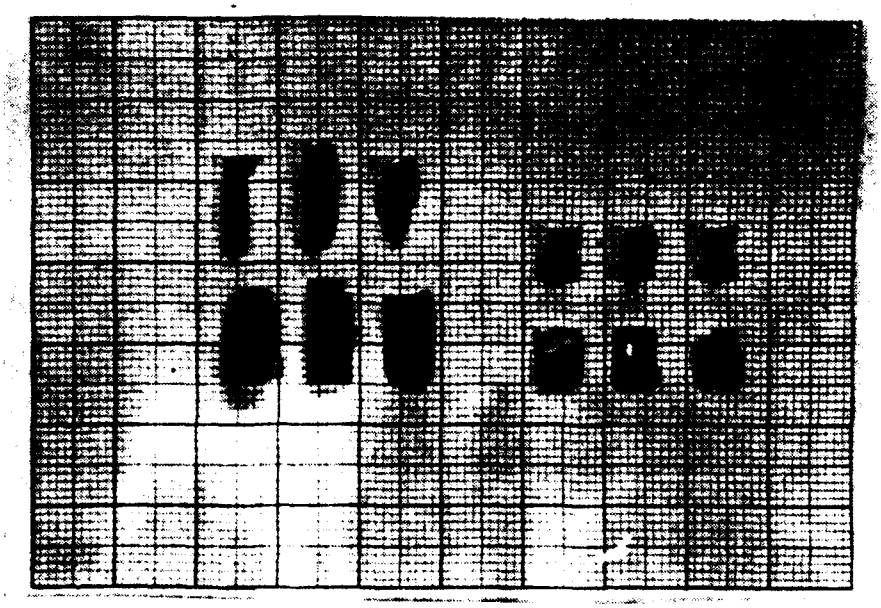

Figure 7. Failed Compression Specimens.

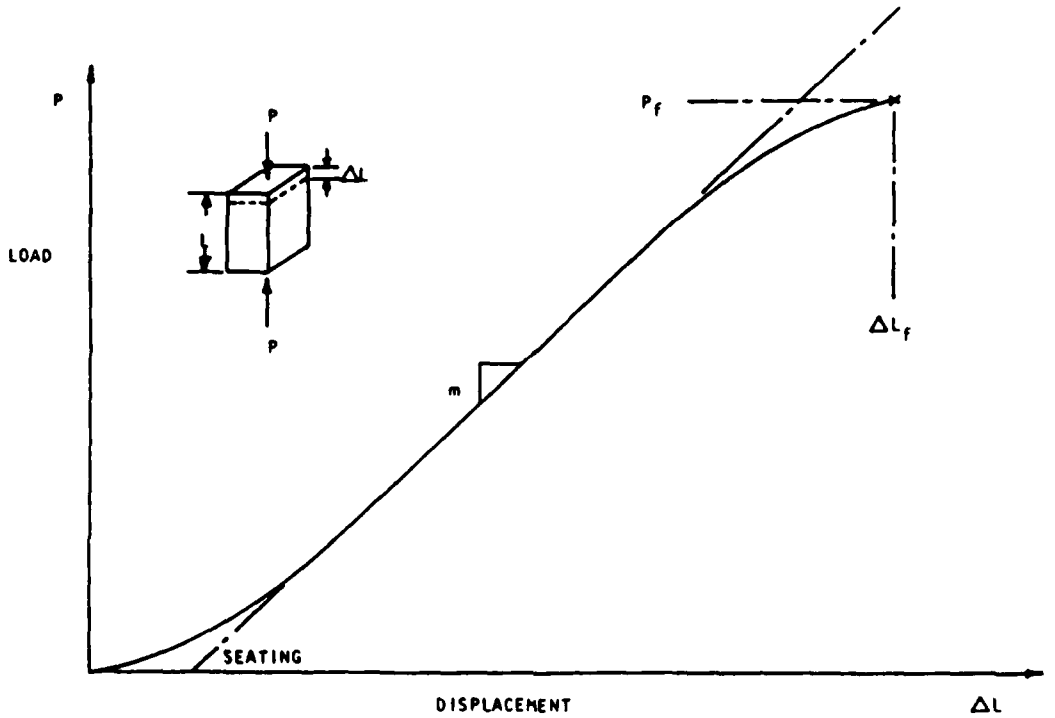

(a)

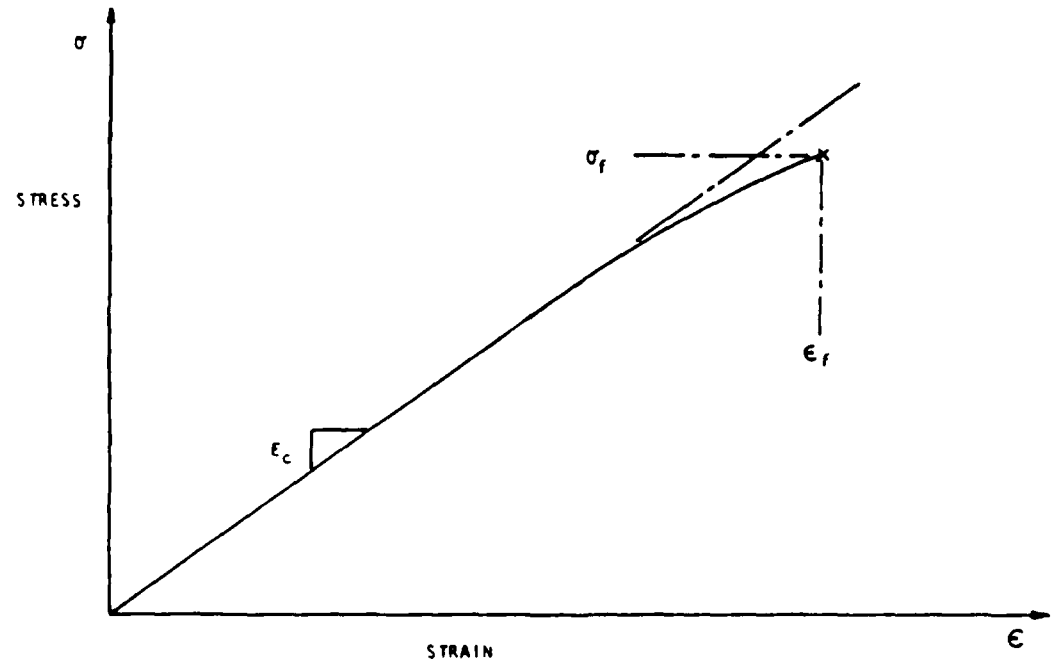

(b)

Figure 8. Typical Forms of (a) Test Record and (b) Reduced Record of Compression Tests.

TABLE 2. COMPRESSIVE TEST RESULTS

5 mm Compression Test (ASTM D695-80)

Sample	Elastic Modulus (x 10^6 psi)	Compressive Strength (psi)	Maximum Strain (in/in)
1915-X2	0.999	43854	0.0509
1915-X3	1.0000	45497	0.0522
1915-X4	1.235	46221	0.0561
1915-X5	0.950	45837	0.0577
1915-X6	0.924	44158	0.0573
Mean	1.022	45113	0.0548
St.D.	0.124	1048	0.0039
1915-Y1	1.015	42951	0.0472
1915-Y2	0.993	45782	0.0537
1915-Y3	1.000	45093	0.0524
1915-Y4	0.991	47256	0.0580
Mean	0.995	45371	0.0530
St.D.	0.015	1567	0.0039

10 mm Compression Test (ASTM D695-80)

Sample	Elastic Modulus (x 10^6 psi)	Compressive Strength (psi)	Maximum Strain (in/in)
1850-X1	1.132	43265	0.0434
1850-X2	1.161	42421	0.0394
1850-X3	1.159	45113	0.0430
1850-X4	1.197	48020	0.0459
1850-X5	1.189	49235	0.0475
Mean	1.168	45611	0.0439
St.D.	0.026	2952	0.0031
1850-Y1	1.244	52766	0.0493
1850-Y2	1.241	54382	0.0500
1850-Y3	1.224	53159	0.0492
1850-Y4	1.239	50857	0.0461
1850-Y5	1.258	52409	0.0467
1850-Y6	1.195	44036	0.0398
Mean	1.224	51268	0.0468
St.D.	0.022	3723	0.0038

C. FLEXURE TESTS

Flexural strength tests were conducted in accordance with the ASTM standard D790-81. From Table 2 of the standard and for a support span-to-depth ratio of 16, the specific dimensions of each specimen were set at 13 mm x 76 mm x 5 mm and 13 mm x 152 mm x 10 mm for the 5 mm and 10 mm thick material, respectively. Lengths shown are for the span between supports. Total specimen length was 192 mm for the 152 mm span and 104 mm for the 76 mm span. Plan dimensions are given in Figure 9 and intact specimens are shown in Figure 10.

The flexure tests followed Method II and Procedure A of the standard. Method II is a four-point bend configuration. The loading points were selected to be at third points between the supports. Procedure A is a designated practice for brittle materials. The load point deflection curve rate was set at 5.0 mm/min for all flexure tests.

Load-deflection curves for the flexure tests were autographically recorded. From simple linear elastic beam theory, the ratio of the beam midpoint deflection to loadpoint deflection is 1.15 for a four-point loading at third points. From this and reduction of the load-deflection curves the flexure modulus, flexural strength, and extreme fiber strain at failure were obtained. Typical forms of the load-deflection curve and reduced data curve are shown in Figure 11. A summary of these results is given in Table 3.

The flexural strength S_f and modulus E_b were calculated by the formulas

$$S_f = P_f L/bd^2 \quad (1)$$

$$E_b = 0.213 L^3 m/bd^3 \quad (2)$$

where P_f is the failure load, L is the length between supports, b is the width, d is the depth, and m is the slope of the straight portion of the load-deflection curve.

Failure of the flexural test specimens was entirely from rupture of the outermost tensile face. After breakage, halves of the test specimens would scatter wildly, so that protective shielding was required during testing. Failed test specimens are shown in Figure 12.

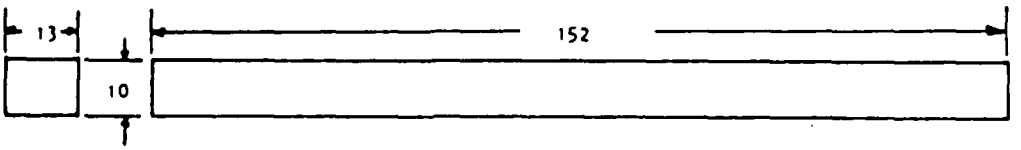

(a)

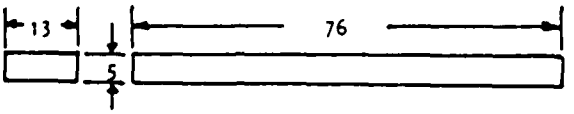

(b)

Figure 9. Flexure Test Specimen Dimensions.
(a) 10 mm, (b) 5 mm Thickness.

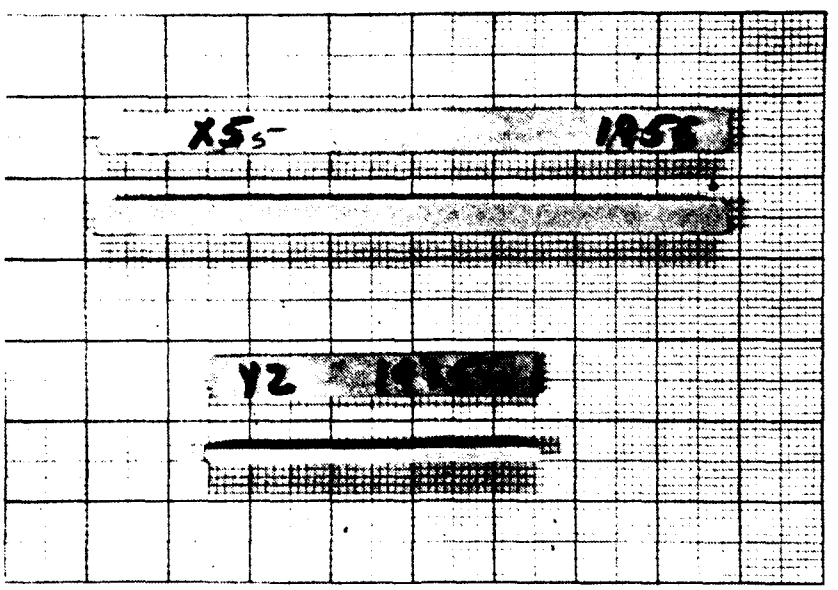

Figure 10. Intact Flexure Specimens.

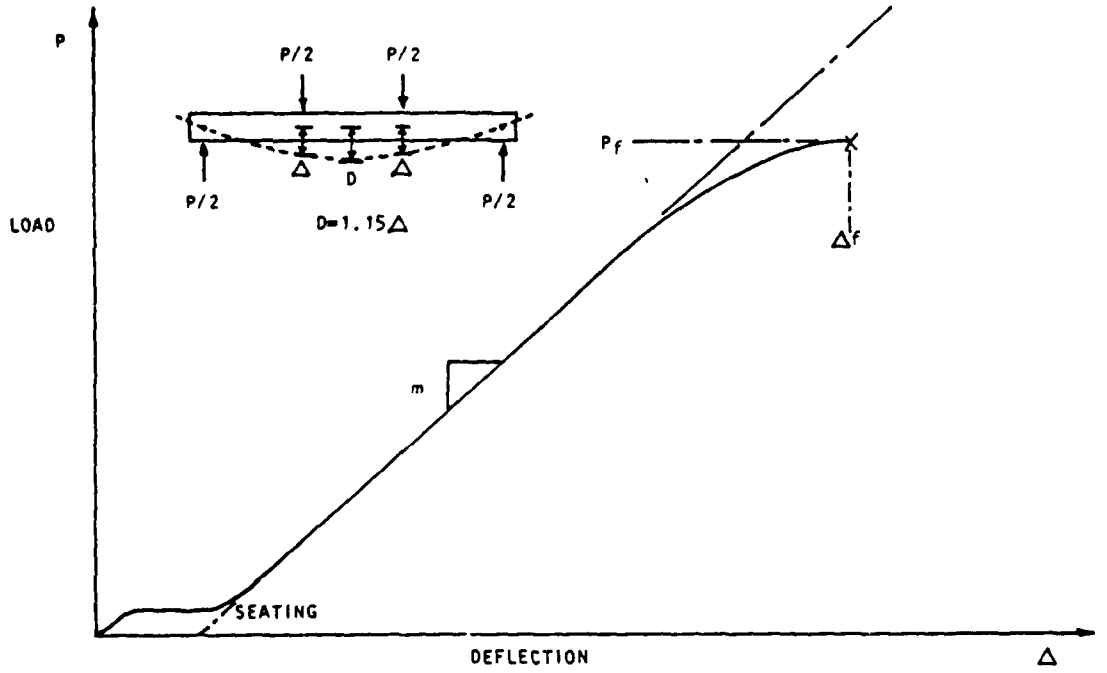

(a)

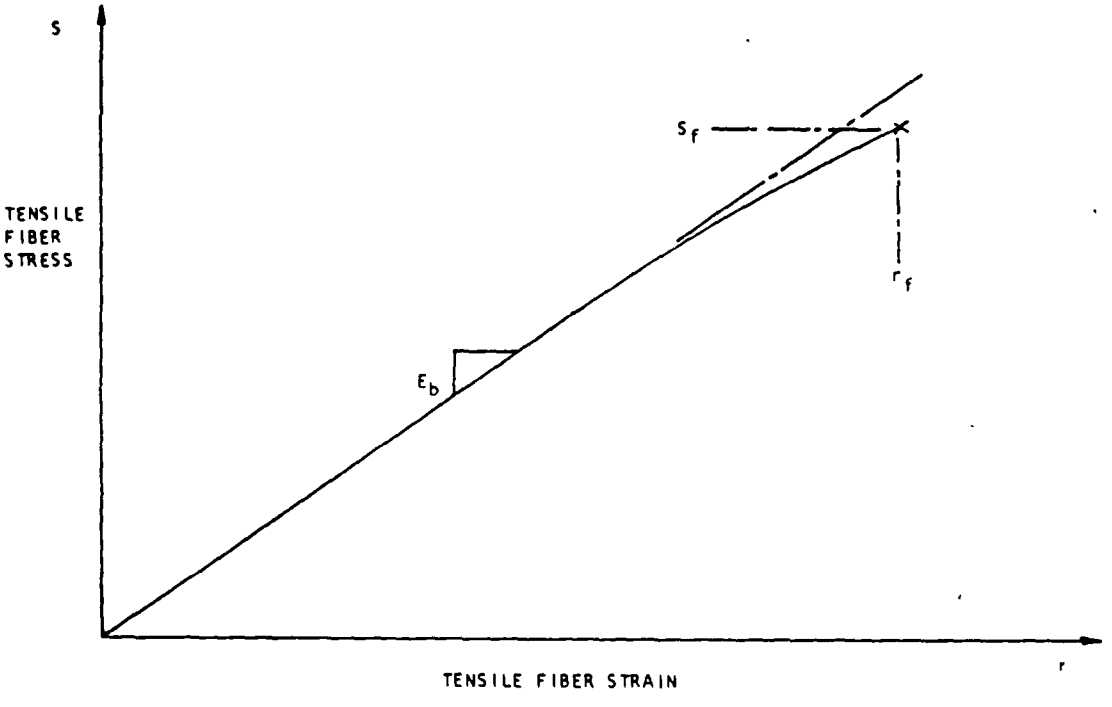

(b)

Figure 11. Typical Forms of (a) Test Record and (b) Reduced Record of Four-Point Bend Tests.

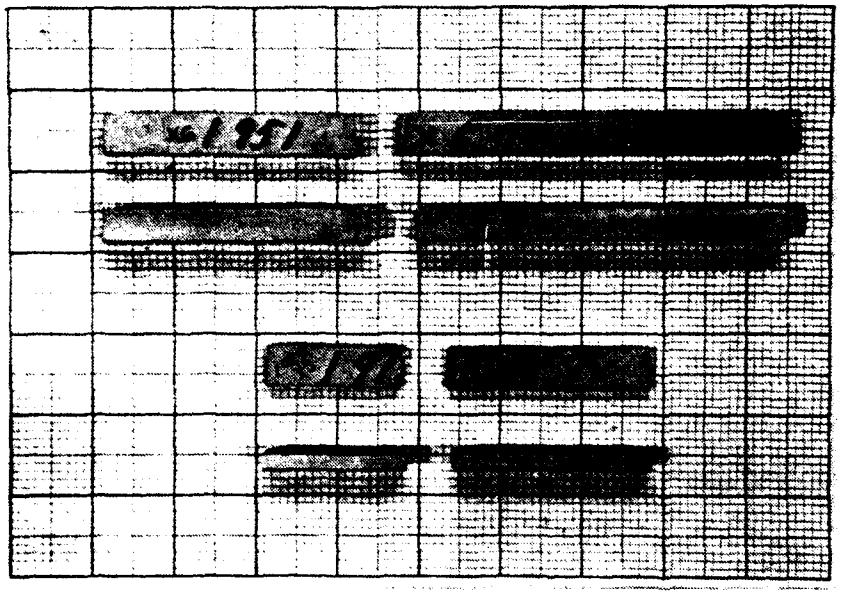

Figure 12. Failed Flexure Specimens.

TABLE 3. FLEXURE TEST RESULTS

5 mm Flexure Test

Sample	Flexure Modulus (x 10^6 psi)	Flexure Strength (psi)	Max Strain (in/in)
1913-X7	5.001	17575	0.00372
1913-X8	4.940	16055	0.00348
1913-X9	5.126	18636	0.00413
1913-X10	5.029	14208	0.00362
1913-X11	4.883	19094	0.00447
Mean	4.996	17114	0.00381
St.D.	0.092	2001	0.00049
1913-Y7	5.317	18722	0.00388
1913-Y8	5.156	19127	0.00407
1913-Y9	5.183	21191	0.00469
1913-Y10	5.088	19705	0.00436
1913-Y11	5.317	18685	0.00393
Mean	5.232	19431	0.00417
St.D.	0.078	1190	0.00034

10 mm Flexure Test

Sample	Flexure Modulus (x 10^6 psi)	Flexure Strength (psi)	Max Strain (in/in)
1951-X6	5.750	17559	0.00386
1951-X7	4.920	17648	0.00396
1951-X8	5.161	17679	0.00386
1951-X9	5.600	18693	0.00424
1951-X10	5.231	17140	0.00365
1951-X11	5.046	18175	0.00437
Mean	5.285	17816	0.00399
St.D.	0.324	542	0.00027
1951-Y6	4.711	14704	0.00340
1951-Y7	5.070	16930	0.00374
1951-Y8	5.046	16905	0.00381
1951-Y9	4.921	17870	0.00427
1951-Y10	4.850	17291	0.00394
1951-Y11	4.717	17694	0.00399
Mean	4.886	16899	0.00386
St.D.	0.156	1144	0.00029

D. FRACTURE TOUGHNESS TESTS

Fracture toughness testing of the material was conducted by conforming to the ASTM standard E399-81. The specimen configuration for the fracture toughness testing was that of a standard compact tension specimen. Dimensions for both the 5 mm and 10 mm thick material are shown in Figure 13. In accordance with section 7.1 of the ASTM standard, the specimen size was determined empirically to constitute plane strain conditions during testing. Intact compact tension specimens are shown in Figure 14.

All relevant testing parameters were met, except for the requirement of an existing fatigue precrack at the root of the starter notch. This condition could not be met because of the inability to prevent complete brittle failure of the specimen during the low-level cyclic fatigue process required to generate the precrack. Fracture toughness testing was, therefore, done without prior precracking on specimens with a straight-through 90-degree V-notch. Therefore, results given for the Mode I plane strain fracture toughness should be considered an upper bound.

The testing of each specimen was done by autographically recording the relative crack opening displacement versus the applied load. The crack opening displacement was measured at the open end of the compact tension specimen starter notch by use of a double cantilever clip gage. Direct computation of the toughness of the material was made by interpretation of the test history (Figure 5) and the test specimen dimensions. A summary of these results is in Table 4.

The fracture toughness K_{IC} and the strength ratio R_{SC} are calculated in accordance with ASTM E399-81 by the formulas

$$K_{IC} = P_q \, f(a/w)/BW^{1/2} \tag{3}$$

and

$$R_{SC} = 2P_{max}(2W + a)/B(W - a)^2\sigma_{ys} \tag{4}$$

The meanings of the dimensions and loads in Equations (3) and (4) are illustrated in Figures 13 and 14; σ_{ys} is the yield strength in tension and $f(a/w)$ is the value of an algebraic function of a/w given in section A4.5.3 of

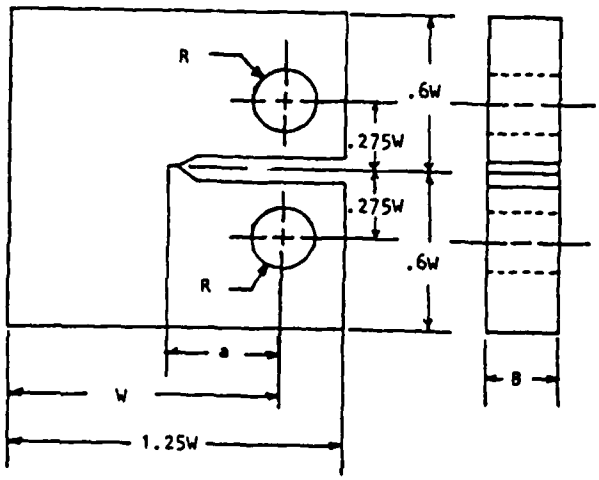

Dimensions, mm		Tolerance
a - initial crack length	20.0	------
W - width	50.0	± .025
R - radius	12.7	± .025
B - thickness	5.0 or 10.0 (approximate)	

Figure 13. Compact Tension Specimen.

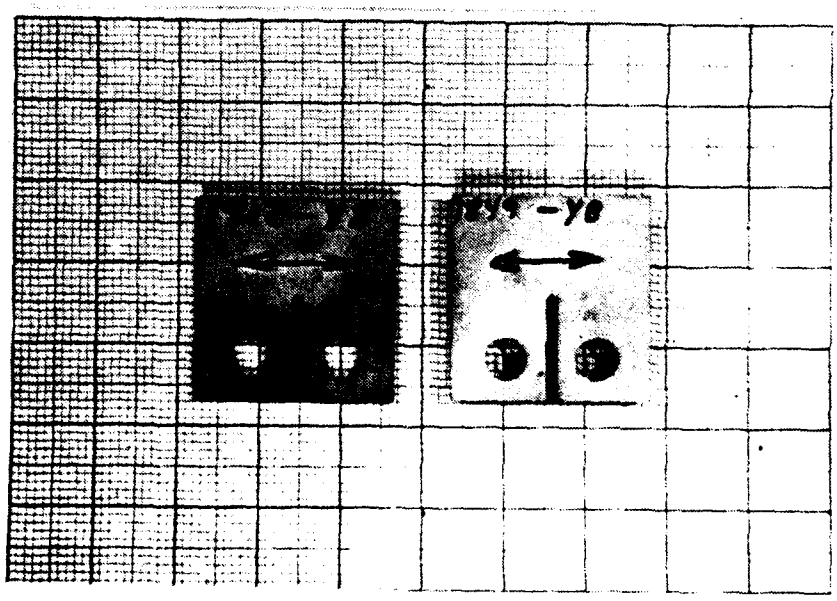

Figure 14. Intact Fracture Specimens.

TABLE 4. FRACTURE TOUGHNESS TEST RESULTS

5 mm Fracture Toughness (ASTM E399-81)

Sample	Toughness K_{IC} ($ksi\sqrt{in}$)	Strength Ratio R_{SC} (%)
1912-X4	1.23	17.1
1912-X6	1.30	18.2
1912-X7	1.25	17.4
1912-X8	1.36	18.0
Mean	1.285	17.7
St.D.	0.058	0.512
1912-Y4	1.19	15.1
1912-Y6	1.17	15.1
1912-Y8	1.24	15.3
Mean	1.20	15.2
St.D.	0.036	0.115

10 mm Fracture Toughness (ASTM E399-81)

Sample	Toughness K_{IC} ($ksi\sqrt{in}$)	Strength Ratio R_{SC} (%)
1949-X3	1.20	16.3
1949-X4	1.06	14.8
1949-X7	1.01	14.3
Mean	1.09	15.1
St.D.	0.098	1.04
1949-Y1	1.02	15.1
1949-Y8	0.99	14.4
1949-Y9	1.13	16.3
Mean	1.05	15.3
St.D.	0.074	0.96

the ASTM standard. R_{SC} is the ratio of the apparent strength of the specimen to the ultimate tensile strength of an unnotched specimen. In the Table the ratio has been converted to a percent by multiplying by 100.

Failure of the compact tension specimens was abrupt with a Mode I crack extension running through the length of the body. Failed specimens are shown in Figure 16.

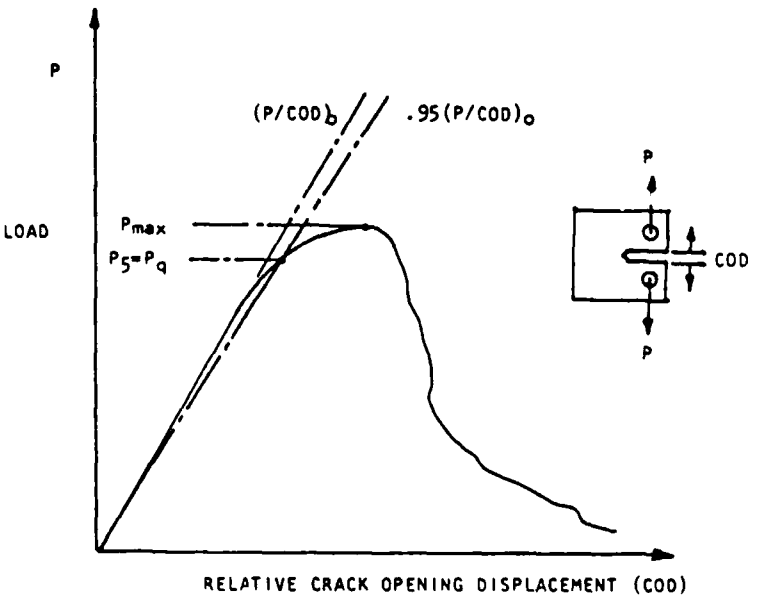

Figure 15. Fracture Test Record.

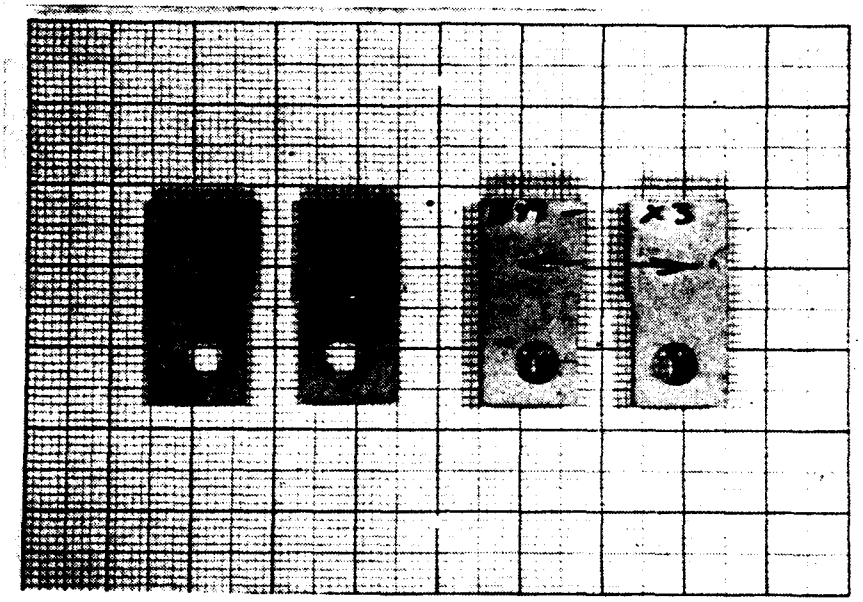

Figure 16. Failed Fracture Specimens.

E. SPECIMEN BLANKS

Before the supplied panels were cut into the required specimen dimensions, the panels were marked with the rough shape of each specimen blank and labeled. The labeling of the specimens consisted of a four-digit panel designation, principal testing direction (x or y), and a specimen number. The x-direction is the direction of the final rolling in the plate fabrication. The general layouts of these blanks are shown in Figures 17 to 20. The roughly cut blanks were a couple of millimeters greater in each of the directions than actually required by the ASTM standard.

Since this is a high-strength, brittle material, the final machine finishing was done with carbide tooling at moderately low speeds. This avoided chipping of the specimens, while providing smooth surfaces.

Within each of the test panels supplied, varying thicknesses in the range of 0.2 mm and 0.6 mm had been noticed. This caused some difficulty in the machining process but was not a major problem.

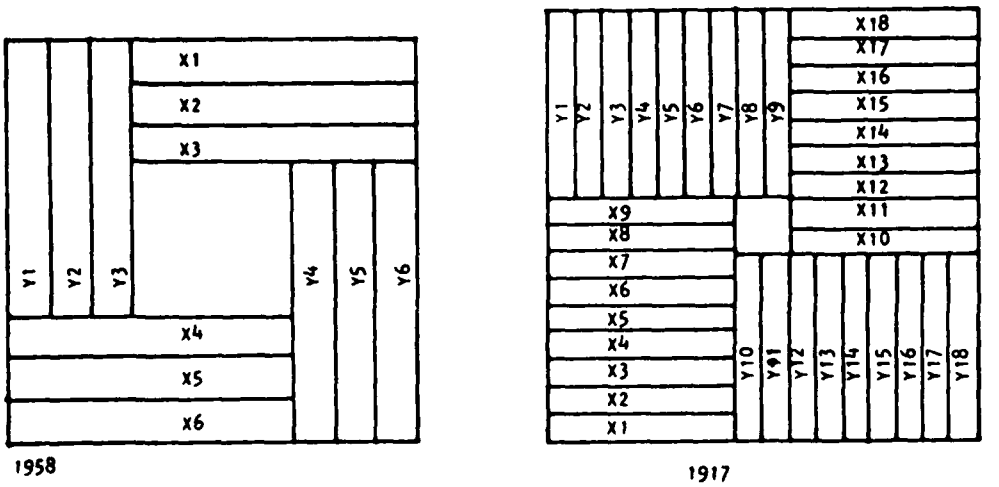

Figure 17. Layout for Tensile Test Specimen Blanks.
(a) 10 mm, (b) 5 mm Thickness.

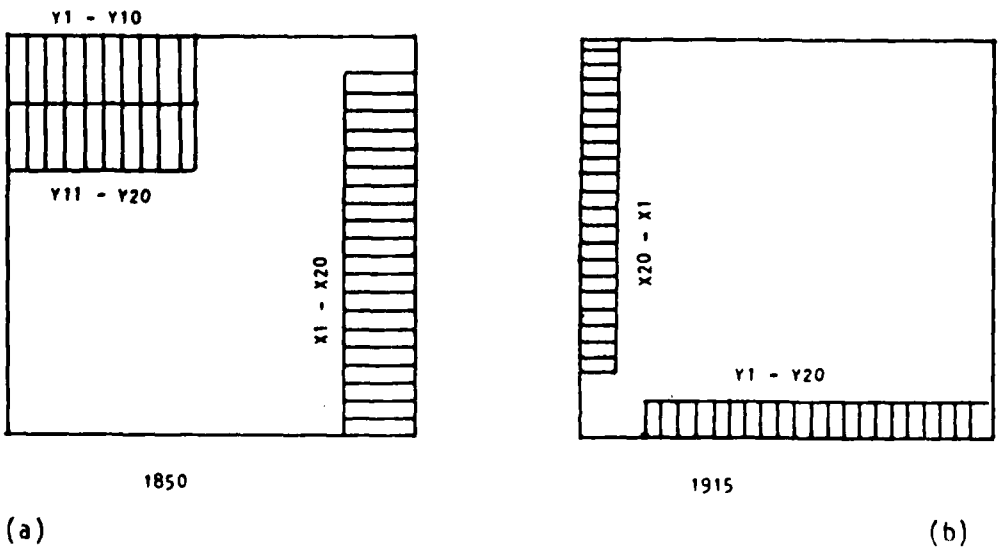

Figure 18. Layout for Compression Test Specimen Blanks.
(a) 10 mm, (b) 5 mm Thickness.

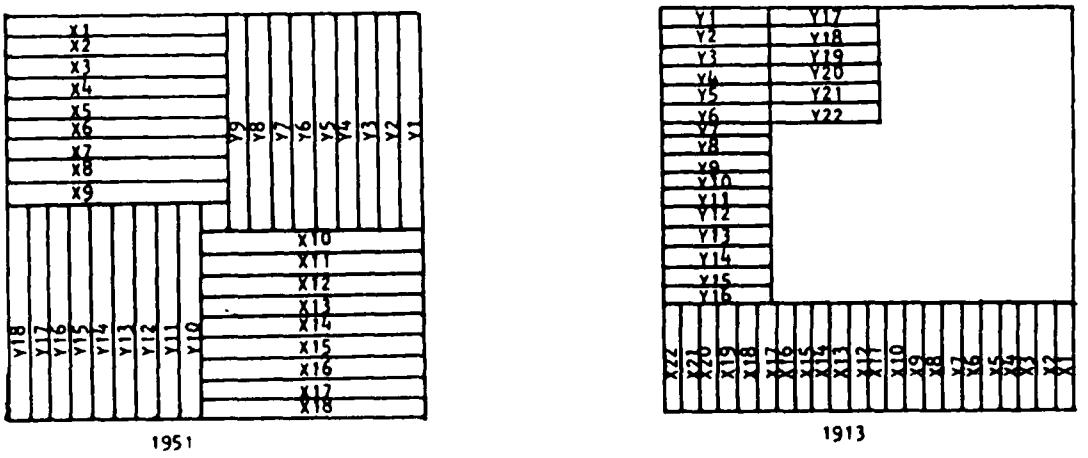

Figure 19. Layout for Flexure Test Specimen Blanks. (a) 10 mm, (b) 5 mm Thickness

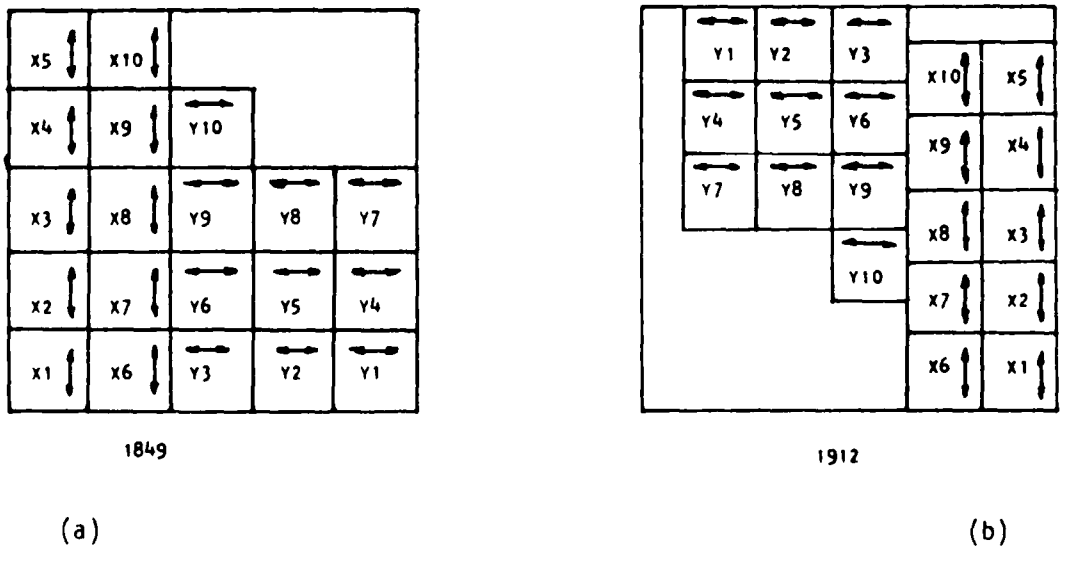

Figure 20. Layouts for Compact Tension Fracture Toughness Specimen Blanks. (a) 10 mm, (b) 5 mm Thickness.

SECTION III

ENVIRONMENTAL HISTORY EFFECTS ON FLEXURAL PROPERTIES

A. MOISTURE HISTORY EFFECTS

Environmental testing was conducted on flexure test specimens that had been immersed in a distilled water bath for periods of 24 hours or 7 days. The bath of distilled water was de-aired and kept at room temperature throughout the soaking duration. The dimensions, loading configuration, and loading rate were the same as those of the dry run flexure tests per ASTM D790-81; see Figure 9. Specimens were cut from Plate Numbers 1913 and 1951, at locations shown in Figure 19.

The environmental parameters evaluated from these tests were water absorption as measured by per cent weight increase, flexure modulus, flexural strength, and extreme fiber strain at failure. Typical relationships for the reduced load-deflection curves and the per cent of weight increase with water absorbed during soaking are shown in Figures 21 and 22. A summary of these results is given in Tables 5 and 6, and trends with times of immersion are shown in Figures 23 to 26.

During the soaking period, a soft chalky film formed at the surface of the water bath. Air bubbles were also noticed to accumulate densely on the material surface, and they did not appear to separate from the surface of the material.

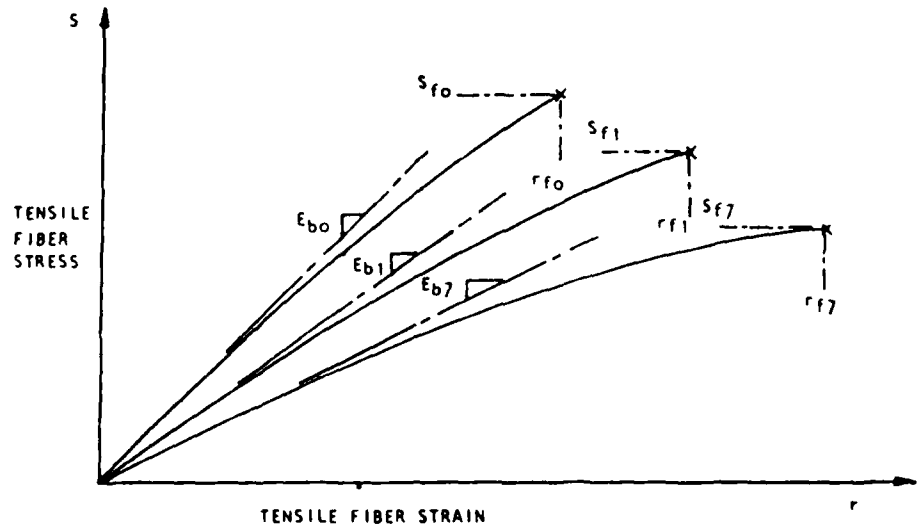

Figure 21. Typical Flexural Stress-Strain Curves After 0, 1 or 7 Days Soaking.

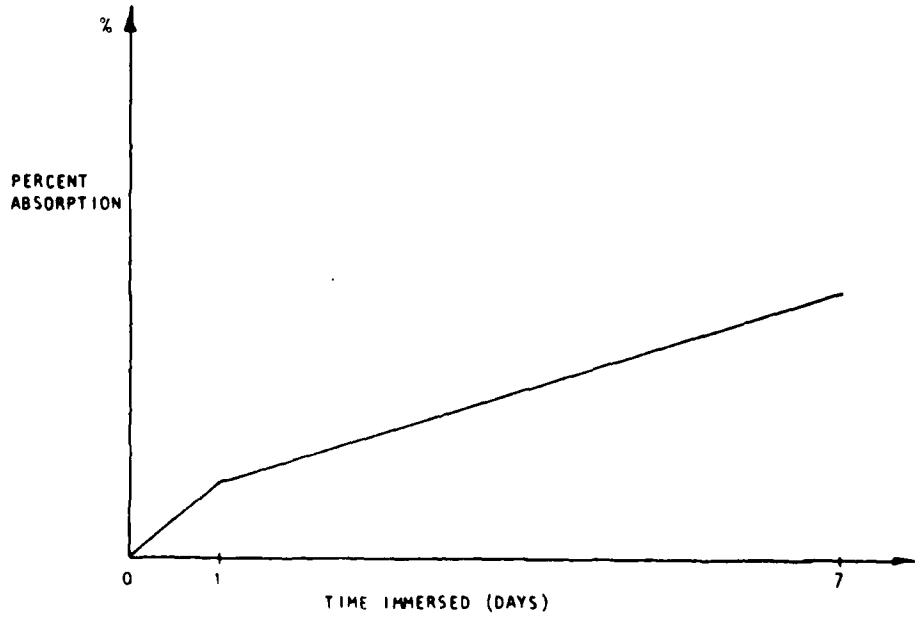

Figure 22. Typical Water Absorption (Schematic).

TABLE 5. FLEXURE TESTS OF 5 MM THICK SPECIMENS AFTER MOISTURE EXPOSURE

5 mm Flexure Test - 24-Hour Immersed

Sample	Flexure Modulus (x 10^6 psi)	Flexure Strength (psi)	Max Strain (in/in)	Absorption (%)
1913-X16	3.600	14893	0.00493	0.20
1913-X17	3.853	15584	0.00496	0.26
Mean	3.727	15239	0.00495	0.23
St.D.	0.179	489	0.00002	0.04
1913-Y16	3.677	13636	0.00406	0.00
1913-Y17	2.967	11641	0.00463	0.32
1913-Y18	3.763	14660	0.00475	0.00
Mean	3.469	13312	0.00448	0.11
St.D.	0.437	1535	0.00037	0.18

5 mm Flexure Test - 7-Day Immersed

Sample	Flexure Modulus (x 10^6 psi)	Flexure Strength (psi)	Max Strain (in/in)	Absorption (%)
1913-X13	2.550	11648	0.00792	1.72
1913-X14	2.786	12049	0.00790	1.85
1913-X15	2.701	12049	0.00758	1.65
Mean	2.679	11915	0.00780	1.74
St.D.	0.119	232	0.00019	0.10
1913-Y13	2.916	13281	0.00691	1.32
1913-Y14	3.551	15343	0.00659	0.11
1913-Y15	3.095	14459	0.00648	0.94
Mean	3.187	14361	0.00666	0.79
St.D.	0.327	1034	0.00022	0.62

TABLE 6. FLEXURE TESTS OF 10 MM SPECIMENS AFTER MOISTURE EXPOSURE

10 mm Flexure Test - 24-Hour Immersed

Sample	Flexure Modulus (x 10^6 psi)	Flexure Strength (psi)	Max Strain (in/in)	Absorption (%)
1951-X16	4.128	16218	0.00435	0.06
1951-X17	3.930	15118	0.00414	0.22
1951-X18	3.930	15118	0.00435	0.12
Mean	3.996	15485	0.00428	0.15
St.D.	0.114	635	0.00012	0.08
1951-Y16	3.997	14816	0.00394	0.17
1913-Y18	3.680	13654	0.00412	0.29
1956-Y1	3.876	14637	0.00410	0.20
Mean	3.926	14369	0.00405	0.22
St.D.	0.218	626	0.00010	0.06

10 mm Flexure Test 7-Day Immersed

Sample	Flexure Modulus (x 10^6 psi)	Flexure Strength (psi)	Max Strain (in/in)	Absorption (%)
1951-X13	3.915	14543	0.00475	0.46
1951-X14	3.330	14123	0.00489	0.46
1951-X15	3.759	14921	0.00515	0.46
Mean	3.668	14529	0.00493	0.46
St.D.	0.303	399	0.00020	0.00
1951-Y13	3.700	13861	0.00473	0.49
1951-Y14	3.728	14001	0.00473	0.55
1951-Y15	3.795	13315	0.00480	0.60
Mean	3.674	13726	0.00475	0.55
St.D.	0.070	362	0.00004	0.06

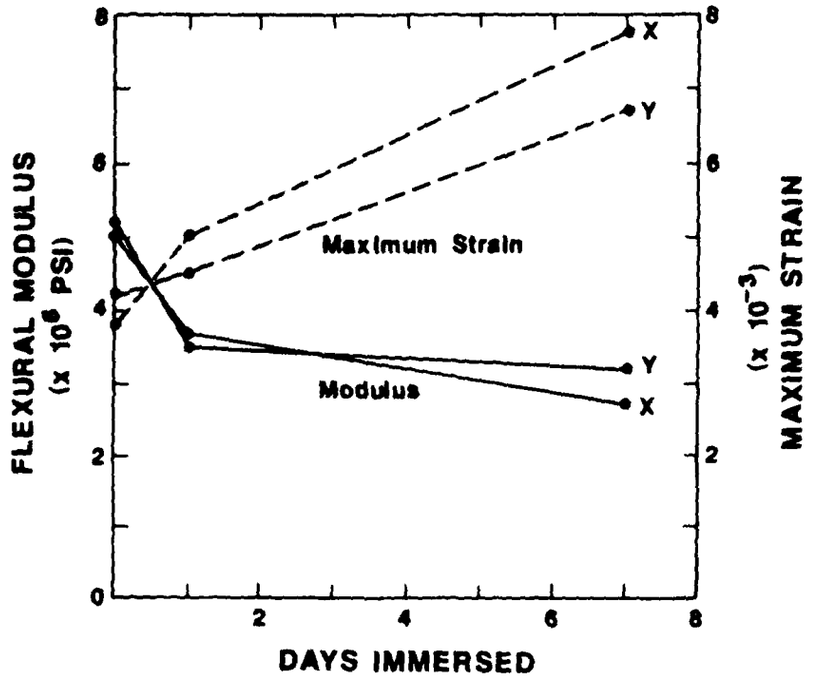

Figure 23. Trends of Average Modulus and Maximum Fiber Strain With Time Immersed for 5 mm Specimens.

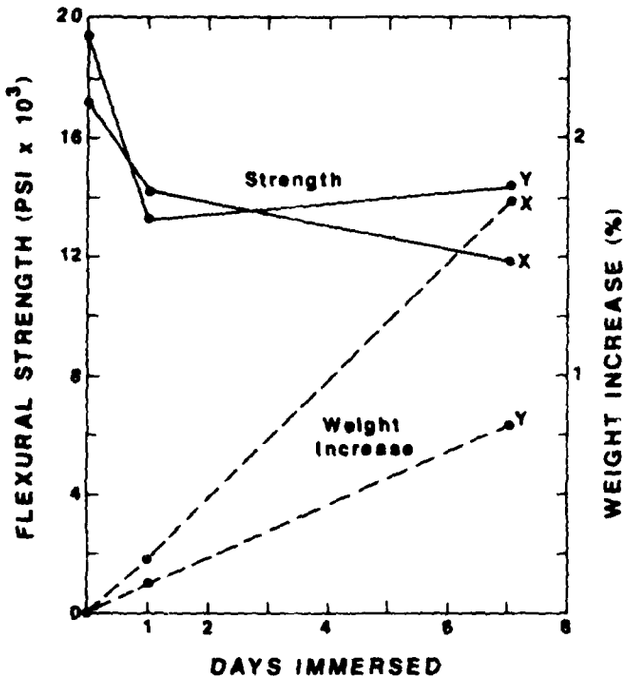

Figure 24. Trends of Strength Decrease and Weight Increase with Time Immersed for 5 mm Specimens.

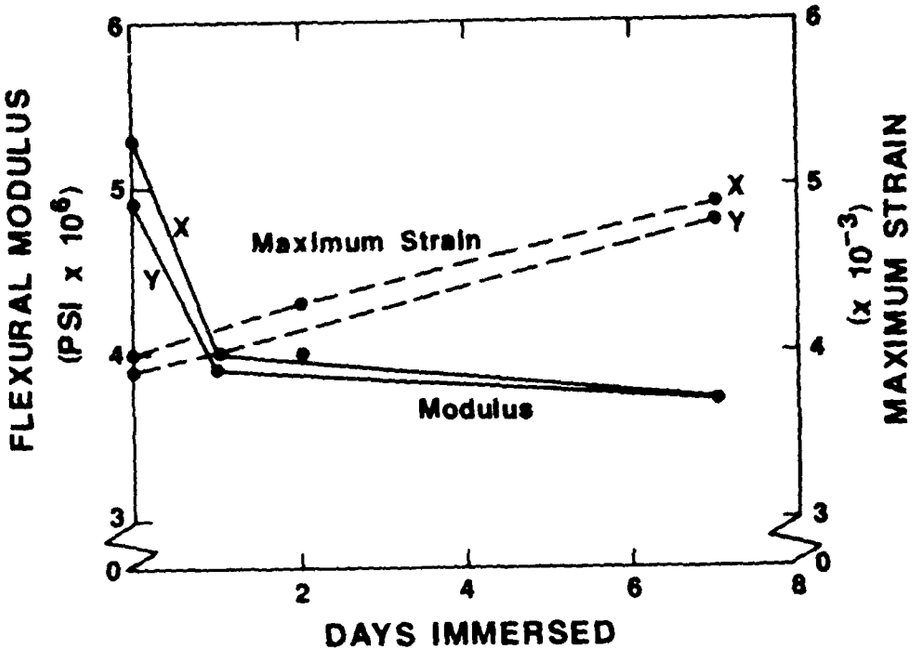

Figure 25. Trends of Average Modulus and Maximum Fiber Strain with Time Immersed for 10 mm Specimens.

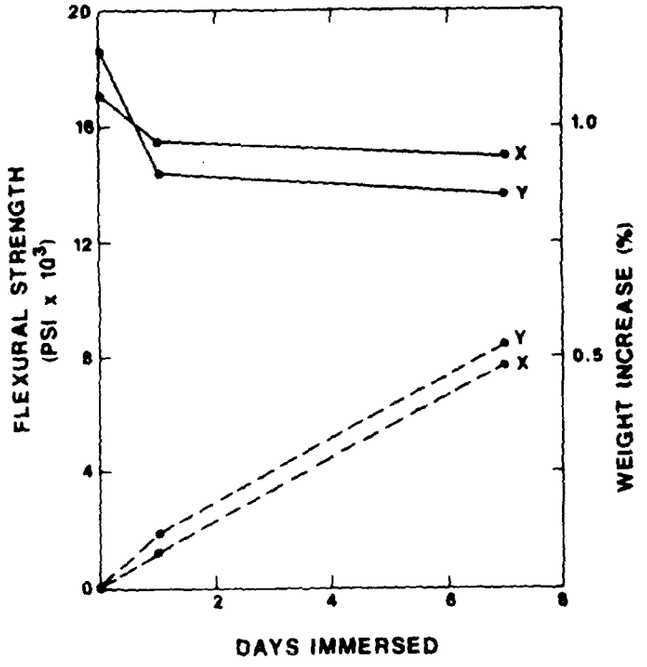

Figure 26. Trends of Strength Decrease and Weight Increase with Time Immersed for 10 mm Specimens.

B. THERMAL HISTORY EFFECTS

Four-point bend flexural tests were performed on 5 mm thick specimens. The dimensions and loading configuration were the same as those of the flexural tests described in Section II.C per ASTM D790-81. Additional control specimens, not subjected to a thermal history, were tested, cut from the same plates as the thermal history specimens.

Some preliminary tests on 10 mm thick specimens subjected to a 120°C environment for 24 hours showed that many of the specimens, which were from plates that had evidently been formed by laminating together two 5 mm plates, delaminated during the thermal exposure, and all of them showed less than 10 per cent of the flexural strength of the control specimens. Most of the remainder of the test program was carried out on 5 mm thick specimens.

After some exploratory trials, it was determined that a temperature range from 80°C to 150°C with exposure times ranging from 1 to 24 hours was a suitable test spectrum. After removal from the autoclave, the specimens were allowed to cool at room temperature for 1 to 1.5 hours before testing. Results reported in the following table are averages for four replications of the flexural strength and flexural modulus (except for a few cases where there were only three replications). Since these parameters varied somewhat from plate to plate, the values reported in the following table have been normalized by dividing by the average value for four control specimens from the same plate. As the table shows, all the thermal histories caused an increase in the flexural modulus after a 24-hour exposure. In some cases, shorter exposure times decreased the modulus, most notably at 120°C, which was also the temperature where the greatest increase in modulus occurred (28 per cent) in 24 hours.

TABLE 7. THERMAL ENVIRONMENTAL HISTORY EFFECTS ON FLEXURAL PROPERTIES

(Strength and modulus have been normalized by dividing by the average value for control specimens from same plate.)

EXPOSURE TEMPERATURE 80°C						PLATE NO. 1941
Exposure Time (hr)	0	1	3	5	7	24
Flexural Strength /127 MPa	1.00	0.768	0.733	0.818	0.853	0.955
Flexural Modulus /35.8 GPa	1.00	1.005	1.005	0.972	1.022	1.131

EXPOSURE TEMPERATURE 100°C							PLATE NO. 1940
Exposure Time (hr)	0	0.5	1	3	5	7	24
Flexural Strength /117 MPa	1.00	0.840	0.904	0.878	0.948	1.00	0.956
Flexural Modulus /37.8 GPa	1.00	0.939	0.987	0.989	0.960	0.915	1.077

EXPOSURE TEMPERATURE 120°C							PLATE NO. 1940
Exposure Time (hr)	0	0.5	1	3	5	7	24
Flexural Strength /117.0 MPa	1.00	0.908	0.921	0.980	0.921	0.932	0.745
Flexural Modulus /37.8 GPa	1.00	0.820	0.857	1.06	1.06	1.06	1.28

EXPOSURE TEMPERATURE 150°C						PLATE NO. 1982	
Exposure Time (hr)	0	0.5	1	3	5	9	13
Flexural Strength /125.8 MPa	1.00	0.828	0.944	0.619	0.636	0.425	0.299
Flexural Modulus /41.4 GPa	1.00	1.10	1.16	1.20	1.21	1.17	1.09

Exposure Time (hr)	21	25	30
Flexural Strength /125.8 MPa	0.343	0.377	0.361
Flexural Modulus /41.4 GPa	1.11	1.14	1.14

Strength was degraded by all the thermal histories, but the decrease showed quite different dependence on exposure time at different temperatures. For example, at 80°C the retained strength after 1 hour was 0.768 of the control value, but further exposure showed 0.955 of the strength retained after 24 hours. At 150°C, on the other hand, the retained strength factor after 1 hour was 0.944 and after 25 hours it was 0.377. Each value reported in the table is the average for four replications. Some individual specimen results are shown in the appendix.

Figures 27 through 30 show the trends in flexural strength with exposure time at four temperatures. The error bars denote actual scatter bands at the various exposure times. The maximum exposure time initially planned was 24 hours, but at 150°C a group of specimens was exposed for 30 hours to rule out significant further degradation.

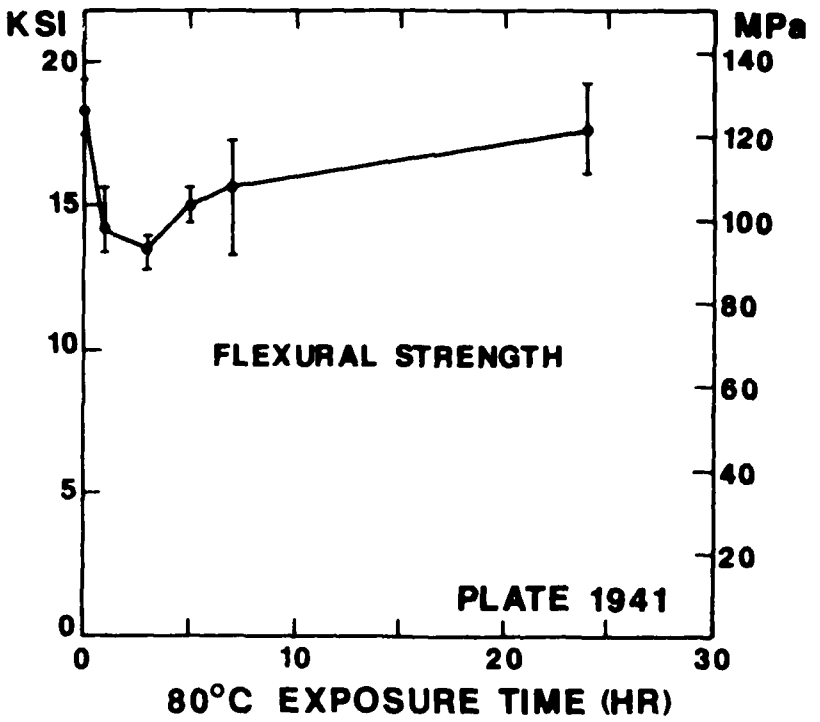

Figure 27. Trend of Flexural Strength with Hours of Exposure at 80°C.

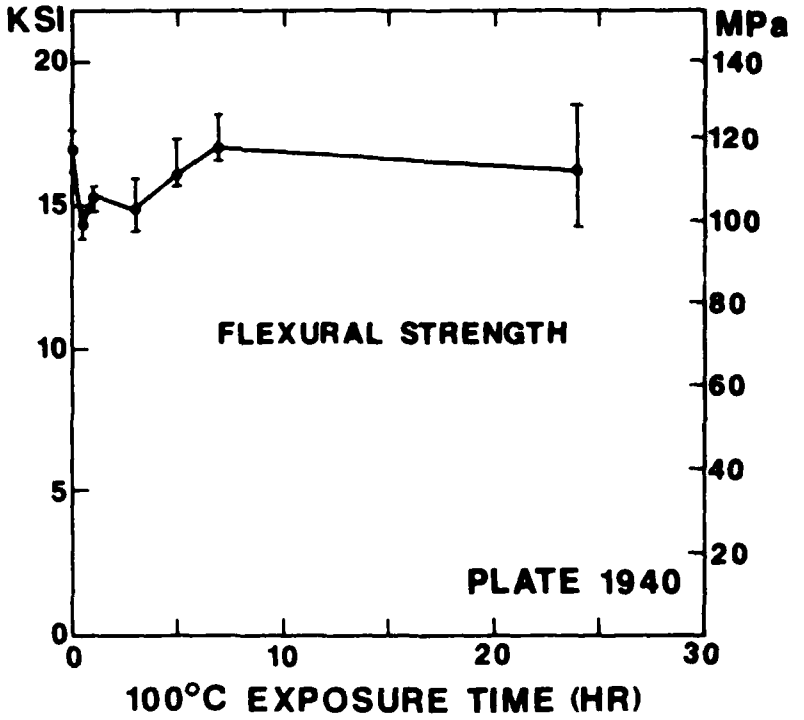

Figure 28. Trend of Flexural Strength with Hours of Exposure at 100°C.

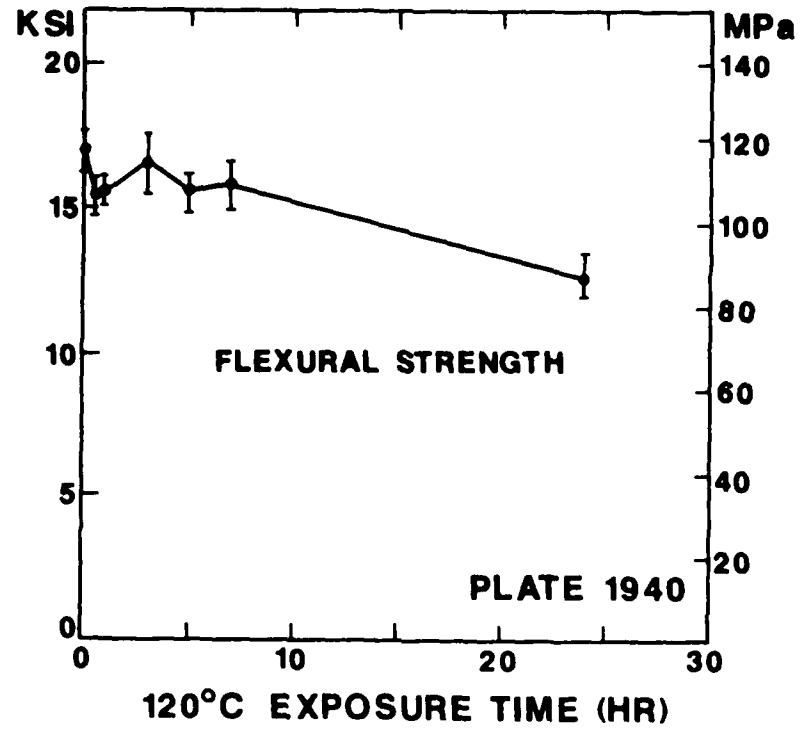

Figure 29. Trend of Flexural Strength with Hours of Exposure at 120°C.

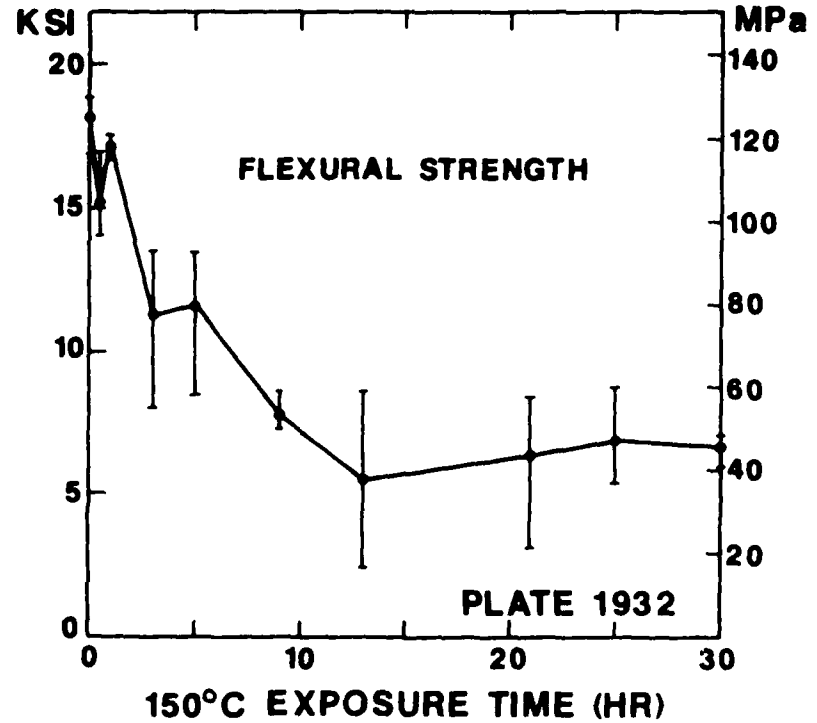

Figure 30. Trend of Flexural Strength with Hours of Exposure at 150°C.

SECTION IV
DYNAMIC TESTS

A. HIGH-STRAIN-RATE COMPRESSIVE TESTS WITH SHPB

1. Test Equipment and Procedures

The Kolsky apparatus or Split Hopkinson's Pressure Bar (SHPB) system methods used do not follow an ASTM standard. A brief description of the apparatus and procedures is, therefore, given here. For a historical background on the development of SHPB systems, and more details about their application, see the section by T. Nicholas in the book Impact Dynamics by Zukas et al. (1982), Reference 1. Two SHPB systems were used. Tests of 10 mm diameter specimens were made with a small system with 19 mm diameter pressure bars and a 58 cm (23 inch) long striker bar propelled by a torsion spring. This system was inadequate for testing 19 mm diameter specimens. Fortunately a new system with 76 mm diameter pressure bars and a 76 cm (30 inch) long striker bar propelled by a gas gun, designed for testing concrete, was completed at the University of Florida during this investigation. Although it had a larger than desirable area ratio of pressure bar to specimen, it was used to test the 19 mm specimens.

Figure 31 shows a schematic of the SHPB with a Lagrange diagram (x - t plane) above it illustrating the propagation of the longitudinal elastic stress waves in the striker and two pressure bars. Dimensions shown are for the new larger system. Maximum loading time of approximately 300 microseconds is determined by the time required for the elastic compressive wave set up in the striker bar to return as an unloading tensile wave. The strain gages on the incident pressure bar are positioned so that this length of incident compressive pulse, ε_I, has passed the gage station and the trace has returned to zero, so that there is a dwell period before the reflected wave, ε_R, from the specimen arrives.

A full strain-gage bridge is permanently mounted on each pressure bar, 152 cm (60 inches) from the specimen interface. The amplified signals are recorded by a transient recorder consisting of a four-channel Nicolet 4094 digital storage oscilloscope.

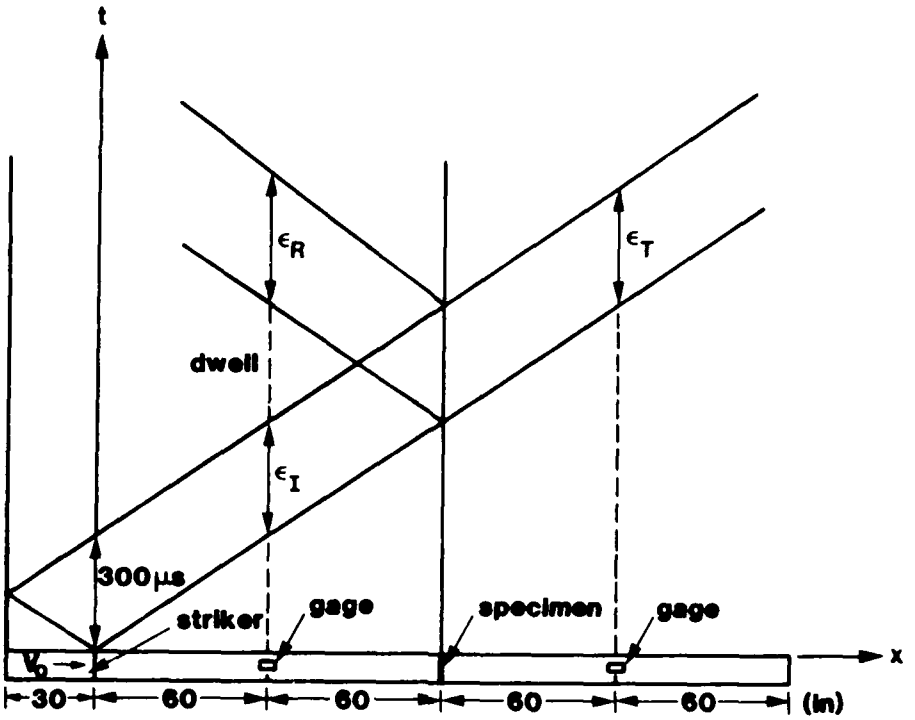

Figure 31. Schematic of Bars and Lagrange Diagram

The recorded signals are displayed by the oscilloscope and also stored on floppy diskettes for subsequent analysis. Figure 32 shows an example of the axial strain signals versus time, recorded by a Hewlett Packard 7470A digital plotter from the stored signals in the digital oscilloscope. Compressive strain is plotted upward. After the passage of the first incident pulse, of nominal length 300 microsec (from the beginning of the rise to the beginning of the fall), there is a dwell time before the arrival of the reflected pulse from the specimen, which is recorded at the same gage station as the incident pulse. Another channel shows the pulse transmitted through the specimen into the transmitter bar. Because the two gage stations are equidistant from the specimen, the transmitted pulse arrives at the transmitter-bar gage station at approximately the same time as the reflected pulse arrives back at the incident-bar station, delayed only by the transit time of the leading edge of the pulse through the specimen.

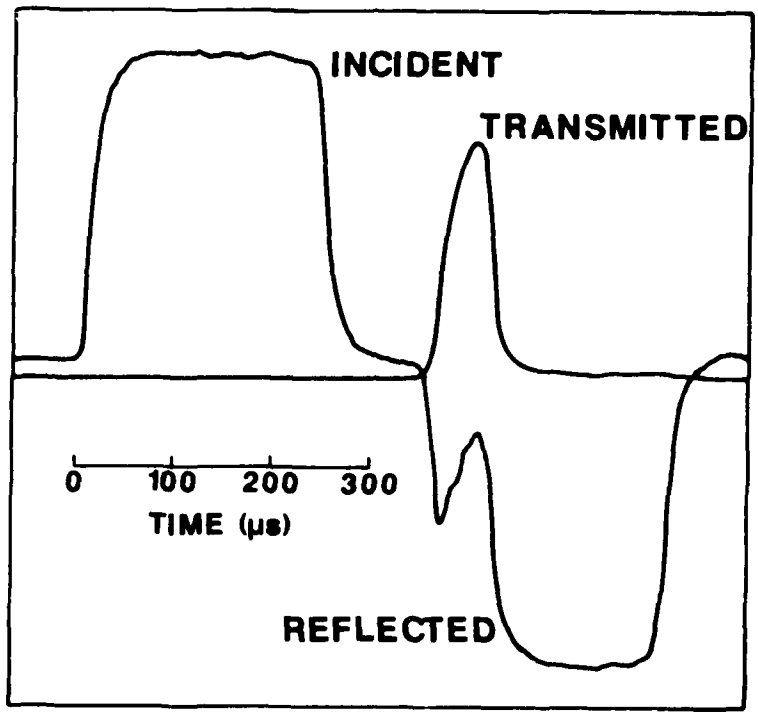

Figure 32. Strain Pulses in Pressure Bars - Larger System with 19-mm Specimen.

For purposes of analysis, the digitally recorded pulses are time-shifted, so that time zero coincides with the initial arrival at the specimen interface. One-dimensional elastic wave analysis in the pressure bars then furnishes both force and velocity versus time at each interface of the short specimen, from which the dynamic stress-strain relation is deduced.

For a strain pulse propagating in the positive direction (away from the striker) in a pressure bar, elastic bar-wave theory furnishes the relationship

$$v = - c_0 \varepsilon \tag{5}$$

between the particle velocity v and the strain ε (negative for compression), where c_0 is the elastic bar-wave propagation speed. In the incident bar at the interface with the specimen the incident strain pulse ε_I gives velocity $-c_0\varepsilon_I$ and the reflected strain pulse ε_R

propagating in the negative direction gives particle velocity $+c_0\varepsilon_R$, so that the net particle velocity v_I of the incident bar interface is

$$v_I = -c_0(\varepsilon_I - \varepsilon_R) \tag{6}$$

The transmitter bar interface particle velocity v_T is similarly found as

$$v_T = -c_0\varepsilon_T \tag{7}$$

where ε_T is the strain in the transmitted pulse. All these strains and particle velocities vary with time, while c_0 is constant. The nominal strain rate $\dot{\varepsilon}_s$ in a specimen of initial length L_s is $(v_T - v_I)/L_s$ or

$$\dot{\varepsilon}_s = -\frac{c_0}{L_s}[\varepsilon_T - \varepsilon_I + \varepsilon_R]. \tag{8}$$

Equation (8) gives, at any time, the average strain rate along the specimen, (negative for compression) regardless of the specimen length, if the three recorded strain pulses at the gages are appropriately shifted in time (ε_I forward and the other two backward) before combining them. This can be accomplished by a simple computer program with digitally recorded data. In many analyses the further assumption is made that the stress in the specimen is essentially uniform along the short specimen length after the initial rise; then the same force acts on each pressure bar interface so that

$$EA(\varepsilon_I + \varepsilon_R) = EA\varepsilon_T \tag{9}$$

where E and A are the elastic modulus and cross section area of the pressure bars. This implies that

$$\varepsilon_I + \varepsilon_R = \varepsilon_T, \tag{10}$$

so that Equation (8) takes the simpler form

$$\dot{\varepsilon}_s = -\frac{2c_0}{L_s}\varepsilon_R. \tag{11}$$

If the assumption of Equation (9) is not valid, then Equation (8) can be integrated instead of Equation (11) to determine specimen strain versus time. This will require a simple digital computer analysis because of the different time shifts between ε_I and the other pulses.

When the simpler Equation (11) can be used, the integration can be performed with an integrating operational amplifier in the recording circuit. Then, with appropriate scaling, the reflected pulse of Figure 32 represents specimen strain rate, the transmitted pulse represents specimen stress and the integrated reflected pulse represents the specimen strain, all plotted versus time. They can be read out point by point from the memory of the digital storage oscilloscope. They can also be replotted as stress versus strain on the digital oscilloscope display and then copied by the xy-plotter.

Although the 10 mm long specimens of the present investigation were short enough that the simpler analysis would have given almost the same results, the method of Equation (8) was used to obtain the strain rate for all the data reported in this investigation.

The specimen stress at the transmitter bar interface, σ_{sT}, is given by

$$\sigma_{sT} = E(A/A_s)\varepsilon_T \tag{12}$$

while the specimen stress at the incident bar interface, σ_{sI}, is given by

$$\sigma_{sI} = E(A/A_s)(\varepsilon_I + \varepsilon_R) \tag{13}$$

where A_s is the cross section area of the specimen, which should be less than or equal to the pressure bar cross section area A, and E is the pressure bar elastic modulus. An estimate of the average stress along the specimen length is then given by

$$\bar{\sigma} = \frac{1}{2}(\sigma_{sI} + \sigma_{sT}) \tag{14}$$

while an error estimate for the stress difference from the average is given by

$$\frac{1}{2}|\sigma_{sI} - \sigma_{sT}|.$$

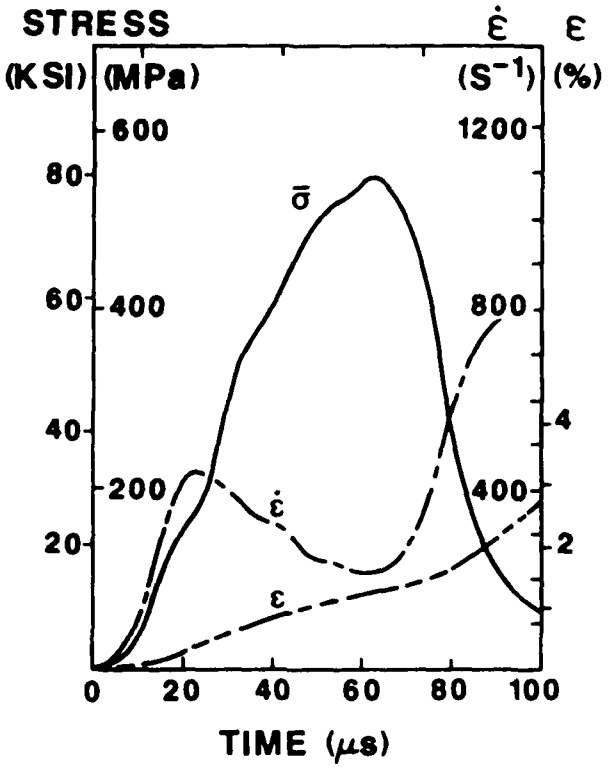

Figure 33. Example of Average Specimen Stress $\bar{\sigma}$, Strain Rate $\dot{\varepsilon}$ and Strain ε Versus Time.

Figure 33 shows an example of plots of the average stress (by Equation 14), specimen strain rate (by Equation 8), and strain ε (obtained by numerical integration of the strain rate), all plotted versus time measured from the instant when the leading edge of the incident pulse arrived at the specimen. This is the processed data deduced from the recorded pulses of Figure 32. The results are replotted as stress versus strain in Figure 34. Two stress scales are shown, kips per square inch and megapascals.

As is shown in Figure 33, the specimen strain rate (average along the length) is not constant during the test but decreases from a maximum that occurs near what is believed to be the end of an essentially elastic deformation to a minimum very near the maximum stress and then increases again as the specimen fails completely. The decrease in strain rate is not a purely material effect, but is an interaction between the specimen and the incident pressure bar, which is slowed by the resisting force of the specimen. In the following subsection the test results will be reported as maximum stress versus the strain rate at the maximum stress.

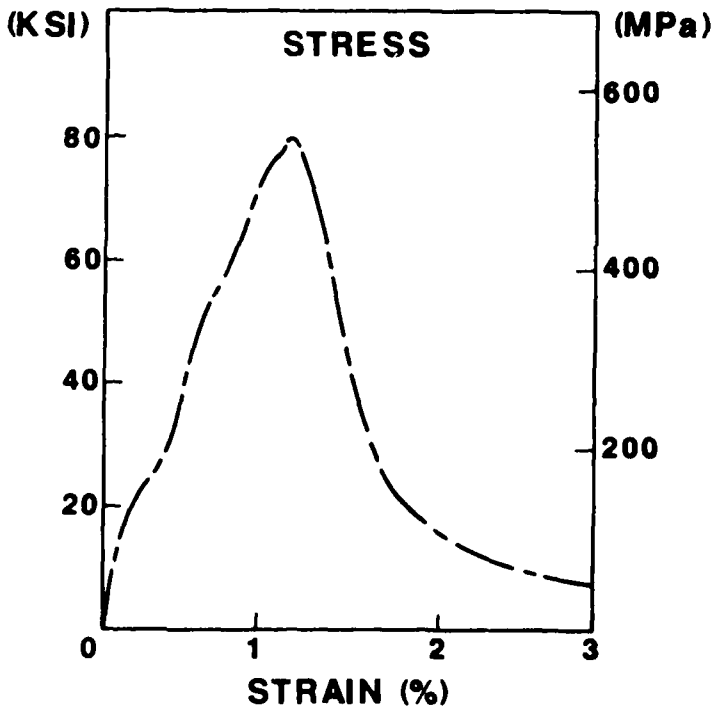

Figure 34. Stress-Strain Curve for Example of Figure 33.

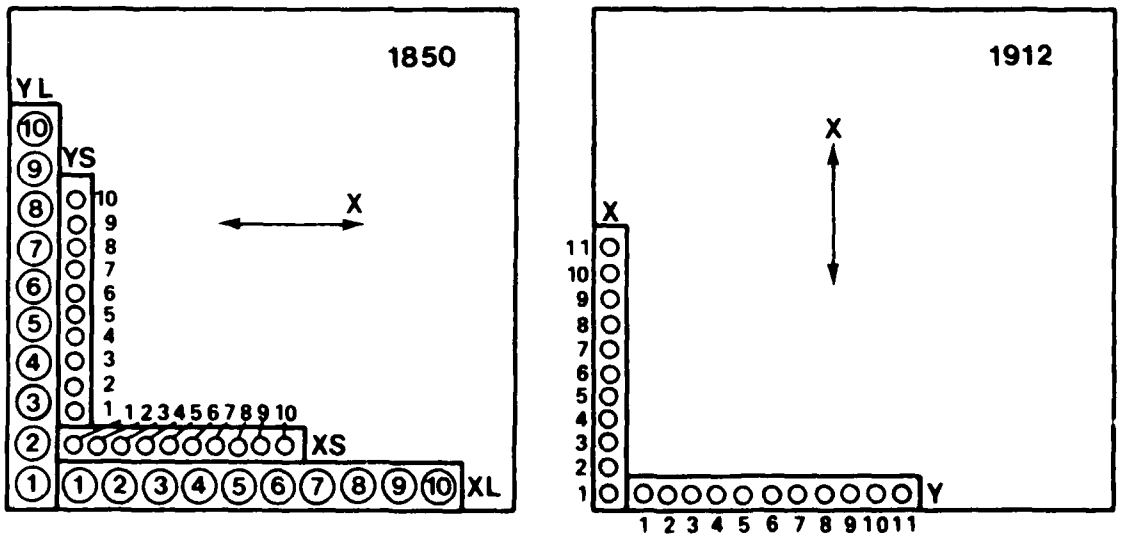

Figure 35. Locations From Which Dynamic Compression Specimens Were Cut In Plates 1850 and 1912. Arrows Marked X Indicate Final Rolling Direction.

2. Dynamic Compressive Test Results

Figure 35 shows the locations in the plate from which large (XL and YL) 19 mm diameter specimens and small (XS and YS) 10 mm diameter specimens were cut from Plate 1850. All these dynamic compression specimens are for thickness direction tests of nominally 10 mm long cylinders. The X-direction is the direction of the final rolling in the preparation of the plate, and the Y-direction is perpendicular to it. The right-hand part of the figure shows locations in the 5 mm thick Plate 1912 from which another series of specimens of length 5 mm and diameter 10 mm were cut.

Figure 36 displays the ultimate compressive strength versus the strain rate at the maximum stress for seven of the XS specimens, along with five of the in-plane static strengths found in the tests of Section II.B. This was an unusually consistent set of dynamic test results. Figure 37 shows these same points, along with seven of the YS specimen

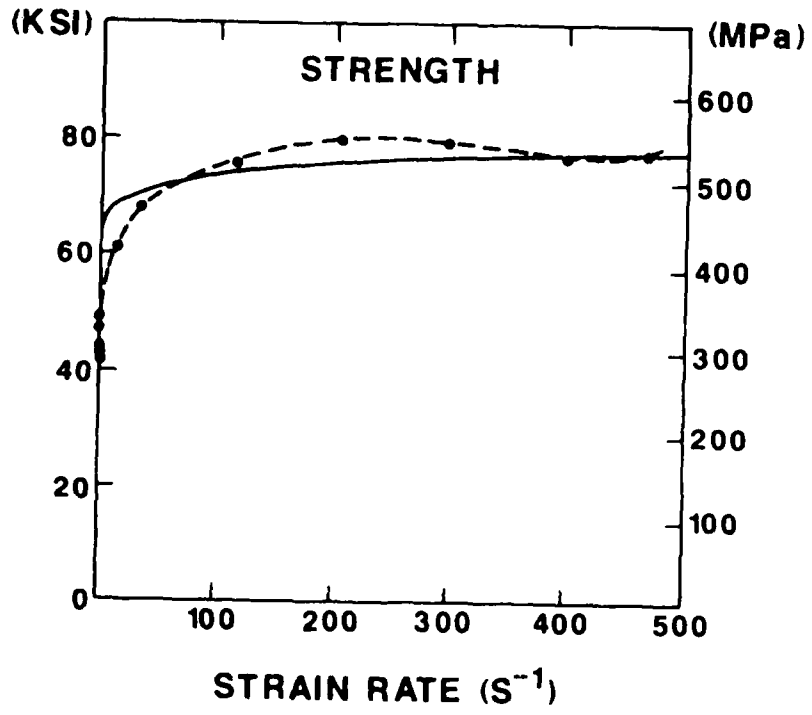

Figure 36. Ultimate Strength Versus Strain Rate at the Ultimate Strength for Seven 10 mm Thick by 10 mm Diameter Specimens of Type XS. Also shown are five static compression test results.

dynamic test results and additional static tests and exhibits greater scatter in the results. All the numerical values for the points plotted in the figures of this section are tabulated in three tables in the appendix.

In Figure 36, the two lowest-speed dynamic tests (at failure strain rates of 10/sec and 35/sec) were obtained by a technique of direct impact of the 1.83-meter (6-foot) long incident pressure bar against the specimen instead of the usual split-bar technique where the loading pulse is furnished by a 58 cm (23-inch) long striker bar and transmitted to the

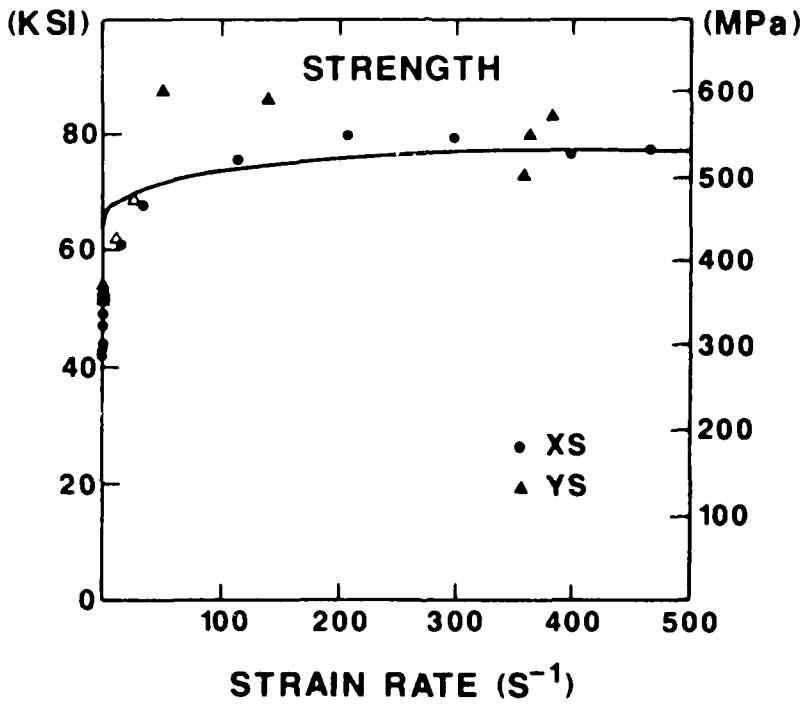

Figure 37. Dynamic Compression Test Results of 10 mm Specimens Showing Ultimate Strength Versus Strain Rate at the Maximum Stress. Also shown are 10 static compression test strengths.

specimen through the incident pressure bar. Two more direct-impact low-speed tests are shown by the hollow triangles in Figure 37. The direct impact by the incident bar provides a longer loading pulse than the usual striker-bar pulse, so that enough loading time is available for failure to occur at the lower speed. This provided data in the important transition region between the static tests and the usual SHPB range (above about 50/sec).

Above the transition region in Figure 36, the strength appears to reach a maximum at a failure strain rate of about 200/sec and then to decline at higher rates. The scatter in Figure 37, however, makes such a specific conclusion questionable. What can be concluded from these results is that there is a transition region from the static range with strengths around 50 ksi (345 MPa) to the Hopkinson bar range with strengths around 80 ksi (550 MPa), with possibly a slight decrease at the higher rates.

All the results reported in Figures 36 and 37 are for 10 mm diameter specimens, tested with the small SHPB system. These have been reproduced in Figure 38 along with additional points from tests of 19 mm diameter specimens marked X for the XL series and + for the YL series. These larger specimens, tested in the new larger SHPB system, show a great deal of scatter, possibly because of the large area mismatch between specimen and pressure bar, and possibly because the specimens were cut from positions near the edge of the plate.

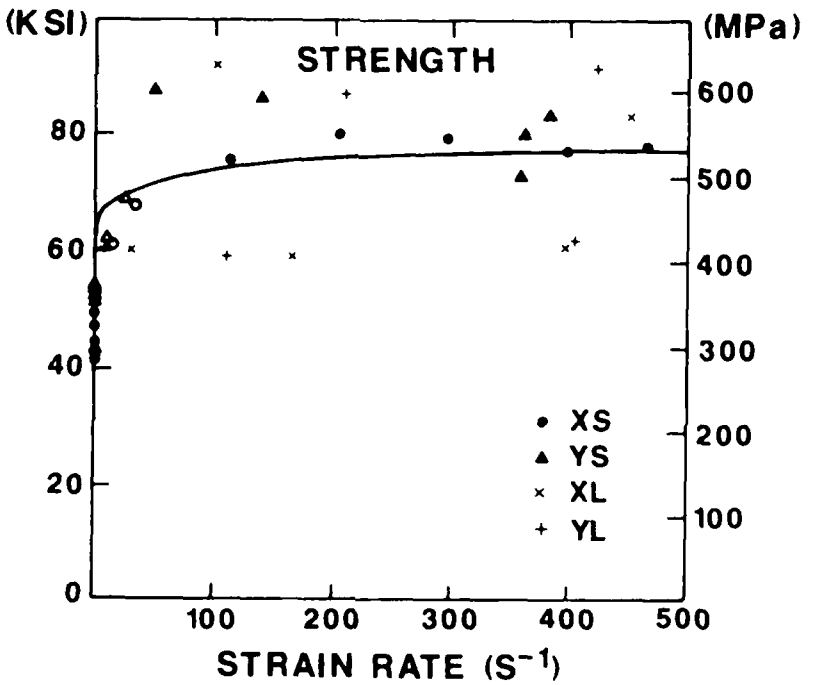

Figure 38. Dynamic Compression Test Results Showing Ultimate Strength Versus Strain Rate at the Maximum Stress. Points Marked With Solid Circles and Triangles are for 10 mm Diameter Specimens, Reproduced From Figure 37. Ten Static Compression Test Strengths are Shown on the Left Ordinate Scale.

Figure 39 reproduces the dynamic data of Figure 38 along with six more points at still higher rates. It was noticed in some of these higher-rate tests that considerable heating occurred. Brilliant sparks were observed even with the laboratory lights on, and cakes of flattened specimens felt warm when they were removed from the ends of the steel pressure bars after the tests. It is possible that some thermomechanical effects are responsible for the drop-off in ultimate strength in some of the tests at the higher rates.

Figure 40 shows the results for 10 mm diameter specimens cut from the nominally 5 mm thick Plate 1912, tested in the small bar system. The hollow squares (X-series) and diamonds (Y-series) were obtained by direct impact of the incident bar against the specimen to produce a longer

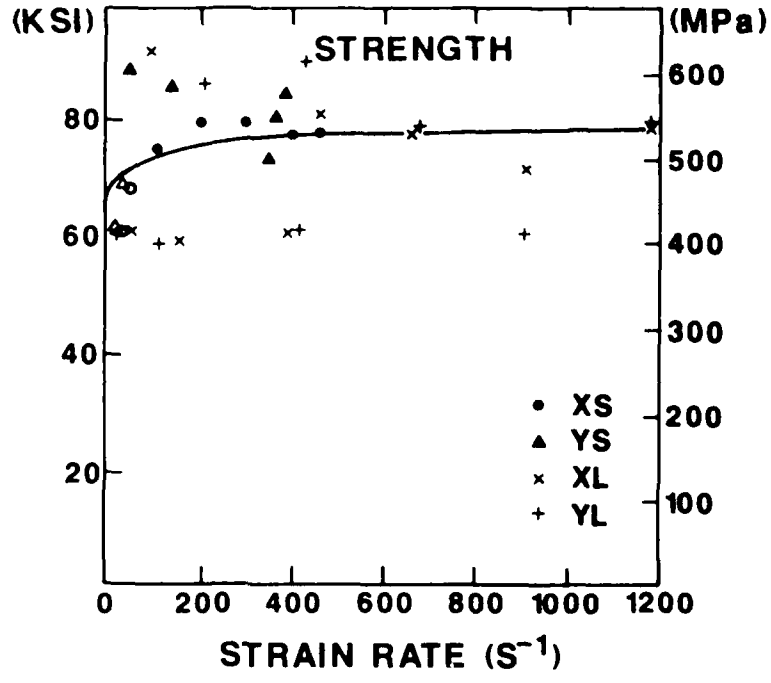

Figure 39. Dynamic Tests of Figure 2 Reproduced Along with Four Tests at Higher Strain Rates. Plate 1850.

loading pulse than the striker bar of the normal Hopkinson's Bar system provides. The solid squares and diamonds represent points obtained by the normal Hopkinson's Bar technique.

Trends in the dynamic testing regime are a little difficult to establish from this data, because of the scatter, but all the dynamic ultimate strengths are around or above 60 ksi, well above the static strengths (average about 50 ksi) shown on the left ordinate scale in Figure 38.

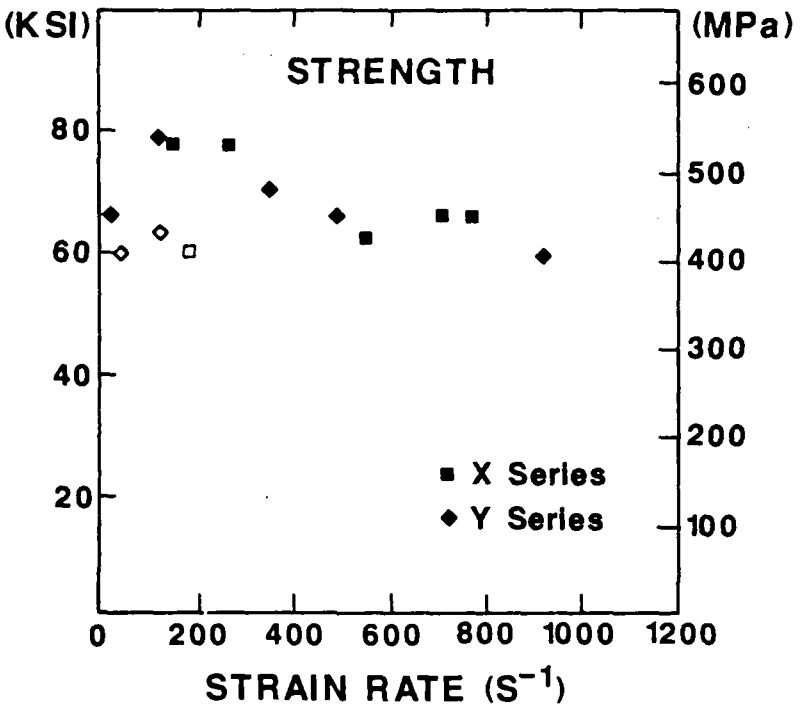

Figure 40. Results for 10 mm Diameter, 5 mm Long Specimens. Hollow Square and Hollow Diamonds are for Direct Impact by the Incident Bar. Plate 1912.

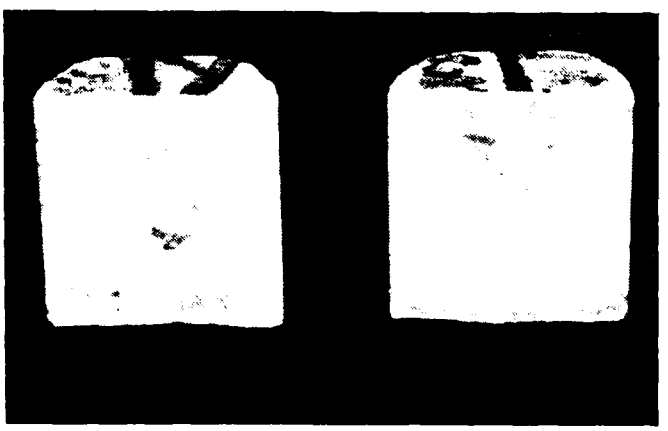

Figure 41. Longitudinally Fractured Specimen. Length = Diameter = 10 mm.

Failure at the lower impact speeds was by a single longitudinal crack as shown in Figure 41. At higher speeds, further fragmentation occurred into a fine angular gravel.

B. DYNAMIC MODULUS AND DAMPING FROM VIBRATION TESTS ON BEAMS

1. Steady Forced Vibrations

The experimental equipment and procedures used for the flexural vibration damping and modulus measurements are quite similar to those described by Gibson et al. in Reference 2, which also gives references to earlier papers dealing with the development of the method. The apparatus was assembled at the University of Florida while Professor Gibson was a visiting professor there.

The specimen, a flat beam, is centrally supported on a shaker as illustrated in Figure 42, forming two symmetrically placed cantilevers. The shaker is driven by an oscillator through a power amplifier with variable frequency and controllable power. The acceleration at the support is monitored by an accelerometer from whose record both the

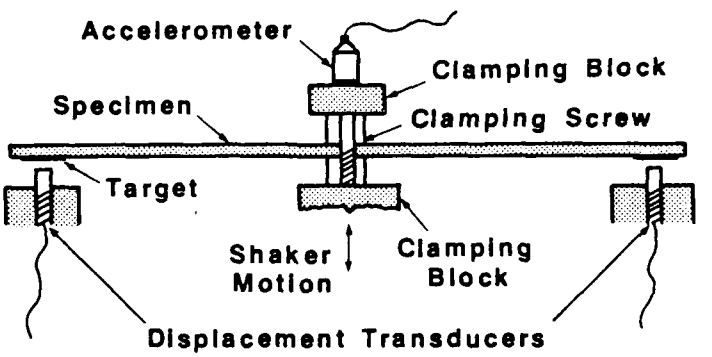

Figure 42. Modified Specimen-Transducer Configuration.

applied force and the support displacement amplitude at resonance are determined. Displacements are also monitored near each tip by a non-contacting eddy-current probe acting on an aluminum-foil target cemented to the specimen. Both tips are monitored to ensure approximately symmetrical motion.

For harmonic motion at a resonant frequency $f_r = \omega_r/2\pi$, a separation of variables solution of the partial differential equation for the deflection of an undamped cantilever of stiffness EI, density ρ and cross-sectional area A is

$$y(x,t) = \mathrm{Re}\{A_1 \sin \lambda_r x + A_2 \cos \lambda_r x + A_3 \sinh \lambda_r x + A_4 \cosh \lambda_r x) \exp(i\omega_r t)\} \quad (15)$$

where $$\lambda_r = (\rho A \omega_r^2/EI)^{1/4} \quad (16)$$

is the eigenvalue and x is the coordinate measured from the support at x = 0. The constants A_1 to A_3 can be determined in terms of A_4 by using the two free-end boundary conditions at x = L and the zero slope condition at x = 0. Then it can be shown that the tip-to-support deflection amplitude ratio is

$$a(L)/a(0) = |(\cos \lambda_r L + \cosh \lambda_r L)/(1 + \cos \lambda_r L \cosh \lambda_r L)| \quad (17)$$

For the undamped beam, this ratio becomes infinite when the denominator vanishes. Thus

$$\cos \lambda_r L \cosh \lambda_r L + 1 = 0 \quad (18)$$

is the eigenvalue equation for the resonant frequencies.

Damping is accounted for in the analysis by replacing the modulus E by the complex modulus E^*

$$E^* = E' + iE'' = E'(1 + i\eta) \quad \text{where } i = \sqrt{-1} \quad (19)$$

E' is the storage modulus,
E" is the loss modulus,
and $\eta = E''/E'$ is the damping ratio.

The complex eigenvalue is

$$\lambda_r^* = [\rho A \omega_r^2/E'I(1 + i\eta)]^{1/4}. \quad (20)$$

For light damping the principal complex root is

$$\lambda_r^* = \lambda_r[1 - i(\eta/4)]. \tag{21}$$

Equation (17) with the eigenvalue replaced by the complex eigenvalue according to Equation (21) then leads to

$$\eta = C_r[a(0)/a(L)] \tag{22}$$

where C_r depends upon $\lambda_r L$. The values of $\lambda_r L$ and C_r have been tabulated in Reference 2 for the first five modes of vibration.

Since the displacement is not measured exactly at the tip, the procedure is further refined by using the mode-shape function $\phi_r(x)$ given in Reference 2. Then in Equation (22)

$$a(L) = [\phi_r(L)/\phi_r(x_0)]\, a(x_0) \tag{23}$$

where x_0 is the position of displacement measurement. Also the displacement amplitude $a(0)$ of the support is obtained from the measured acceleration amplitude there, $\ddot{a}(0)$, at resonance by

$$a(0) = \ddot{a}(0)/\omega_r^2. \tag{24}$$

In the first series of tests, the acceleration amplitude was held constant, while the frequency was varied until the maximum tip displacement amplitude occurred at the lowest resonant frequency f_r. This determined $\omega_r = 2\pi f_r$ for the first mode of vibration. The storage modulus E', which for light damping is approximately equal to the usual elastic modulus E, is then calculated by

$$E' = \rho A \omega_r^2 / \lambda_r^4 I \tag{25}$$

where I is the area moment of inertia of the cross section, and the damping factor η is given by Equations (22) through (24). Results are given in Table 8 for four specimens, two nominally 7 mm thick and two nominally 10 mm thick. The thicker plates had a higher resonant frequency and also about 4.5 per cent higher storage modulus, which may be a difference in specimens rather than a frequency dependence of the modulus.

TABLE 8. FLEXURAL VIBRATION DAMPING AND MODULUS RESULTS (FIRST SERIES)

Spec. No.	Thickness (mm)	Length L (mm)	Width (mm)	Density (g/cm^3)	f_r (Hz)	E' (GPa)	η
1	7.94	152.2	25.2	2.43	245	47.5	0.031
2	7.98	152.2	25.83	2.41	250	48.7	0.030
3	10.91	152.0	25.26	2.46	347	50.8	0.032
4	10.88	152.2	24.79	2.48	344	51.0	0.037

Averages: 7 mm, E' = 48.1 GPa (6.98×10^6 psi), η = 0.0305 Plate No. 2080
10 mm, E' = 50.9 GPa (7.39×10^6 psi), η = 0.0345 Plate No. 1957
All 4, E' = 49.5 GPa (7.18×10^6 psi), η = 0.0325

Two variations of the test were carried out. The lowest-mode resonant frequency of the 7 mm thick specimens from Plate 2080 was varied from about 250 Hz to 483 Hz by shortening the cantilever length from 150 mm to 110 mm to determine whether a frequency dependence could be noted, and these tests were repeated in a vacuum bell jar to verify that air damping was not significant. As the results summarized in Table 9 show, there was no noticeable frequency dependence over this limited range of frequencies for either the 7 mm specimens or the 10 mm specimens from Plate 1957 for which the resonant frequency was varied from about 348 Hz to about 667 Hz.

The small difference noted between the storage moduli of the two sizes of specimens tested in the first test series is therefore attributed to differences in the specimens rather than to any frequency dependence. For the tests reported in Table 9, three lengths for a given thickness were obtained by cutting off the ends of the longer specimen after testing, so that the central part of the beam consisted of the same material in all three lengths. Two beams were prepared for each thickness, giving four tests in air for each length.

The same specimens were also tested in vacuum to verify that the air damping was negligible for these small amplitudes of vibration. As may be seen in Table 9, there was no significant difference between the measurements in air and those at a gage pressure of -53.34 cm (-21 inches) of mercury, obtained by placing the whole apparatus in a bell jar. In fact, for this whole series of tests there was little variation from the average values of the Modulus of Elasticity and Damping Factors as shown below.

$$\text{Modulus } E = 51.8 \text{ GPa } (7.51 \times 10^6 \text{ psi}) \qquad (26)$$

$$\text{Damping Factor } \eta = 0.032.$$

TABLE 9. RESULTS OF VIBRATION MODULUS AND DAMPING TESTS

Length (mm)	Pressure	Thickness (mm)	f_r (Hz)	E (GPa)	η
150	atm	7	257	52.0	0.0331
150	atm	7	242	52.1	0.0305
150	atm	10	347	50.9	0.0336
150	atm	10	349	52.3	0.0302
150	-21 in	7	257	52.2	0.0304
150	-21 in	7	243	52.5	0.0285
150	-21 in	10	347	50.8	0.0322
150	-21 in	10	349	52.5	0.0276
122	atm	7	401	52.7	0.0309
122	atm	7	374	50.6	0.0322
122	atm	10	544	51.9	0.0342
122	atm	10	538	51.4	0.0339
122	-21 in	7	402	52.7	0.0309
122	-21 in	7	374	50.6	0.0302
122	-21 in	10	545	52.5	0.0319
122	-21 in	10	539	51.5	0.0327
110	atm	7	500	52.5	0.0304
110	atm	7	464	51.0	0.0315
110	atm	10	657	50.5	0.0367
110	atm	10	677	52.8	0.0343
110	-21 in	7	501	52.6	0.0292
110	-21 in	7	464	51.1	0.0306
110	-21 in	10	657	50.5	0.0361
110	-21 in	10	677	52.9	0.0333

2. Damping Factors from Free Vibration Decay

The free-vibration tests were undertaken because some preliminary free vibration tests had apparently shown a much greater damping based on the logarithmic decrement in free vibration than was found in the forced-vibration tests. The relationship between the various measures of damping can be seen from the following simple argument.

If a cantilever beam is regarded simply as a linear spring of stiffness k resisting the vertical motion of a mass m, then the deflection y as a function of time is given by the following equations.

$$\text{Without damping } y = y_0 \exp(i\omega_0 t), \text{ where } \omega_0 = (k/m)^{1/2} \qquad (27)$$

and y_0 is the amplitude of the undamped motion. With damping, k is replaced by the complex stiffness k^*.

$$k^* = k(1 + i\eta), \text{ where } \eta \text{ is the damping factor,} \tag{28}$$

the measure of damping reported in the forced vibration measurements. With damping the solution is

$$y = y_0 \exp\{it[\frac{k}{m}(1 + i\eta)]^{1/2}. \tag{29}$$

For $\eta << 1$, $[\frac{k}{m}(1 + i\eta)]^{1/2}$ may be replaced by $(k/m)^{1/2}(1 + \frac{1}{2} i\eta)$ (30)

and the solution becomes

$$y = y_0 \exp(-\frac{1}{2}\omega_0 \eta t) \exp(i\omega_0 t) \tag{31}$$

where now y_0 is the initial displacement.

The ratio of the displacements y(t) and y(t + τ) at times separated by one period $\tau = 2\pi/\omega_0$ of the oscillatory motion represented by the last factor in Equation (31) is

$$y(t)/y(t + \tau) = \exp(\frac{1}{2}\omega_0 \eta\tau) \tag{32}$$

since $y_0 \exp(i\omega_0 t) = y_0 \exp[i\omega_0(t + \tau)]$.

The logarithmic decrement δ is given by

$$\delta = \ln[y(t)/y(t + \tau)] = \pi\eta \tag{33}$$

Thus, according to this simple analysis, the logarithmic decrement in free vibration should be Pi times the damping factor. The analysis is approximate in that the mass in the real system is distributed rather than lumped, but experience with vibrating systems suggests that this simple model works reasonably well for lightly damped systems when comparing a damped free vibration with a lowest-mode forced vibration. Some of the

approximation gets cancelled out by taking the ratio of successive maximum displacements. The fraction of critical damping, ζ, is given by

$$\zeta = c/c_{cr} = \delta/(4\pi^2 + \delta^2)^{1/2} \tag{34}$$

$$\text{or} \quad \zeta = \delta/2\pi \quad \text{when} \quad \delta \ll 2\pi. \quad \text{Thus} \quad \zeta = \eta/2 \quad \text{since} \quad \eta = \delta/\pi. \tag{35}$$

Table 10 lists the values of η calculated in this way for seven free-vibration specimens tested at the University of Florida. Several of them show higher damping factors than the values around 0.03 in Tables 8 and 9, based on forced vibration tests, but they are of the same order of magnitude.

TABLE 10. DAMPING FACTORS FROM FREE VIBRATION TESTS

SPECIMEN NO.	LENGTH (mm)	THICKNESS (mm)	DAMPING FACTOR η
M-1	159	8	0.060
M-2	220	11	0.046
M-3	220	8	0.041
M-4	304	8	0.036
M-5	220	11	0.065
M-6	220	11	0.071
M-7	317	11	0.034

C. DYNAMIC MODULUS FROM WAVE PROPAGATION TESTS

The wave propagation studies were performed before the vibration tests reported in the previous section. As will be seen, the dynamic modulus determinations by several different methods gave a considerable variation in results.

The first wave propagation tests undertaken were performed on some of the same specimens that were later used for dynamic compression SHPB tests. These were ultrasonic wave speed measurements (propagation through the thickness direction of the plates) to determine dynamic moduli. Since the results gave unexpectedly high values for the elastic modulus E, another method was used to determine E from bar-wave velocities measured on a bar cut from one of the plates. This gave a lower value.

It was suspected that the discrepancy between the bar-wave in-plane measurement of E and the determination based on through-the-thickness longitudinal and shear wave velocities might be caused by anisotropy which made the thickness stiffness greater than the in-plane stiffness. If this were the case, it would invalidate the method by which E was calculated from the ultrasonic data. Some additional tests were made to resolve the discrepancy. Some specimens were cut from a 10 mm thick plate with which the ultrasonic measurements could be made both in the thickness direction and in an in-plane direction. These tests showed that the material is macroscopically very nearly isotropic, so that the suspicion of anisotropy was unfounded. There was considerable variation from point to point in the plate, however, indicating some nonuniformity, but all of the measurements gave significantly higher modulus E (of the order of 55 GPa) than previously reported static data or the preliminary bar-wave test result.

Suspicion then shifted to the bar-wave test. An accelerometer mounted on one end of the bar could have loaded the end sufficiently to give longer times between reflections and therefore apparently lower bar-wave speeds. Another method was then used with a shorter bar 93.7 mm (3.69 inches) long, mounted in the split Hopkinson's bar. This gave a somewhat higher bar-wave speed closer to the ultrasonic data. Several additional bar-wave and ultrasonic tests were then made with results as summarized in Tables 11 and 12.

The in-plane bar-wave speed measurements were made on four bars of nominally square cross section cut from the four edges of one of the 10-mm thick panels. Bars B and D are in the rolling direction, while A and C are in the transverse direction, cut from Plate 1957.

Bar-wave measurements in the thickness direction were made as follows. A bar was formed by stacking together 16 of the 10 mm thick, 19 mm diameter, Hopkinson Bar specimens that had been fabricated from Plate 1850. A light film of grease between the specimens caused them to adhere when pressed together. It had been thought that these oil-film interfaces might introduce enough delay into the transmission that a lower speed and consequently lower apparent modulus E would be found in the thickness direction. This was not the case, however, since the modulus determined for the thickness direction of Bar 1850 is slightly higher than

any of the in-plane moduli determined on Plate 1957.

Table 11 summarizes the dynamic modulus results from the different bars as obtained by different measurement methods. The results obtained on any one bar by a given method were highly reproducible with a variation between readings of less than one per cent, mainly occasioned by the resolution of the digital oscilloscope used to record, which resolves to 0.5 microsecond.

TABLE 11. DYNAMIC MODULUS AS DETERMINED FROM BAR-WAVE SPEEDS BY DIFFERENT METHODS

METHOD	ACCELEROMETER		SHPB		STRAIN GAGE	
	c_o (m/s)	E (GPa)	c_o (m/s)	E (GPa)	c_o (m/s)	E (GPa)
BAR						
B	4090	40.8	4220	43.5	4240	43.8
D	4320	45.5	4340	46.0		
A	4240	43.9	4290	44.9	Plate 1957	
C	4220	43.5	4320	45.7	Density 2440 kg/m^3	
Thickness Direction, Plate 1850			4230	46.9	Density 2620 kg/m^3	

The accelerometer method tests were made with a small accelerometer mounted on one end of the bar. The other end was tapped with a light hammer to induce longitudinal vibrations. Except for the initial transient, the period of the longitudinal vibration is equal to the round-trip transit time of the bar-wave. Several successive oscillations were displayed on the oscilloscope and the total time divided by the number of oscillations to get the transit time. In the SHPB method, the bar was mounted between the two pressure bars of the Split Hopkinson Pressure Bar system and the transit time recorded by subtracting known transit time from the pressure bar/specimen interfaces to the gages mounted on the pressure bars. Only one bar was tested with a strain gage mounted directly on the specimen (Bar B). Again, except for the initial transient, the period of the oscillation observed was equal to the round-trip transit time along the bar. The strain-gage method gave almost exactly the same result as the SHPB method for Bar B, while the accelerometer

method gave an apparent slightly slower wave speed and lower modulus. This may be caused by the small added mass of the accelerometer and added length of the attachment through a small plastic nut that was cemented to the end of the bar with the accelerometer screwed into it, although it is not clear why the discrepancy between the two methods is greater for Bars B and C than for Bars D and A. In any case the SHPB method is judged to be the most reliable, and the indicated differences among the four bars are believed to be real material differences. The modulus was determined by the formula

$$E = \rho c_0^2. \tag{36}$$

The density ρ was determined by weighing and measuring each plate.

From the bar-wave tests, it is concluded that the dynamic elastic modulus E for this material varies within the following range

$$E = 44 \text{ to } 47 \text{ GPa} \quad (6.4 \times 10^6 \text{ to } 6.8 \times 10^6 \text{ psi}), \tag{37}$$

which falls within the range of static tensile moduli reported in Section II.A. The longitudinal vibrations in these measurements were at a frequency of the order of 6 kHz. Since the variation between directions in Table 11 is of the same order as the variation between two specimens in the same direction, the material is approximately isotropic in its elastic response. Therefore, the analysis used to deduce the modulus from ultrasonic wave speeds, which assumes isotropic response, is a reasonable approach.

The ultrasonic wave speeds were measured with a Panametrics Time Intervalometer System 5054, which applies a short broadband pulse repetitively to a quartz transducer on one face of the specimen, which can be used both for sending the ultrasonic pulse and receiving reflections from the opposite face. A second receiving transducer was mounted on the opposite face, which records the arrival of the first pulse and of successive reflections back from the first face. Both the longitudinal wave speed c_1 and the shear wave speed c_2 were determined. For c_1 two Panametrics V-106 transducers with half-power bandwidth 2.25/0.5 MHz were used. For c_2 two Panametrics V-153 shear transducers with bandwidth 1.0/0.5 MHz were used.

A precisely controlled variable oscilloscope sweep speed was used to display and overlap two successive signals on two successive sweeps. The sweep repetition period required to overlap the signals is the time between the two signals. The two signals used were the first arrival at the receiving end and the first reflection back to the sending end. The moduli are then calculated by Equations (38) and (39), well-known equations of the theory of elasticity, where λ is the Lamé constant and ρ is the density. Results are given in Table 12.

TABLE 12. RESULTS OF ULTRASONIC TESTS

DIRECTION	c_1 (m/s)	c_2 (m/s)	G (GPa)	λ (GPa)	E (GPa)	Density (kg/m^3)
ROLLING	5330	3000	22.0	25.3	55.8	
TRANSVERSE	5030	2920	20.8	19.7	51.7	
THICKNESS	5230	2970	21.5	23.7	54.6	
Plate 1957						2440
Plate 1850	5380 (Thickness direction only)	3100	25.2	25.4	63.0	2620

$$\lambda + 2G = \rho c_1^2 \qquad \text{Shear Modulus} \quad G = \rho c_2^2 \tag{38}$$

$$\text{Young's Modulus} \quad E = \frac{G(3\lambda + 2G)}{\lambda + G} \qquad \text{Poisson's Ratio} \quad \upsilon = \frac{\lambda}{2(\lambda + G)} \tag{39}$$

Table 13 summarizes the modulus ranges as determined by various methods.

TABLE 13. ELASTIC MODULUS RESULTS

Static Tensile [Section II.A]
E = 38 to 47 GPa (5.5×10^6 to 6.8×10^6 psi)

Bar Wave Tests [Eq. (37)]
E = 44 to 47 GPa (6.4×10^6 to 6.8×10^6 psi)

Vibration Tests [Eq. (36)]
E = 52 GPa (7.5×10^6 psi)

Ultrasonic Waves [Table 12]
E = 52 to 63 GPa (7.5×10^6 to 9.1×10^6 psi)

The flexural vibration tests (at from 242 to 677 Hz) and the ultrasonic wave tests in the MHz range seem to suggest a frequency dependence of the modulus, but the bar wave tests at a longitudinal vibration frequency of around 6 kHz do not fit the pattern, since they fall within the range of static tensile moduli.

D. BALLISTIC IMPACT TESTS ON PLATES

1. Unreinforced Single Panels

The first ballistic tests were made on 7 mm thick plates. Two 7 mm panels were cut into 152 mm (6 inch) square plates. The eight plates were subjected to ballistic impacts by a flat-ended steel cylinder fired from a gas gun. The impactor dimensions were diameter 9.52 mm (3/8 inch) and length 25.4 mm (1 inch). The mass of the impactor was 14.8 grams. The two panels tested were given the numbers 2096 and 2102, and the four plates from each panel labeled A, B, C, and D. Two plates from each panel were impacted at approximately 30 m/s and two from each panel at approximately 25 m/s in a preliminary test series to check on reproducibility and estimate the impact speed needed for perforation. The plates were clamped on four sides.

No perforations occurred, but in all the plates of the higher-speed group a roughly conical spall occurred on the back side, which reached almost through the thickness, leaving less than one millimeter in one case. Cracks were also formed from the impact point to the boundary in all impacts at both speeds, and two of the plates then came apart with very little force required when they were handled, including one of the lower-speed group. It thus, appears that the plates had been severely damaged and had essentially no residual strength after impact. The nature of the brittle failures was made clear by enhancing the crack patterns with flaw detectors (Figures 43 to 58).

Figures 43 and 44 show typical crack patterns on the back face after impact at the two speeds. In the low-speed impact of Figure 43, there was no spall visible without the enhancement, but the enhancement showed that several cracks ran all the way to the boundary. In Figure 44, at the higher speed, the heavier cracks visible had actually separated, and the

pieces have been put back together for the photography. The lighter cracks became visible after enhancement.

Because the cracks extended all the way to the boundary, it was decided to test larger specimens. A new specimen holder was fabricated and three 23.5 cm x 23.5 cm (9.25 in x 9.25 in) of the same thickness (7 mm) were impacted at speeds of 25.1, 28.3, and 32.1 m/s. The lowest and highest speeds in this series were almost the same as in Figures 43 and 44, and the damage patterns were similiar, as may be seen in the back face photographs of Figures 45 and 46.

At the lowest speed none of the cracks in the larger plate extend all the way to the boundary, as may be seen in Figure 45. At approximately the same speed, cracks extended all the way to the boundary of the smaller plate in Figure 43. At the higher speed of Figure 46 the spall region is similar to that of Figure 44 and cracks extend all the way to the boundary. Some improvement in impact resistance was found with laminated plates.

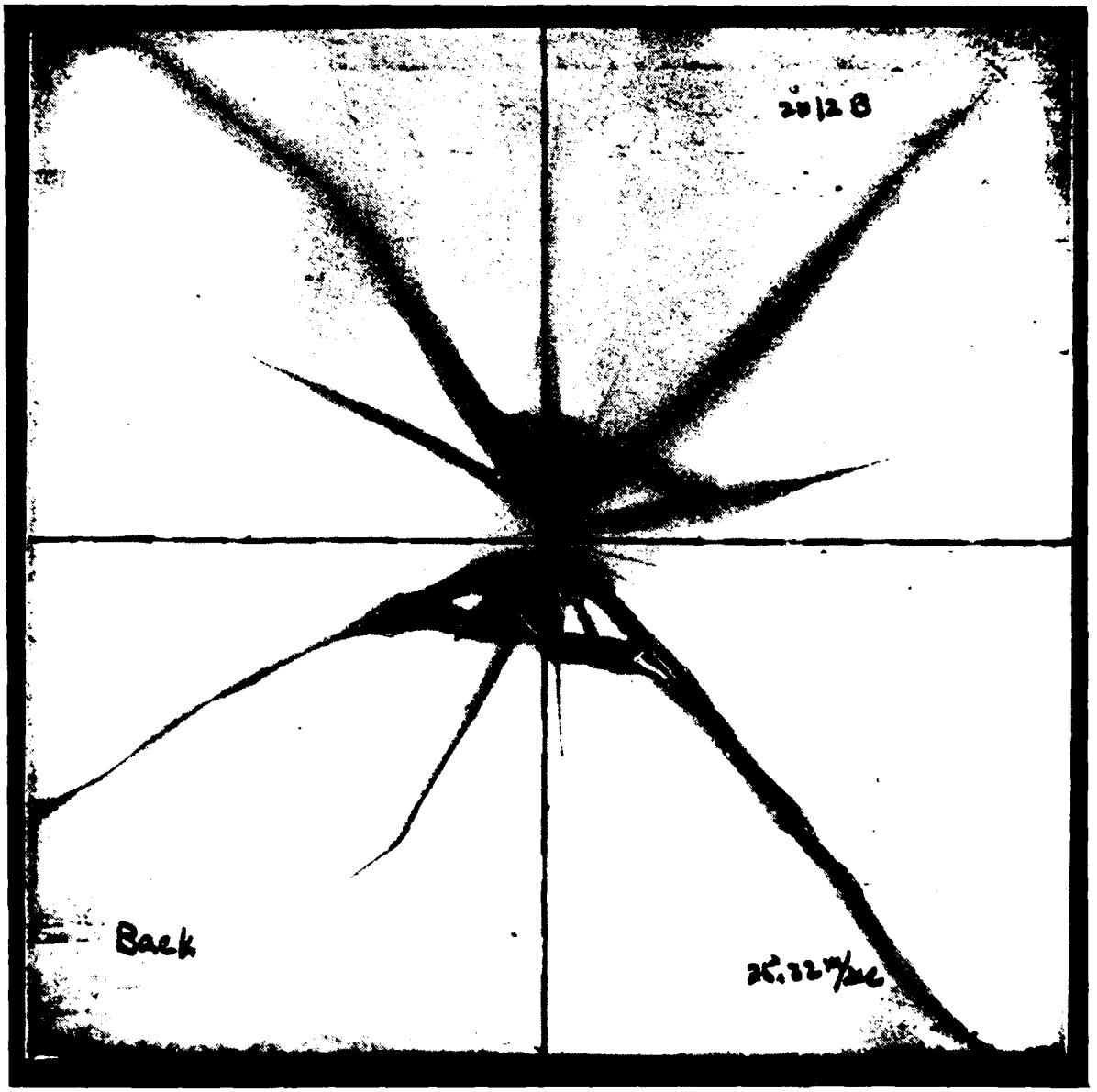

Figure 43. Back Face of 152 mm Square, 7 mm Thick Plate After Impact at 25.32 m/s.

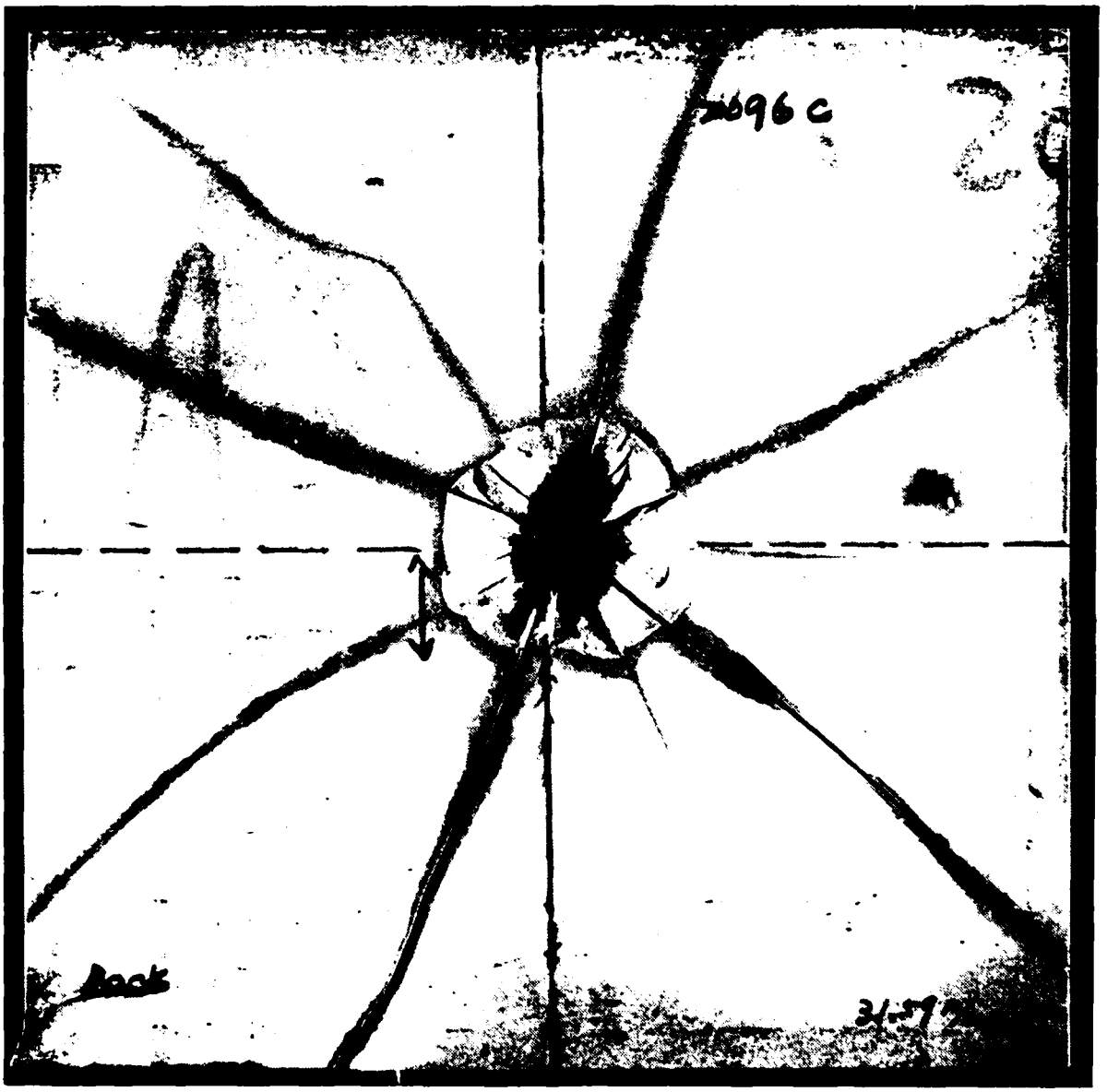

Figure 44. Back Face of 152 mm Square, 7 mm Thick Plate After Impact at 31.59 m/s

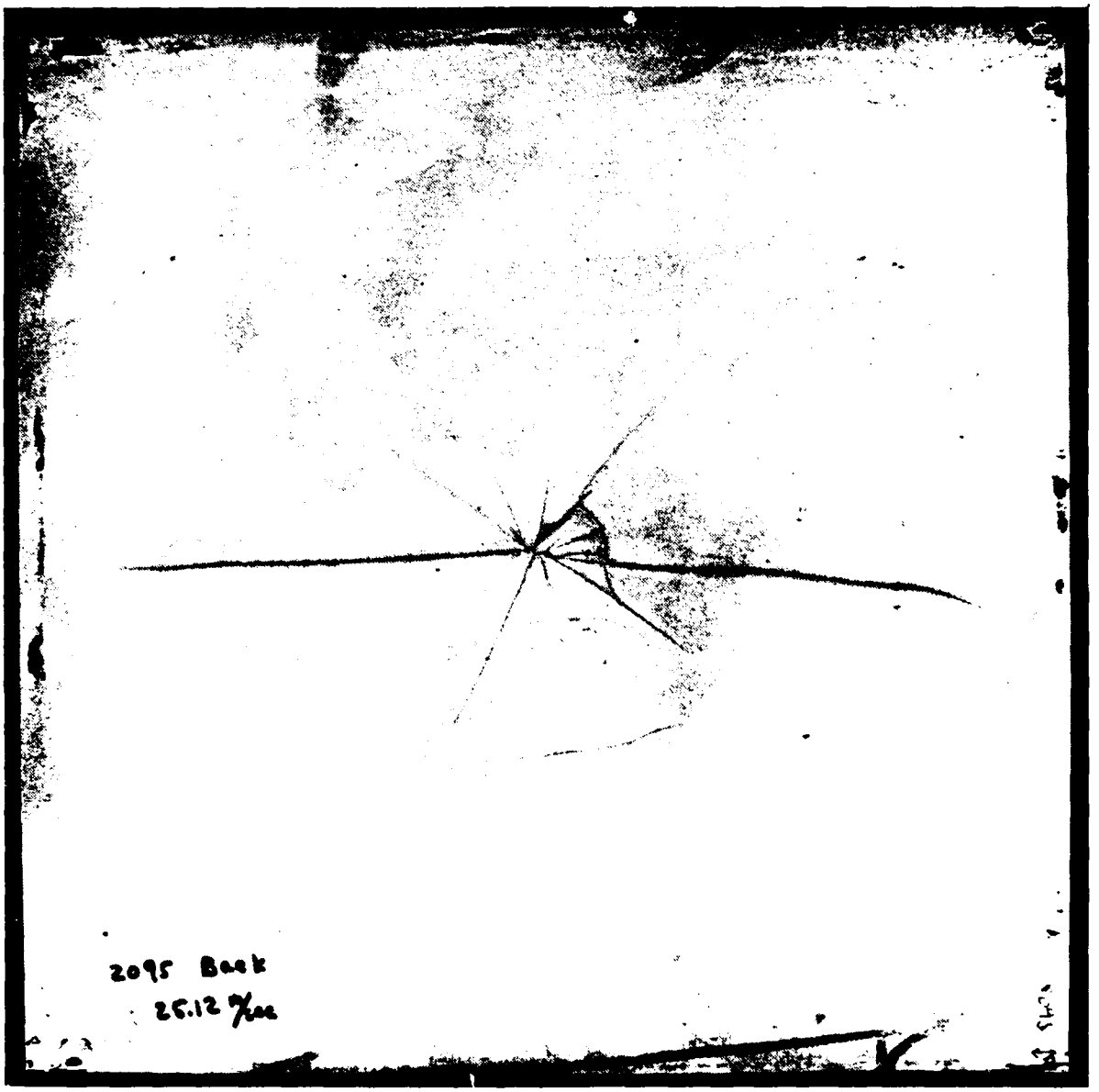

Figure 45. Back Face of 235 mm Square, 7 mm Thick Plate 2095 After Impact at 25.3 m/s.

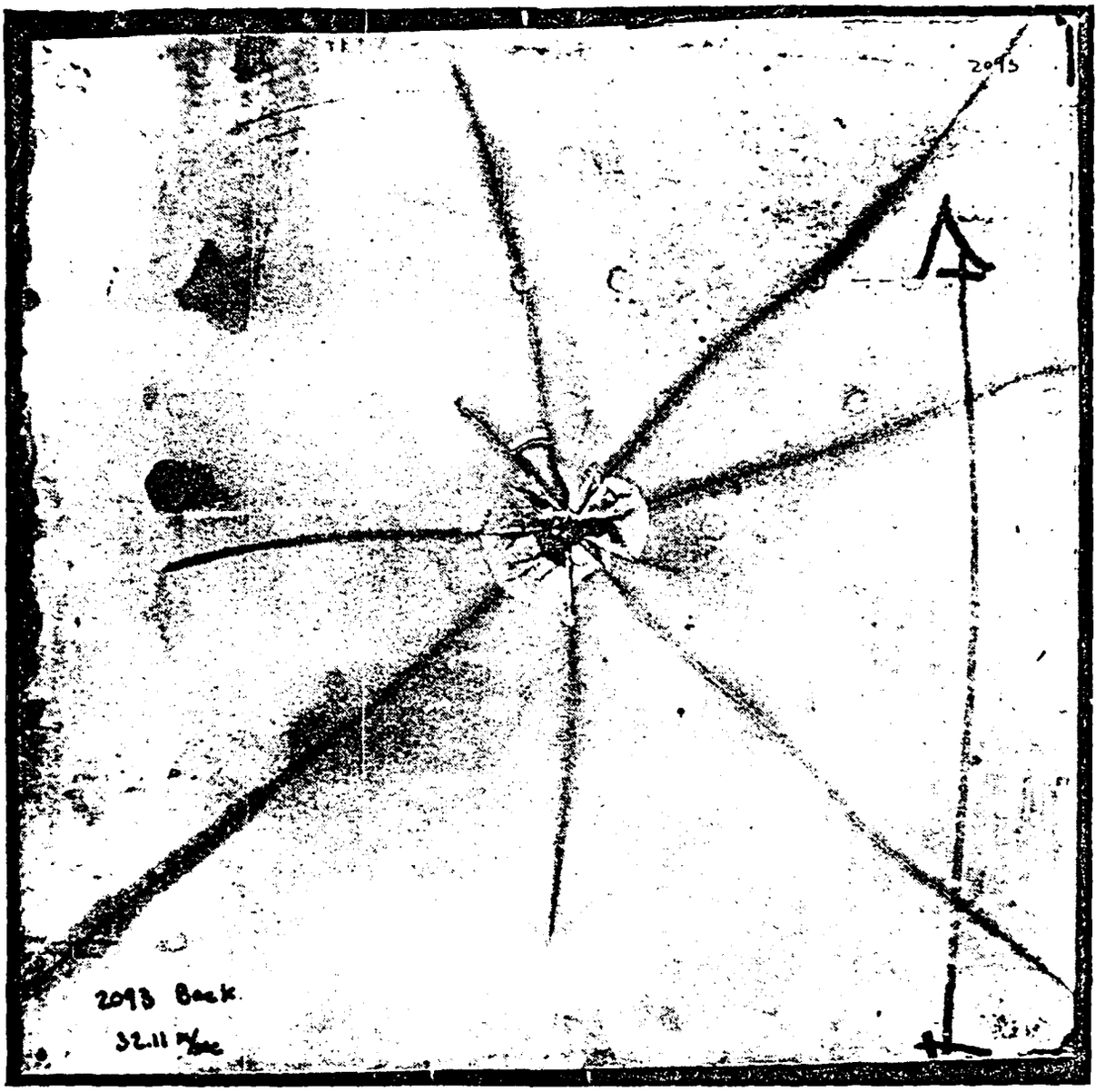

Figure 46. Back Face of 235 mm Square, 7 mm Thick Plate 2093 After Impact at 32.1 m/s.

2. Laminated Plates

Two NIM 127® panels (Nos. 2080 and 2081) of size 350 mm x 350 mm x 7 mm (13.8 inches x 13.8 inches x 0.28 inch) were cut into eight 152 mm (6-inch) square plates. Four two-plate sets:

2080A/2081A, 2080C/2081D, 2080D/2081C, 2080B/2081B

were chosen, matched to minimize the voids between the two plates in a set and placed so that the rolling directions of the two plates in a set were orthogonal. The contiguous faces were painted evenly with epoxy resin (Measurements Group, Inc., M-bond adhesive resin Type AE with curing agent Type 15). Then they were placed between two aluminum plates and clamped by four C-clamps at room temperature for 15 hours. To avoid hard contact, several layers of tissue paper were placed between the aluminum plates and the specimens before clamping. After the clamps were removed, the bonded specimens were left intact at room temperature for 1 week before the impact tests. The thickness of each two-plate set was measured with a micrometer before and after bonding. The average thickness increase from the adhesive resin layer was found to be less than 0.25 mm (0.01 inch). Before impact testing, three of the specimens were examined with the ultrasonic C-scan system. Some small regions indicated imperfect bonding.

The impactor was a blunt-ended steel cylinder of diameter 9.52 mm (3/8 inch), length 25.4 mm (1 inch) and mass 14.6 grams (0.515 ounce). Results of four impact tests are summarized in Table 14 and discussed below.

TABLE 14. RESULTS OF BALLISTIC IMPACTS ON LAMINATED SPECIMENS

No.	SPECIMEN plate pair	IMPACT SPEED	REBOUND SPEED	DAMAGE
1	2080A/2081A	28.44 m/s	6.35 m/s	None apparent
2	2080C/2081D	38.86 m/s	9.84 m/s	None apparent
3	2080D/2081C	53.14 m/s	no rebound	Extensive cracking, no spall
4	2080B/2081B	54.39 m/s	no rebound	Delamination, cracking, and spall from inside face of front plate.

Number 1 was run first at the average of the two impact speeds that caused extensive damage in single panels, as illustrated in Figures 43 and 44. Number 4 was run next at about double this speed; then Number 2 was run at an intermediate speed and finally Number 3 was a replication of the test of Number 4. Ultrasonic inspection showed no apparent debonding in Numbers 1 and 2. No cracks were visible even with flaw-enhancement fluid. Figures 47 to 54 illustrate some of the damage on Numbers 3 and 4. Figures 47 and 48 show photographs of the front and back surfaces of Number 3. Figures 49 and 50 show the outside and inside faces of the front plate of the delaminated specimen, Number 4. A small conical fragment that was spalled from the inside face of the front plate has been replaced in Figure 49. Figure 51 shows the inside face again with the conical fragment removed and Figure 52 shows an enlargement of the conical hole with the conical fragment placed upside down near the hole. Figures 53 and 54 show the outside and inside faces of the back plate of the delaminated Specimen 4 with extensive cracking but no spall from back plate.

As compared with the single panels of Figures 43 and 44, the laminated panels had better impact resistance -- no apparent damage at 38.86 m/s, but extensive damage at 53 and 54 m/s. This is still not a severe impact.

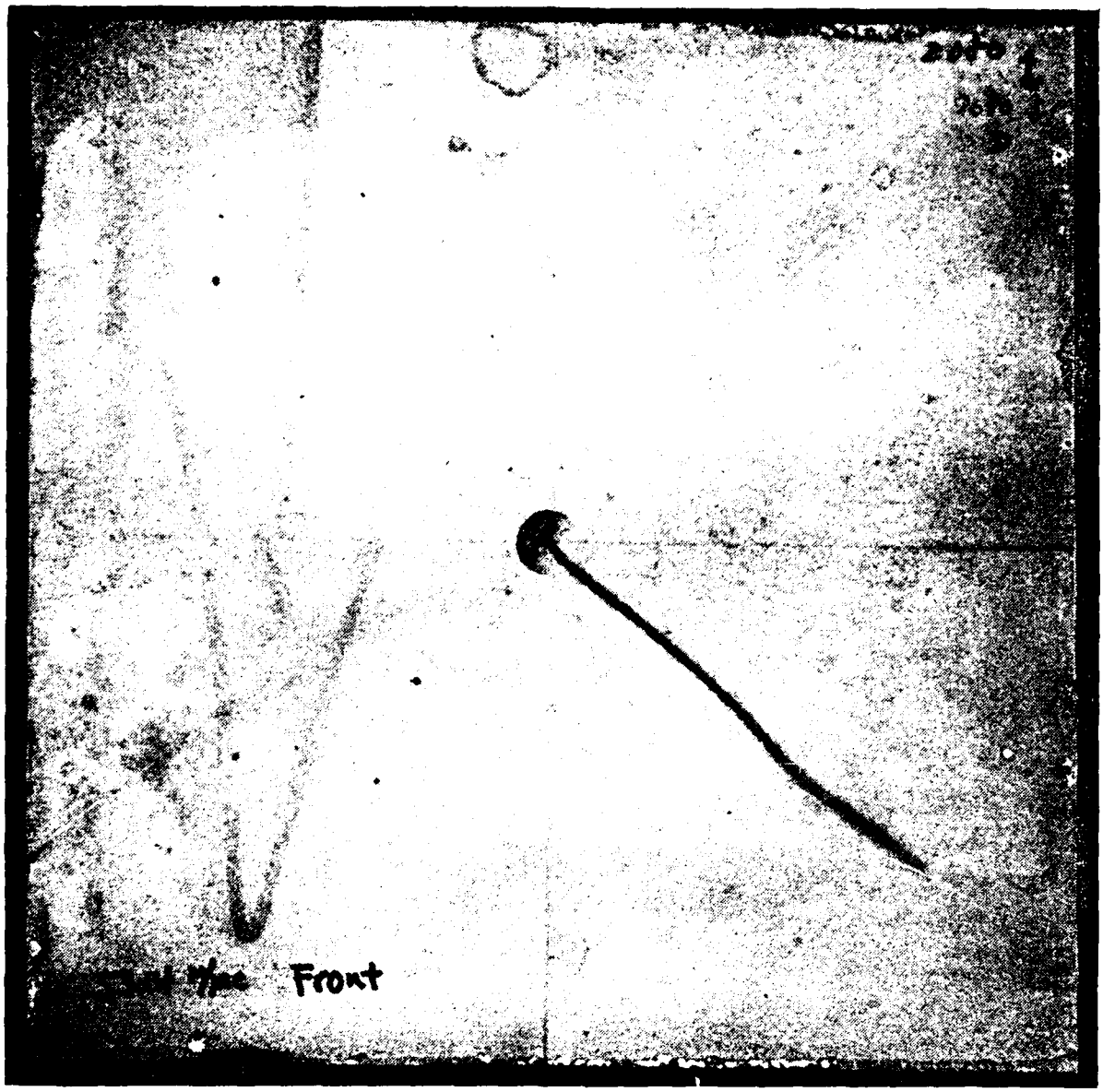

Figure 47. Front Face of Laminated Specimen Number 3 After Impact at 53.14 m/s.

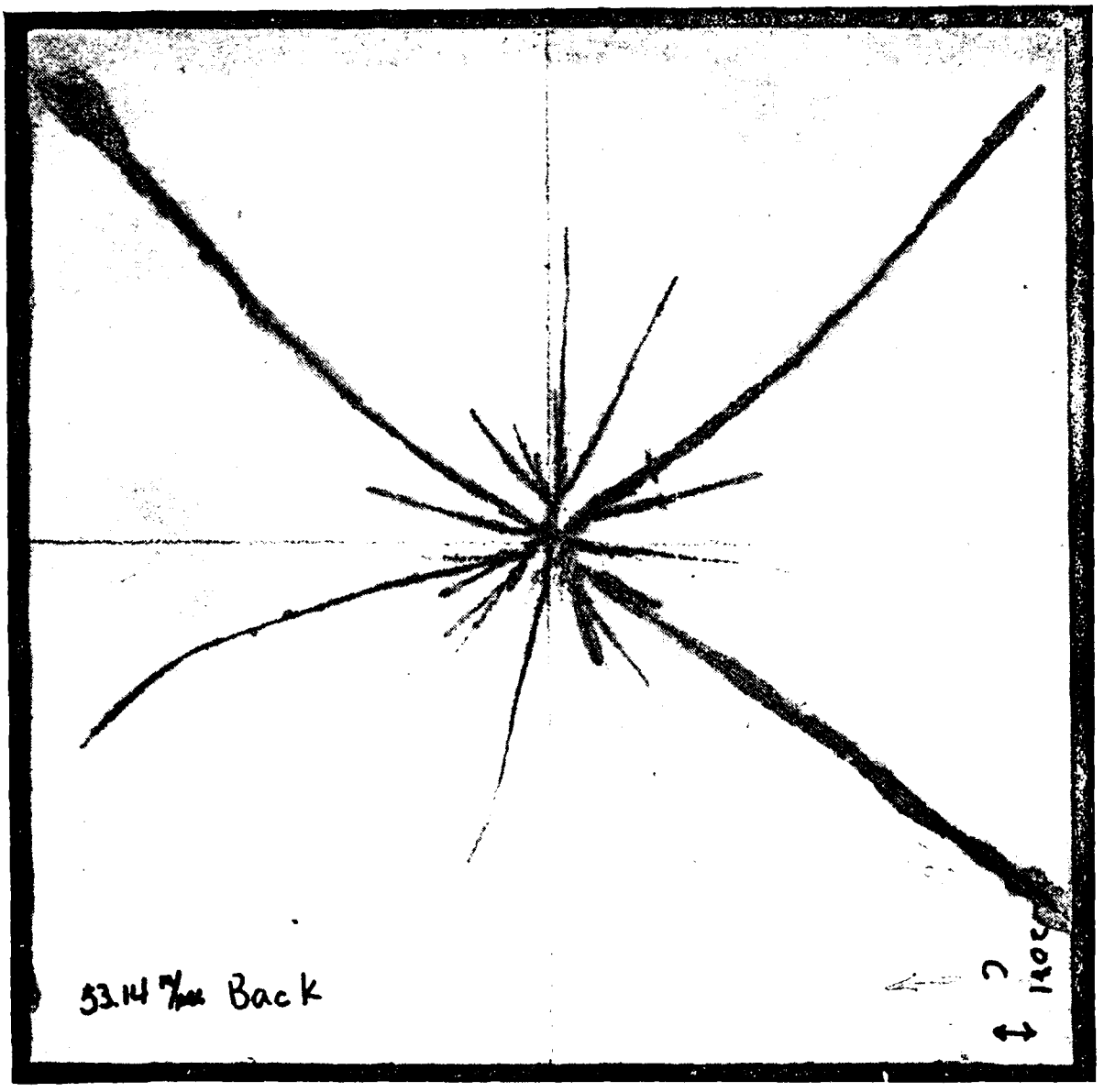

Figure 48. Back face of Specimen Number 3 with Extensive Cracking but No Spall.

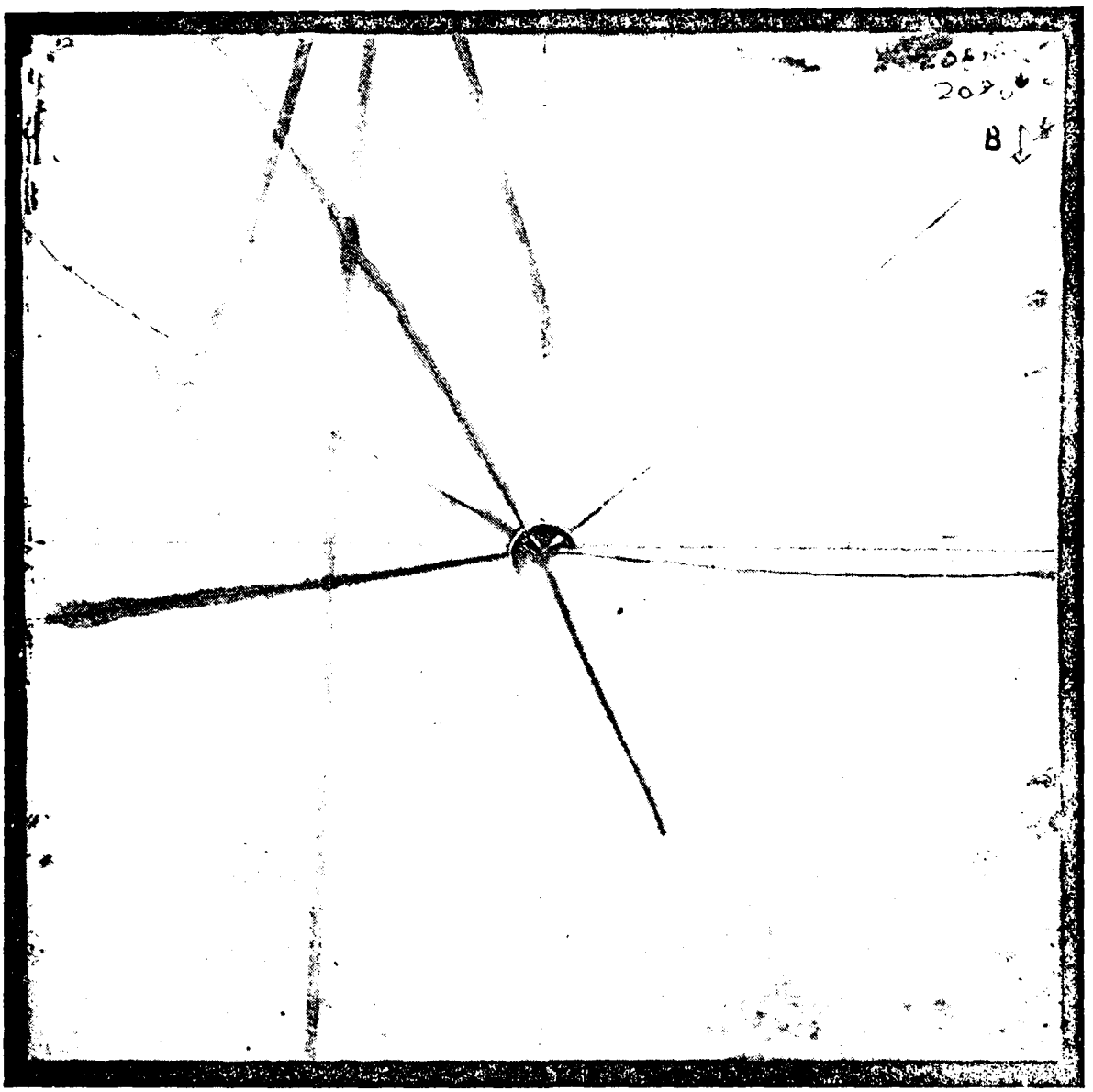

Figure 49. Outside Face of Delaminated Front Plate 2030B of Specimen Number 4 after Impact at 54.39 m/s.

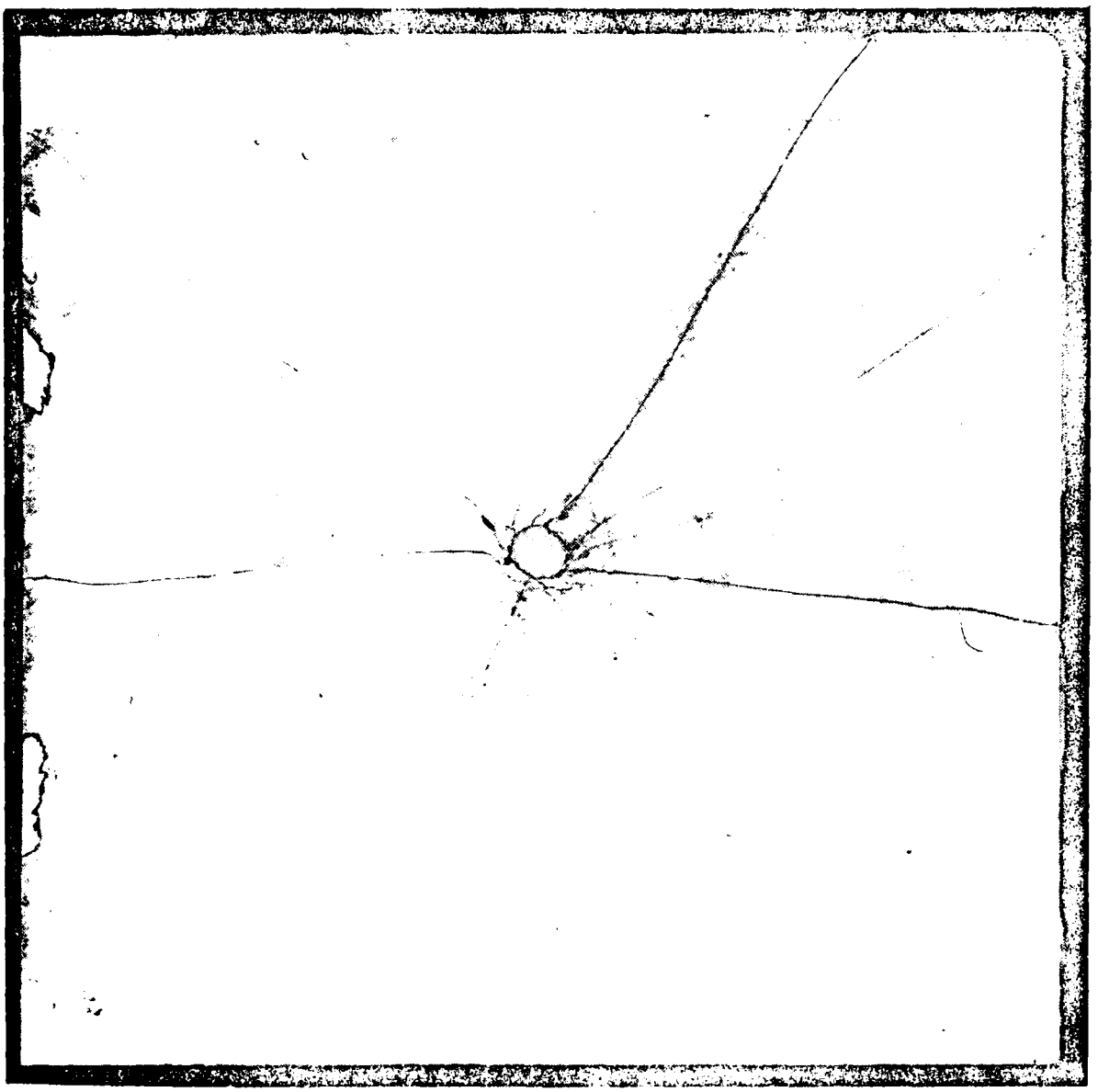

Figure 50. Inside Face of Delaminated Front Plate of Specimen Number 3 With Conical Spall Fragment Replaced at Center.

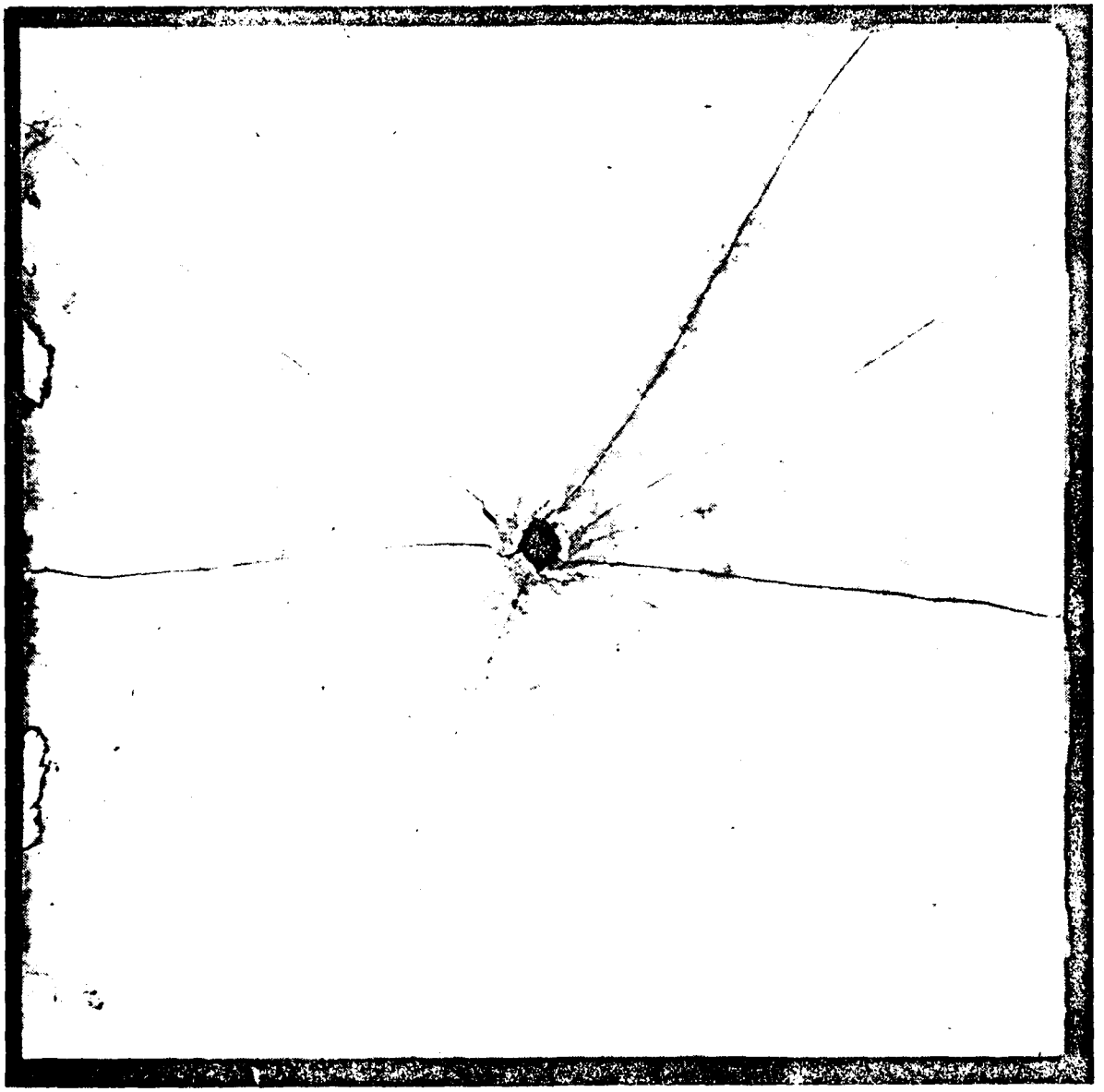

Figure 51. Inside Face of Delaminated Front Plate of Specimen Number 4 With Conical Spall Fragment Removed.

Figure 52. Enlarged View of Conical Spall Hole of Figure 44 and Conical Fragment Placed Upside Down Above the Hole.

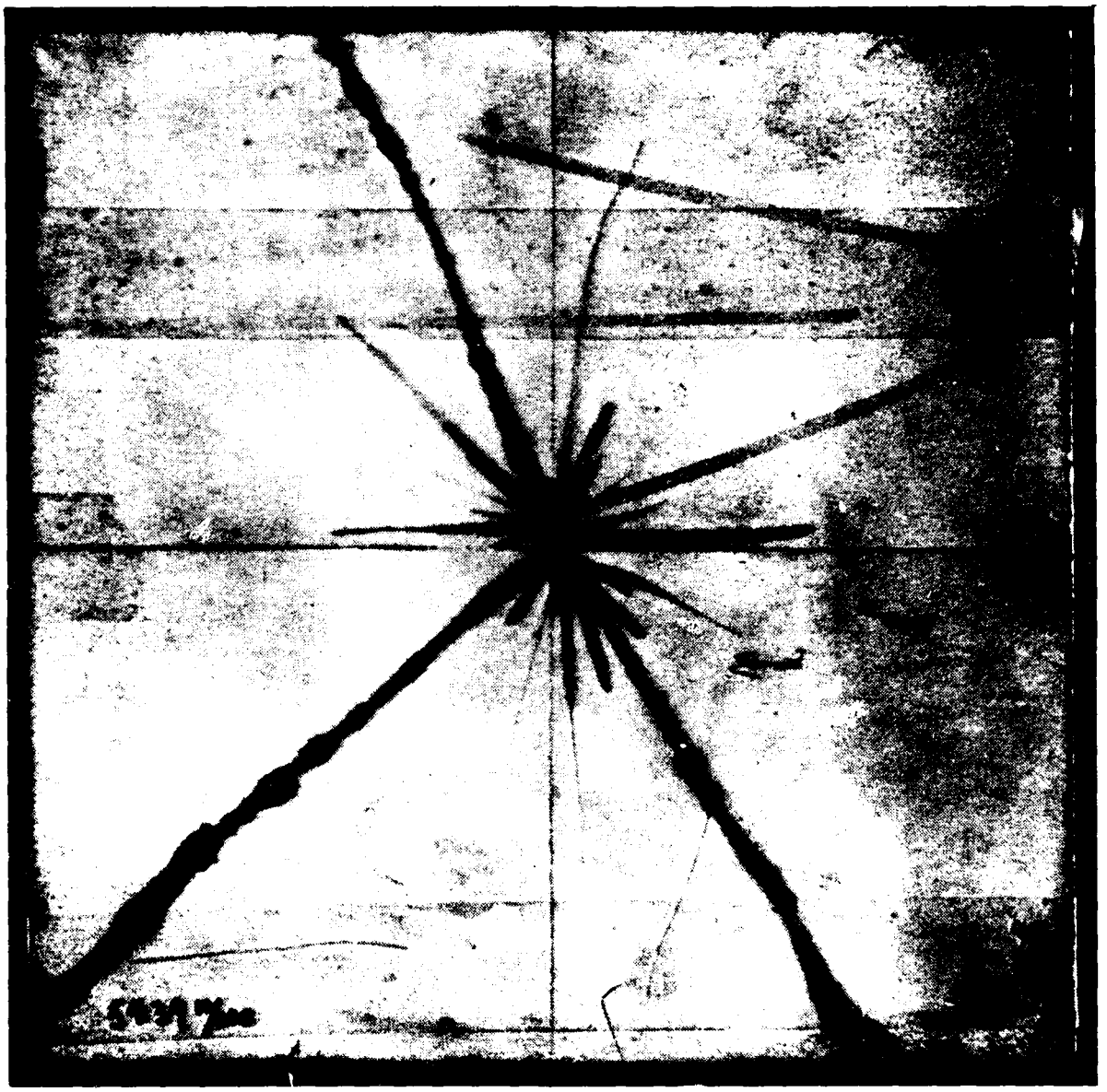

Figure 53. Outside Face of Delaminated Back Plate 20818 with Extensive Cracking But No Spall.

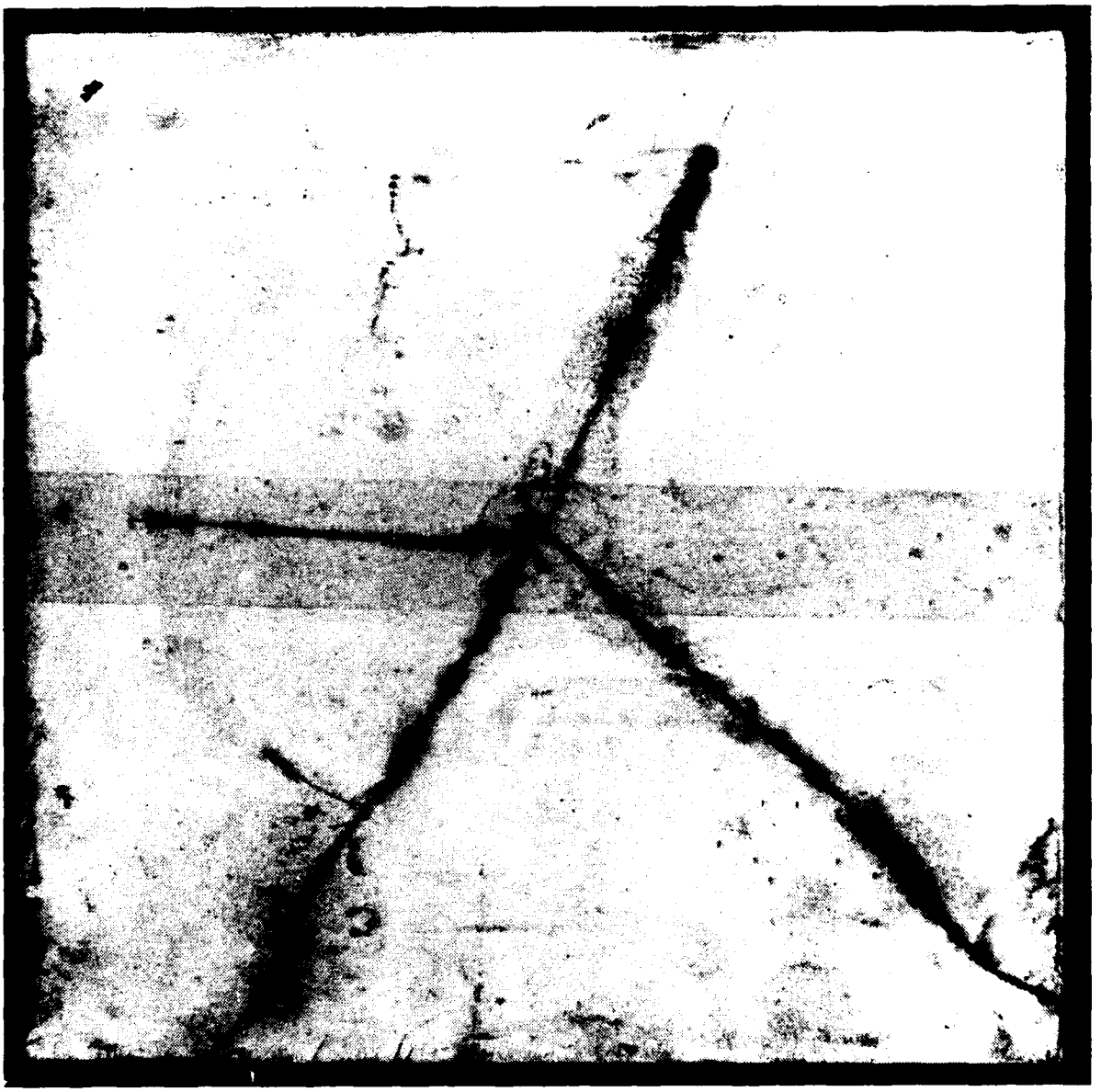

Figure 54. Inside Face of Delaminated Back Plate 2081B of Specimen Number 4.

3. Nylon-Mesh Reinforced Panels

During a visit by the principal investigator to the laboratories of the New Inorganic Materials group of Imperial Chemical Industries PLC at Runcorn, England, a 7 mm thick nylon-mesh-reinforced plate that had been ballistically impacted and had stopped a 38-caliber bullet at 300 m/s was shown.

This motivated some tests at the University of Florida on reinforced plates. Two 7 mm NIM 127R® panels were each cut into four 15.2 cm (6-inch) square plates similar to those of the tests on the unreinforced plates that were badly damaged by impacts at 25 m/s and 30 m/s as illustrated in Figures 43 and 44. The impactor was a blunt-ended steel cylinder of diameter 9.52 mm (3/8 inch), length 25.4 mm (1 inch) and mass 14.6 grams (0.515 ounce). The first test on a reinforced plate showed complete perforation at 82.2 m/s with the immediately apparent damage confined to the vicinity of the hole on the back face. Flaw enhancement fluid, however, revealed some cracks running from the damage area but apparently not reaching the boundary; see Figures 55 and 56. The damaged plate appeared to have considerably more integrity and retained strength than the unreinforced plates. It was decided to make some kind of residual strength tests to give some quantification to this observation.

Accordingly each damaged plate was subjected to a three-point bend test. One of the four plates cut from each panel was tested as an undamaged control specimen for comparison. The other three were first impacted at three different speeds (of order 30, 50, and 80 m/s). Figures 57 and 58 show back-face damage in two plates impacted at subperforation speeds. The spall diameter in the 52.5 m/s impact is comparable to that of the perforated plate of Figures 55 and 56, but some back-face material still adheres near the center. The cracks are somewhat more extended than in the perforated plate, some reaching the boundary. Spall and cracking are both less extensive in the 30.8 m/s impact of Figure 58 than in the 52.5 m/s impact of Figure 57.

Retained strength after impact could be characterized in several different ways. Tests could be made in tension, compression or bending, for example, and different types of tests on various sizes of coupons cut from the damaged plates could produce different results. The three-point

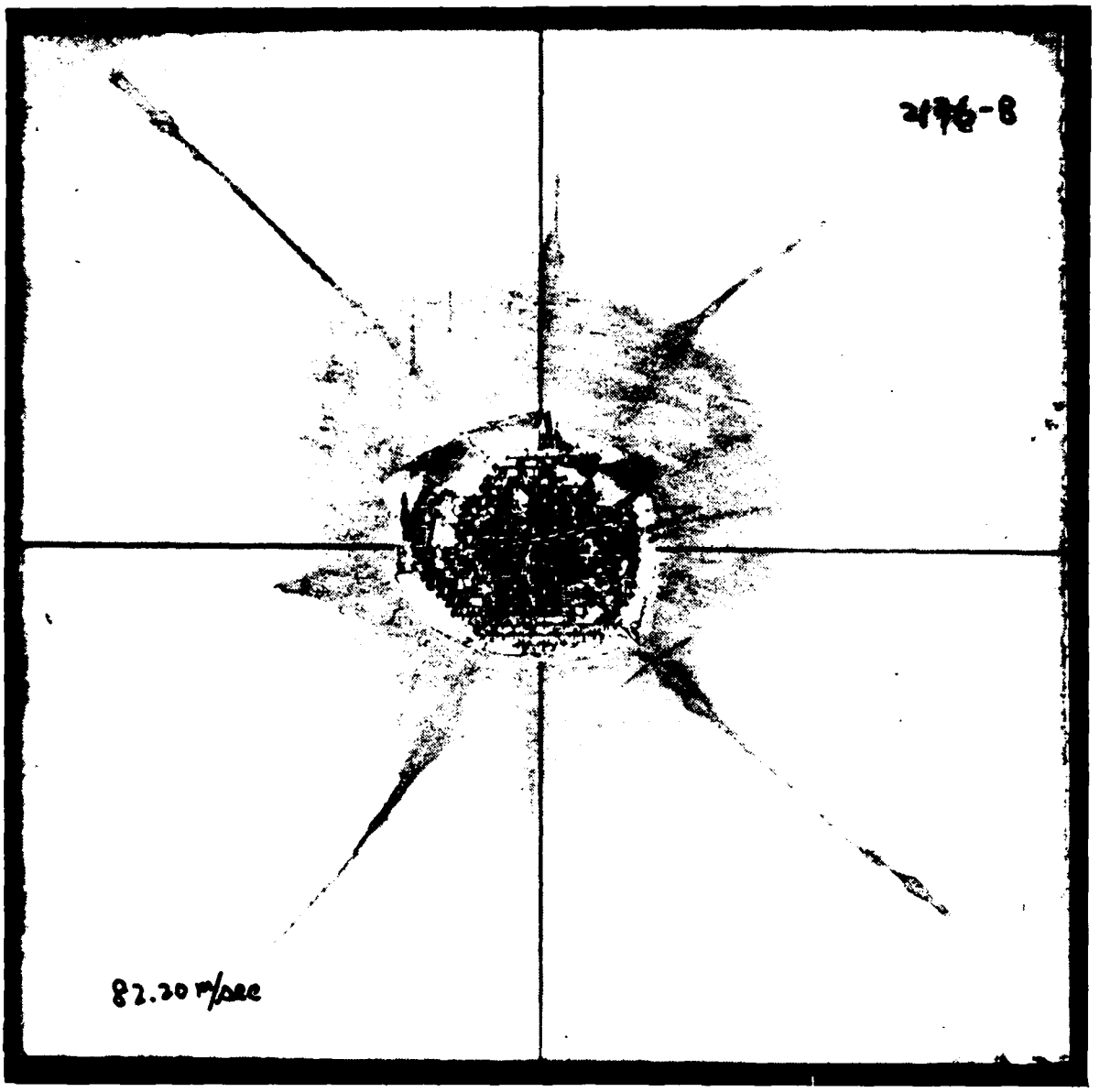

Figure 55. Back Face of NIM 127R® Plate Impacted at 82.2 m/s Showing Damage Around Perforation and Cracks Revealed By Enhancement.

Figure 56. Front Face of NIM 127R® Plate Impacted at 82.2 m/s Impacted by Blunt Impactor Showing Perforation and Cracks Revealed by Enhancement.

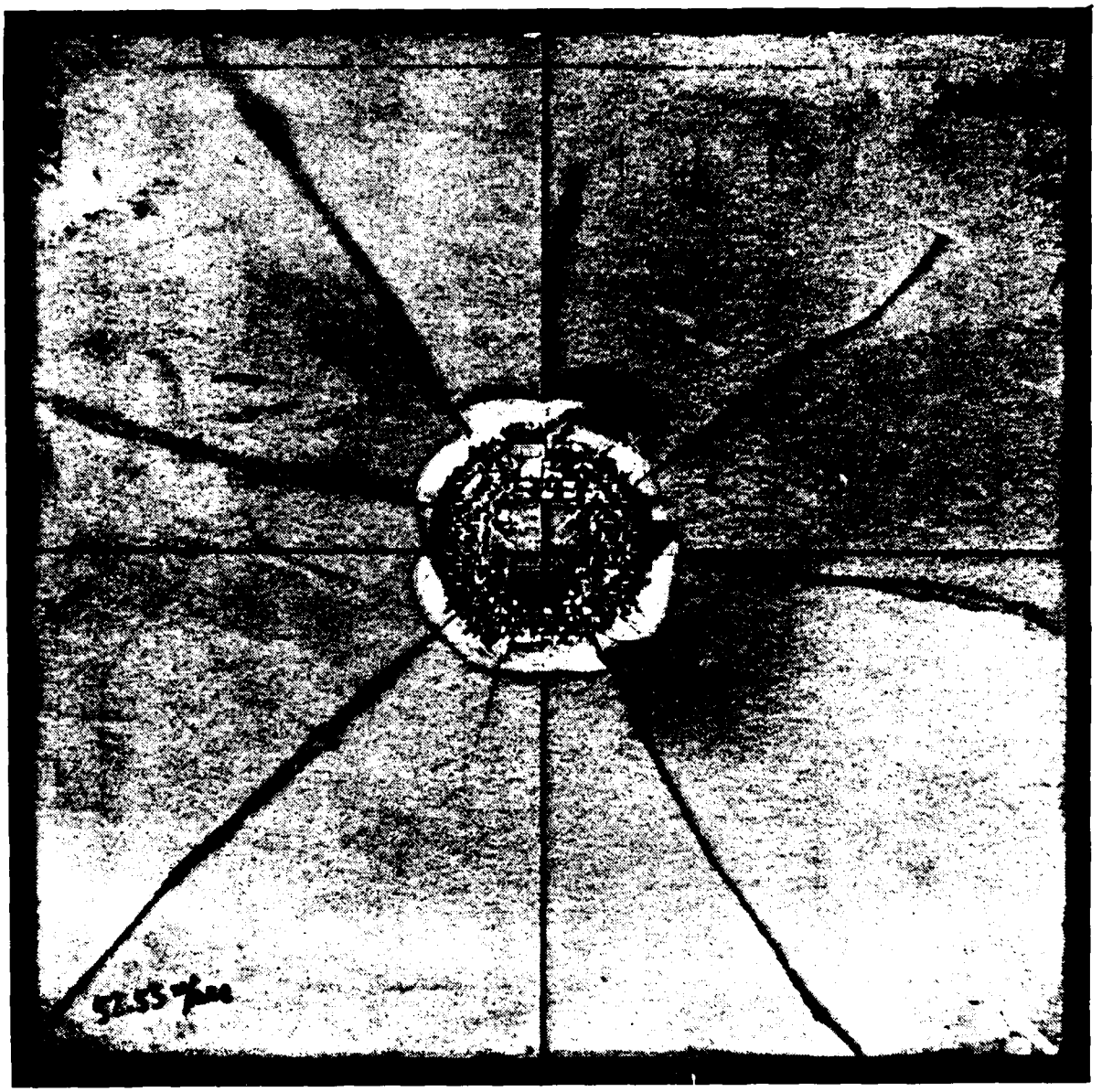

Figure 57. Back Face of NIM 127R® Plate Impacted at 52.5 m/s Showing Damage But No Perforation. Cracks Revealed By Enhancement.

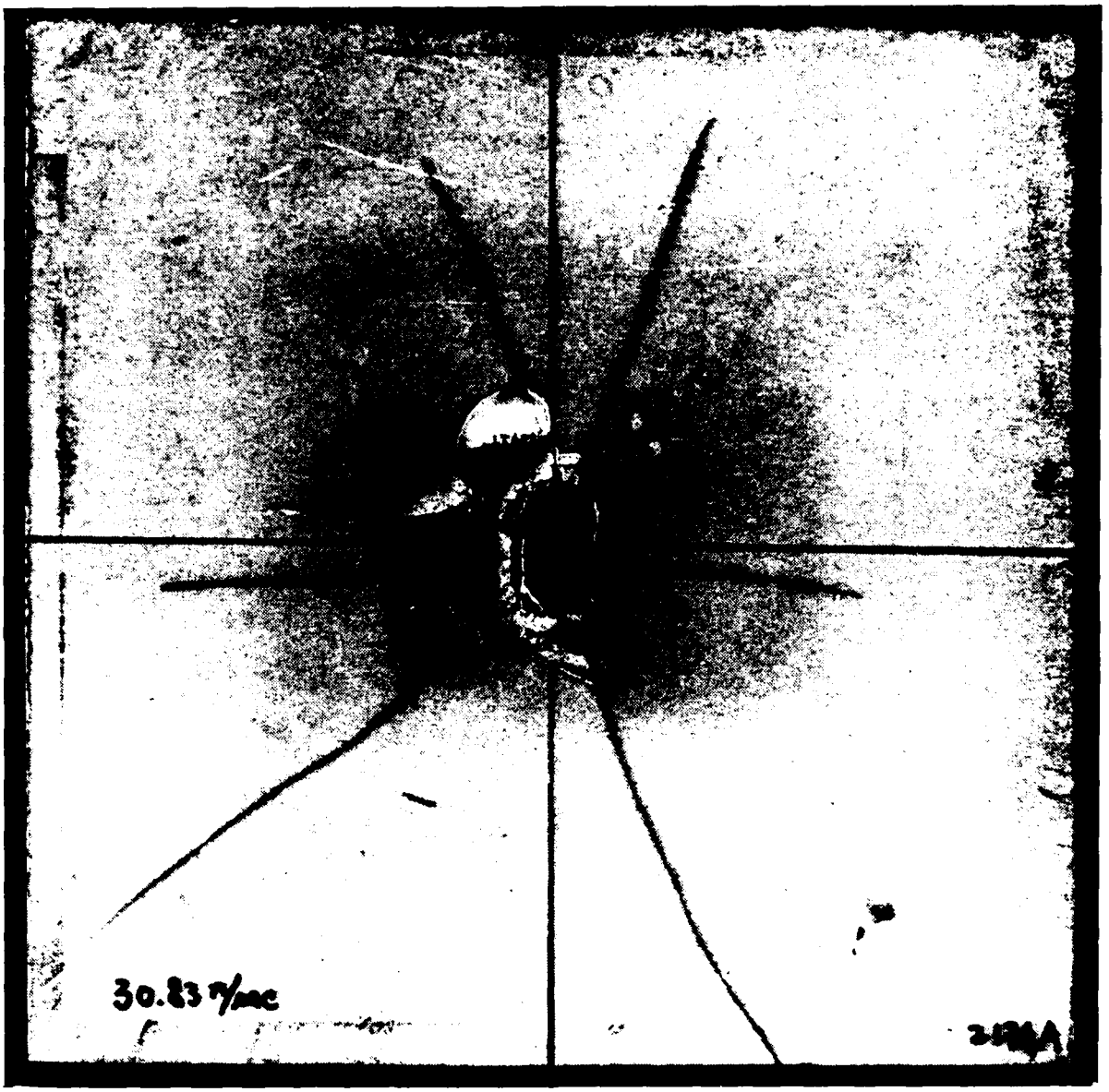

Figure 58. Back Face of NIM 127R® Plate Impacted At 30.8 m/s Showing Limited Damage Near Impact Point and Cracks Revealed By Enhancement.

bend test was arbitrarily selected because it was easy to perform, gave a clearly identifiable point of maximum load, and had been surprisingly reproducible in previous tests on fiber-reinforced epoxy plates. All the tests were made on the full-size 15.24 by 15.24 mm (6-by 6-inch) plates, supported near two edges by rounded wedge supports 12.7 mm (5 inches) apart and centrally loaded across the full width by a wedge with a rounded edge. The tests measured the residual flexural strength of the whole structural element rather than the local strength. The results are particular to the size of the specimen. A larger plate subjected to the same impact and subsequently tested for its structural strength would show a larger fraction of its strength retained. The residual strength factors quoted should, therefore, not be interpreted as absolute values characteristic of the material, but as relative rankings for the impacts at different speeds.

Two examples of the load-deflection curves in the three-point bend tests on damaged plates are given in Figures 59 and 60. The loading ram speed was 1.27 mm/min (0.05 in/min). The point marked P_f identifies the first load at which substantial further cracking occurred accompanied by a load drop. P_{max} is the maximum load sustained. The example of Plate 2174B is more typical than the other one shown in that its final P_{max} is considerably higher than P_f. The final failure at the maximum load was accompanied by formation of a crack all the way across the width of the plate directly underneath the loading wedge. The undamaged control specimen response was essentially linear all the way to a load P_o at which the load dropped almost to zero as the crack formed all the way across the specimen under the loading wedge. The control tests were stopped at that point.

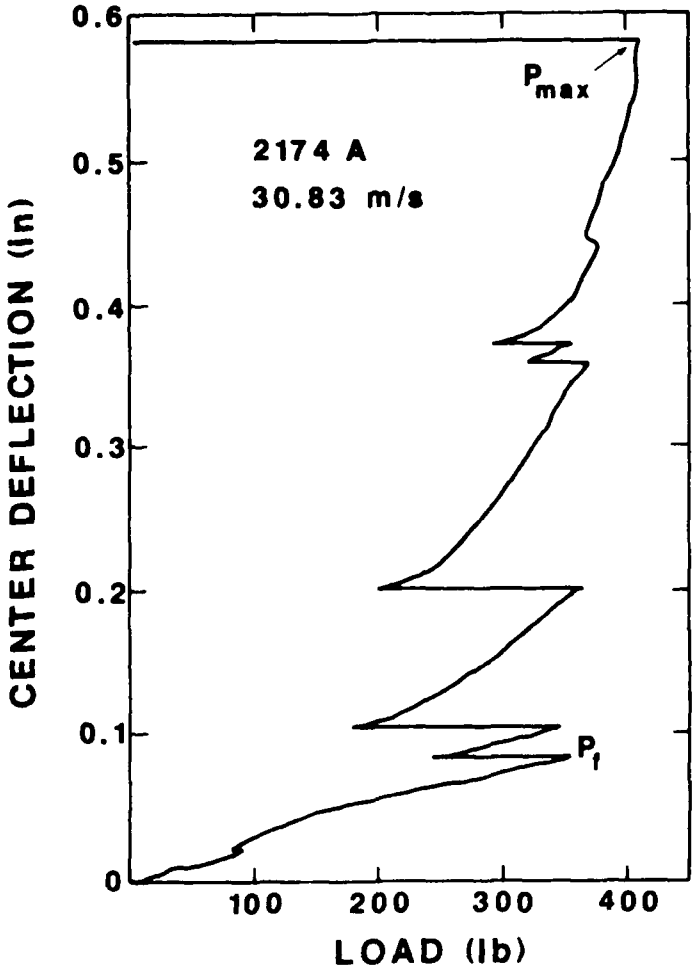

Figure 59. Load-Deflection Curve for Damaged Plate 2174A After Impact at 30.83 m/s.

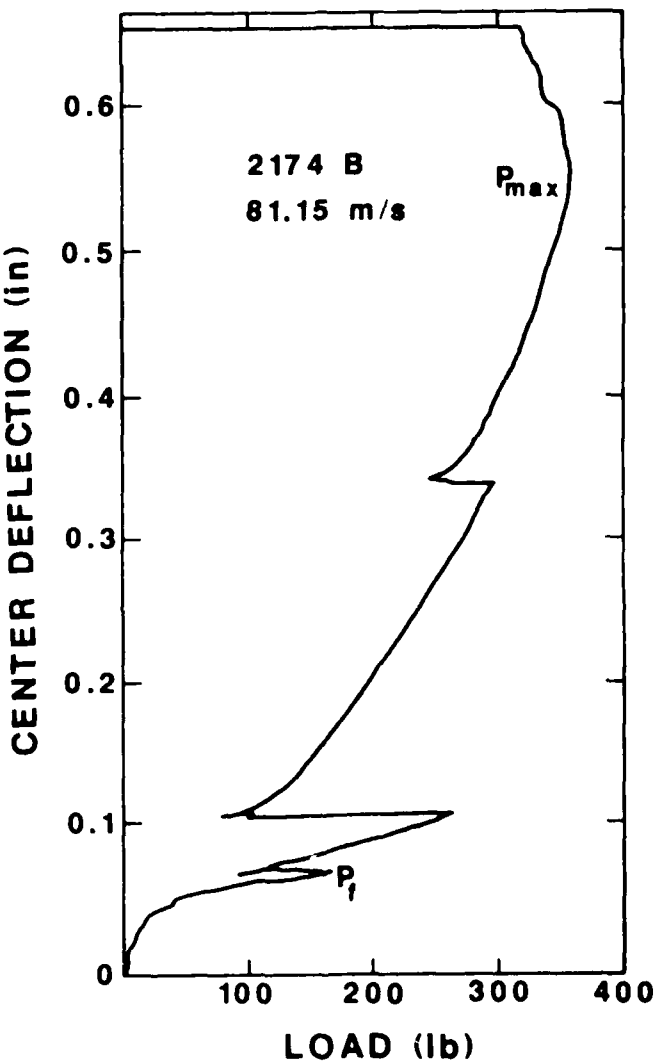

Figure 60. Load-Deflection Curve for Damaged Plate 2174B After Impact at 81.15 m/s.

Table 15 summarizes the failure load results for the eight tests. Besides the loads P_o of the undamaged plates and P_f and P_{max} of the damaged plates some strength-reduction factors P_f/P_o and P_{max}/P_o are listed for each of the damaged plates. It should be kept in mind that these strength-reduction factors are peculiar to the particular test configuration and plate size.

TABLE 15. CYLINDRICAL BEND TEST RESULTS FOR NIM 127R® PLATES

PLATE NO.	2174A	2174C	2174B	2174D	2176A	2176C	2176B	2176D
Impact speed (m/s)	30.8	51.8	81.2	0	30.8	52.5	82.2	0
P_o kgf (lb)				371 (774)				336.6 (742)
P_f kgf (lb)	161 (355)	85.5 (195)	74.4 (164)		76.2 (168)	113.4 (250)	65.8 (145)	
P_f/P_o	0.459	0.251	0.211		0.226	0.337	0.195	
P_{max} kgf (lb)	186 (410)	174.6 (385)	163.3 (360)		173.3 (382)	127.9 (282)	152 (335)	
P_{max}/P_o	0.530	0.497	0.465		0.515	0.380	0.451	

The nylon mesh reinforcement gives a significant improvement in the impact resistance, but the impact loadings used here were not very severe.

SECTION V
SUMMARY OF TEST RESULTS

A. STANDARD STATIC TEST RESULTS

Table 16 summarizes the strengths, moduli and maximum strain determined in the standard tensile, compressive and flexural tests described in Section II and Poisson's ratio as determined in the tension tests. The flexural and compressive strength results and flexural modulus fall in the ranges of typical values reported by the manufacturer. The tensile strengths reported are at the low end of the range of 70 - 100 MPa quoted by the manufacturer. The compressive moduli reported here are not believed to be accurate. The static compressive moduli are probably of the order of the flexural moduli.

TABLE 16. SUMMARY OF STATIC TENSILE, COMPRESSIVE AND FLEXURAL PROPERTIES

Specimens From 5 mm Thick Plates

	Tensile	Compressive	Flexural
Strength	67 MPa (9.7 KSI)	310 MPa (45 KSI)	126 MPa (18.3 KSI)
Maximum Strain	0.002 IN/IN	0.05 IN/IN	0.004 IN/IN
Modulus	46 GPa (6.6×10^6 psi)	7.0 GPa* (1.01×10^6 psi)	35 GPa (5.1×10^6 psi)
Poisson's Ratio	0.26		

Specimens From 10 mm Thick Plates

	Tensile	Compressive	Flexural
Strength	73 MPA (11 KSI)	330 MPa (48 KSI)	120 MPa (17.4 KSI)
Maximum Strain	0.002 IN/IN	0.045 IN/IN	0.004 IN/IN
Modulus	39 GPa 5.6×10^6 psi	8.2 GPa* (1.2×10^6 psi)	35 GPa (5.1×10^6 psi)
Poisson's Rates	0.26		

* The compressive moduli reported here are believed to be much too low.

The average values of fracture toughness K_{IC} and the strength ratio R_{SC} (apparent notched strength expressed as a percentage of the unnotched strength) determined by compact tension tests as described in Section II.D are given in Table 17.

TABLE 17. FRACTURE TOUGHNESS SUMMARY

5 mm	K_{IC} = 1.20 ksi$\sqrt{in}$	R_{SC} = 15% for 5-mm
10 mm	K_{IC} = 1.05 ksi$\sqrt{in}$	R_{SC} = 15% for 11-mm

The tests were conducted in accordance with the standard ASTM E399-81, except that it was not possible to initiate the prescribed fatigue precrack at the root of the starter notch because of complete brittle failure of the specimen during the low level cyclic fatigue process. The reported results should therefore be considered as upper bounds.

B. MOISTURE ENVIRONMENT EFFECTS

For the specimens from 5 mm thick plates the weight increase after 7 days immersion averaged 1.5 per cent (excluding one reported value of 0.11 per cent). This is of the same order as the value of approximately 1.3 per cent reported by the manufacturer for 3 mm thick plates. For the 10 mm thick plates the average value was 0.5 percent in 7 days.

Trends of strength and modulus decrease and maximum strain increase versus time immersed in water were shown in Figures 23 to 26, as determined by the flexural tests reported in Section III.A. Table 18 summarizes the per cent changes shown in Figures 23 to 26.

TABLE 18. MOISTURE ENVIRONMENT EFFECTS ON PROPERTIES OF FLEXURAL SPECIMENS CUT FROM 5 MM and 10 MM PLATES (approximate per cent changes, as shown in Figures 23 to 26 for 1 or 7 days immersion in water)

	Weight Increase 7 days	Modulus Decrease 1 day	Modulus Decrease 7 days	Strength Decrease 1 day	Strength Decrease 7 days	Maximum Strain Increase 7 days
5 mm Plates	1.5	29	41	17 to 31	24 to 31	85
10 mm Plates	0.5	22	27	8 to 23	11 to 28	23

C. THERMAL ENVIRONMENT EFFECTS

In preliminary tests many of the flexure-test specimens, cut from 10 mm thick plates (formed by laminating two 5 mm plates), delaminated during heating at 120°C and all of them showed less than 10 per cent of the flexural strength of unheated control specimens. The remainder of the thermal environmental study was carried out with 5 mm thick plates.

Because of variations in the control specimen properties between plates, the thermal environmental effects displayed in Table 7 of Section III.B were normalized by dividing the average property value after exposure by the average property value of unheated control specimens cut from the same plate.

Table 7 shows that strength was degraded by all the thermal exposures (at 80, 100, 120 or 150°C for 1 to 30 hours), but the trends with time were quite different at the different temperatures, as may be seen also in Figures 27 to 30. At 80 and 100°C, the strength initially decreased with time at temperature to a minimum at about 3 hours and then recovered to almost its initial value after 24 hours; the initial decrease was greater (27 per cent) at 80°C (27 per cent) than at 100°C (12 per cent) and in both cases recovery was to within 5 per cent of the control specimen strength.

At 120°C the strength decrease was less than 10 per cent during the first 7 hours, but about 25 per cent at 24 hours. At 150°C strength had decreased by about 70 per cent after 13 hours and then leveled off.

The flexural modulus was actually increased by 24 hours of thermal exposure, as much as 28 per cent at 120°C. Some of the shorter exposures produced a decrease, the greatest decrease was 18 per cent after 0.5 hour at 120°C.

AD-A170 019 HYPERSTRENGTH CEMENT TESTING(U) FLORIDA UNIV 2/2
GAINESVILLE DEPT OF ENGINEERING SCIENCES
L E MALVERN ET AL. MAR 86 AFESC/ESL-TR-85-47
UNCLASSIFIED F08635-83-C-0136 F/G 13/3 NL

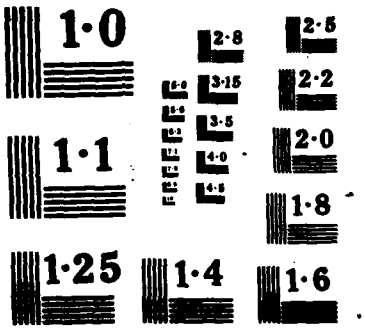
1·0
1·1
1·25
1·4
1·6
1·8
2·0
2·2
2·5
2·8
3·15
3·5
4·0

D. DYNAMIC COMPRESSIVE STRENGTHS

The dynamic compression tests were described in Section IV.A. and results summarized as plotted points of ultimate strength (maximum stress) versus strain rate at the maximum stress in Figures 36 to 40. The strain rate is not constant in these tests, and the strain rate at the maximum stress may not be the optimum parameter to plot against.

Except for initial unusually consistent set of results shown in Figure 36, the results show a great deal of scatter and it is not easy to arrive at a reasonable formula to fit the trend of dynamic strength as a function of strain rate. The dynamic compressive strengths measured varied from 399 MPa to 582 MPa (57.9 ksi to 84.2 ksi). These were substantially higher than the average static compressive strengths of 310 MPa (45 ksi) for 5 mm plates and 330 MPa (48 ksi) for 10 mm plates.

E. DYNAMIC MODULUS AND VIBRATION DAMPING

Table 13 of Section IV.C. summarizes the elastic modulus results. The modulus varies considerably with the different methods of measurement. It is believed that the most useful comparison is the dynamic modulus from bar-wave tests:

Dynamic E = 44 GPa to 47 GPa (6.4×10^6 to 6.8×10^6 psi)

compared with

Static E = 38 GPa to 47 GPa (5.5×10^6 psi to 6.8×10^6 psi)

Other methods gave higher values for the dynamic modulus, up to 63.6 GPa (9.1×10^6 psi) by ultrasonic wave speeds.

Damping factors measured were of the order of 0.03. See Tables 9 and 10 of Section IV.B. Values as high as 0.07 were obtained in some free-vibration damping tests, but the value of 0.03 is considered more representative.

F. BALLISTIC IMPACT TESTS

Four groups of ballistic impact tests were performed, as described in Section IV.D. All were on nominally 7 mm thick panels. Results are summarized in Table 19. All but Group (b) were on 152 mm square (6-inch) targets. In all cases the impactor was a 14.6 gram (0.515 ounce) flat-ended steel

cylinder of diameter 9.52 mm (3/8 inch) and length 25.4 mm (1 inch).

The single plates of Group (a) were extensively damaged by low-speed impacts at 25 to 30 m/s. Damage around the center of the larger plates of Group (b) was similar to that of Group (a), although at the lowest speed no cracks extended all the way to the edges of the larger plate. Very little strength was retained after impact by any of these single plates.

Somewhat better impact resistance was obtained by laminating two of the plates together to form a two-lamina target in Group (c). No apparent damage was sustained in 30 m/s impacts, but extensive damage occurred in 50 m/s impacts. Thus, doubling the thickness (by lamination) approximately doubled the speed at which extensive damage appeared, as compared with Group (a).

The nylon-mesh-reinforced plates of Group (d) performed even better, and the damaged plates had sufficient integrity to exhibit enough retained strength to make it worth measuring. Three-point bend tests were performed on the damaged plates and undamaged control specimens. In Tables 15 and 19, P_o denotes the maximum load supported by undamaged plate, P_f is the first failure load of the damaged specimen where a load drop occurred in the load-deflection curves (see Figures 59 and 60) and P_{max} is the maximum load reached by the damaged specimen. Examples of values of strength-retention fractions P_f/P_o and P_{max}/P_o are given in Tables 15 and 19. The P_f/P_o values show considerable variation, while (except for one case) the P_{max}/P_o factors varied only from 0.45 after 80 m/s impact to 0.53 after the 30 m/s impact. It should be remembered that these factors pertain only to this particular type of test and this particular size of target.

TABLE 19. SUMMARY OF BALLISTIC IMPACT DAMAGE RESULTS
(Target plates formed from 7 mm thick panels)

Target Group	Approximate Impact Speed			
	25 m/s	30 m/s	50 m/s	80 m/s
(a.) Single Plates 152 mm square (6 inch)	Cracks to edge. Almost no strength retained. Figure 43.	Spall, cracks to edge Almost no strength retained. Figure 44.		
(b.) Single Plates 295 mm square (9.25 inch)	Cracks not to edge. Little strength retained. Figure 45.	Cracks to edge. Spall. Little strength retained. Figure 46.		
(c.) Laminated Plates 2 laminas 152 mm square (6 inch)		No apparent damage.	Extensive Damage. Figures 47 - 54. Table 14.	
(d). Nylon-mesh-reinforced Plates 152 mm square (6 inch) cracking		Some spall and cracking.	More spall and cracking.	Perforation, spall. and cracking.
Retained Strength Examples P_f/P_o		Figure 58. 0.23 - 0.46	Figures 57. 0.25 - 0.34	Figures 55, 56. 0.20 - 0.21
P_{max}/P_o		0.52 - 0.53	0.38 - 0.50	0.45 - 0.46
Table 15, Figures 59, 60.				

SECTION VI
CONCLUSIONS

1. The static tensile, compressive and flexural properties, as summarized in Table 16 are impressive. Expecially impressive for a cementitious material is the tensile strength of the order of 70 MPa (10 ksi).

2. The fracture toughness is not impressive, and the fact that an initial fatigue crack could not be formed without completely fracturing the compact tension specimen was an early warning signal of dangers of brittle failure in impact loadings.

3. The strength decrease of up to 31 per cent, modulus decrease of up to 41 per cent and maximum strain to failure increase of up to 85 per cent for 5 mm small flexure specimens immersed in water for 7 days might present some problems for designers of structures exposed to a moisture environment, but would not rule out the possibility of using larger panels, suitably protected, in such structures.

4. The thermal degradation of strength makes the single-lamina panels unsuitable for use where prolonged exposure to temperatures above about 100°C will occur. The laminated 10 mm panels were especially susceptable to delamination damage during heating even without external load. If laminated panels are to be used, some further investigation aimed at avoiding mismatch between the thermal expansions of the laminas and optimizing the adhesive should be carried out.

5. Dynamic compressive strengths of small short cylinders were significantly higher than the static and dynamic moduli somewhat higher.

6. The catastrophic brittle failures of unreinforced plates even at quite low levels of ballistic impact indicate that the material is not suitable for cladding of structures that may be subjected to such impact.

7. The nylon-mesh-reinforced panels performed considerably better than the unreinforced panels in ballistic impact, but were still not impressive. It is possible that a composite plate with a ceramic facing and several layers of the reinforced plates laminated together could be effective, but that has not yet been tried. The cost-effectiveness as well as the performance of such an arrangement would need to be investigated.

REFERENCES

1. Zukas, J. A., Nicholas, T., Swift, H. F., Greszczuk, L. B. and Curran, D. R., Impact Dynamics, New York: Wiley, 1982.

2. Gibson, R. F., Yau, A. and Riegner, D. A., "An Improved Forced-Vibration Technique for Measurement of Material Damping", Experimental Techniques, Vol. 6, No. 2, April 1982.

APPENDIX A --DETAILS OF TEST RESULTS

Tables A-1 to A-4 give the individual specimen results used to calculate the average results for the thermal environment effects reported in Section III.B.

Tables A-5 to A-7 give the numerical results used for plotting the points in Figures 36 to 40, showing the variation of the maximum dynamic compressive stress with strain rate at the maximum stress in the Split Hopkinson Pressure Bar tests described in Section IV.A.

TABLE A-1. DATA FOR 80°C ENVIRONMENT

Specimen No.	Exposure Time (hr)	Cooling Time (min)	P_{max} (kgf)	Flexural Strength (MPa)	Flexural Strength (ksi)	Flexural Modulus (GPa)	Flexural Modulus (x 10^6psi)
41-52	0	---	62.9	128	18.6	36.1	5.22
41-51	0	---	58.6	120	17.4	36.2	5.24
41-53	0	---	65.4	134	19.3	36.1	5.22
41-50	0	---	61.6	126	18.3	34.7	5.02
Average				127	18.4	35.8	5.18
S.D.				5	0.68	0.62	0.09
41-61	1	72	50.2	108.0	15.7	38.2	5.53
41-62	1	79	45.6	92.7	13.4	35.1	5.08
41-63	1	86	44.3	91.8	13.3	34.6	5.01
Average				97.5	14.1	36.0	5.21
S.D.				7.43	1.11	1.59	0.23
41-54	3	72	47.7	95.5	13.9	34.3	4.96
41-57	3	78	47.8	96.0	13.9	39.4	5.70
41-58	3	84	43.8	87.7	12.7	34.3	4.96
Average				93.1	13.5	36.0	5.21
S.D.				3.80	0.57	2.40	0.35
41-60	5	65	49.4	99.3	14.4	36.9	5.34
41-72	5	72	52.3	104.7	15.2	34.3	4.96
41-79	5	79	53.6	107.7	15.6	33.1	4.79
Average				103.9	15.1	34.8	5.03
S.D.				3.48	0.50	1.59	0.23
41-68	7	73	54.4	115.7	16.8	37.6	5.44
41-69	7	81	53.2	118.6	17.2	37.2	5.38
41-70	7	90	44.8	90.7	13.2	34.9	5.05
Average				108.3	15.7	36.6	5.29
S.D.				12.52	1.80	1.19	0.17
41-64	24	87	52.7	110.4	16.0	40.0	5.79
41-65	24	95	58.1	123.1	17.9	41.1	5.95
41-66	24	102	58.4	119.1	17.3	39.2	5.67
41-67	24	109	58.1	132.6	19.2	41.7	6.03
Average				121.3	17.6	40.5	5.86
S.D.				7.98	1.15	0.97	0.14

TABLE A-2. DATA FOR 100°C ENVIRONMENT

Specimen No.	Exposure Time (hr)	Cooling Time (min)	P_{max} (kgf)	Flexural Strength (MPa)	Flexural Strength (ksi)	Flexural Modulus (GPa)	Flexural Modulus (x 10^6psi)
40-1	0	---	48.81	118.9	17.2	39.4	5.70
40-2	0	---	45.97	115.2	16.7	36.1	5.22
41-5	0	---	49.00	121.8	17.7	38.9	5.62
41-5	0	---	45.97	111.9	16.2	36.8	5.32
Average				117	17.0	37.8	5.47
S.D.				3.74	0.56	1.38	0.29
40-5	½	73	38.0	96.0	13.9	30.9	4.47
40-6	½	80	39.2	100.0	14.5	36.7	5.31
40-7	½	88	41.1	102.1	14.8	37.2	5.38
40-8	½	97	38.6	95.1	13.8	37.3	5.40
Average				98.3	14.3	35.5	5.14
S.D.				2.87	0.42	2.68	0.39
40-9	1	83	41.7	101.9	14.8	37.3	5.40
40-10	1	92	43.1	106.8	15.5	38.0	5.50
40-11	1	100	42.5	106.8	15.5	37.6	5.44
40-12	1	107	43.1	107.8	15.6	36.1	5.22
Average				105.8	15.3	37.3	5.40
S.D.				2.30	0.32	0.71	0.10
40-13	3	64	39.8	98.0	14.2	40.4	6.84
40-14	3	70	43.6	105.8	15.3	36.6	5.29
40-15	3	78	43.3	110.0	16.0	37.3	5.40
40-16	3	85	39.2	97.1	14.1	35.4	5.12
Average				102.7	14.9	37.4	5.41
S.D.				5.39	0.79	1.85	0.27
40-21	5	62	47.7	119.6	17.3	36.8	5.32
40-22	5	69	44.8	107.8	15.6	33.9	4.90
40-23	5	76	63.1	105.8	15.3	35.7	5.16
40-24	5	84	45.9	110.4	16.0	38.7	5.60
Average				110.9	16.1	36.3	5.25
S.D.				5.28	0.76	1.74	0.25

TABLE A-2. DATA FOR 100°C ENVIRONMENT (CONTINUED)

Specimen No.	Exposure Time (hr)	Cooling Time (min)	P_{max} (kgf)	Flexural Strength (MPa)	Flexural Strength (ksi)	Flexural Modulus (GPa)	Flexural Modulus (x 10^6psi)
40-17	7	70	46.5	113.7	16.5	42.5	4.70
40-18	7	80	46.8	114.7	16.6	37.0	5.35
40-19	7	88	51.7	125.4	18.2	34.3	4.96
40-20	7	95	46.6	115.6	16.8	34.7	5.02
Average				117.4	17.0	34.6	5.01
S.D.				4.70	0.69	1.60	0.23
40-31	24	84	44.9	109.4	15.9	39.4	5.70
40-32	24	91	40.6	97.7	14.2	36.6	5.29
41-33	24	99	52.7	127.8	18.5	41.2	5.96
41-34	24	109	46.0	112.5	16.3	45.4	6.57
Average				111.9	16.2	40.7	5.89
S.D.				10.74	1.53	3.19	0.46

TABLE A-3. DATA FOR 120°C ENVIRONMENT

Specimen No.	Exposure Time (hr)	Cooling Time (min)	P_{max} (kgf)	Flexural Strength (MPa)	Flexural Strength (ksi)	Flexural Modulus (GPa)	Flexural Modulus (x 10^6psi)
40-60	1/2	77	43.4	101.1	14.7	29.5	4.28
40-61	1/2	84	45.6	107.5	15.6	30.9	4.48
40-62	1/2	40	44.4	105.9	15.4	33.5	4.86
40-63	1/2	97	47.6	110.4	16.0	30.2	4.38
Average				106.2	15.4	31.0	4.50
S.D.				3.37	0.47	1.51	0.22
40-39	1	85	42.7	106.2	15.4	35.6	5.16
40-42	1	93	45.5	109.9	15.9	30.3	4.39
40-40	1	100	40.9	103.4	15.0	31.0	4.50
40-41	1	108	44.7	111.2	16.1	32.5	4.71
Average				107.7	15.6	32.4	4.70
S.D.				3.08	0.40	2.04	0.29
40-35	3	70	67.5	116.7	16.9	37.8	5.48
40-36	3	77	42.6	106.8	15.5	39.3	5.70
40-37	3	85	45.9	113.7	16.5	40.4	5.86
40-38	3	94	48.9	121.6	17.6	42.7	6.19
Average				114.7	16.6	40.1	5.82
S.D.				5.36	0.76	1.79	0.26
40-47	5	67	46.6	111.7	16.2	38.5	5.58
40-48	5	75	44.5	107.5	15.6	39.0	5.66
40-49	5	83	44.1	109.2	15.8	40.4	5.86
40-50	5	92	41.1	102.6	14.9	43.0	6.24
Average				107.8	15.6	40.2	5.83
S.D.				3.33	0.47	1.75	0.26
40-43	7	77	44.9	109.8	15.9	39.7	5.76
40-44	7	84	43.1	102.8	14.9	38.2	5.54
40-45	7	90	47.8	115.0	16.7	38.7	5.61
40-46	7	98	45.7	108.6	15.8	44.3	6.42
Average				109.1	15.8	40.2	5.83
S.D.				4.30	0.64	2.41	0.35
40-51	24	69	35.2	86.1	12.5	49.0	7.11
40-52	24	79	37.5	93.2	13.5	50.3	7.30
40-53	24	90	33.6	82.2	11.9	46.3	6.72
* 40-64	24	97	----	---	---	---	--
Average				87.2	12.6	48.5	7.03
S.D.				4.55	0.66	1.66	0.24

TABLE A-4. DATA FOR 150°C ENVIRONMENT

Specimen No.	Exposure Time (hr)	Cooling Time (min)	P_{max} (kgf)	Flexural Strength (MPa)	Flexural Strength (ksi)	Flexural Modulus (GPa)	Flexural Modulus (x 10^6psi)
32-50	0	---	55.5	130.3	18.9	38.7	5.61
32-52	0	---	54.1	128.0	18.6	40.7	5.90
32-53	0	---	48.8	116.4	16.9	42.3	6.14
32-49	0	---	54.5	128.5	18.6	43.8	6.35
Average				125.8	18.2	41.4	6.00
S.D.				5.49	0.79	1.89	0.28
32-20	1/2	68	52.5	117.5	17.0	45.6	6.61
32-21	1/2	70	46.7	104.9	15.2	44.4	6.44
32-22	1/2	79	43.0	96.6	14.0	44.5	6.45
32-23	1/2	87	43.3	97.7	14.2	46.9	6.80
Average				104.2	15.1	45.4	6.58
S.D.				8.33	1.19	1.01	0.15
32-33	1	73	50.1	120.6	17.5	51.6	7.48
32-34	1	80	50.3	120.1	17.4	47.2	6.85
32-35	1	86	49.4	118.0	17.1	48.7	7.06
32-36	1	94	48.5	116.0	16.8	44.6	6.47
Average				118.7	17.2	48.0	6.96
S.D.				1.83	0.27	2.53	0.37
32-9	3	75	40.9	93.8	13.6	47.3	6.86
32-10	3	84	32.3	74.0	10.7	50.4	7.31
32-11	3	91	24.1	55.2	8.01	50.4	7.31
32-12	3	99	38.8	88.4	12.8	50.1	7.27
Average				77.9	11.3	49.6	7.19
S.D.				14.95	2.16	1.30	0.19
32-37	5	66	24.3	57.7	8.37	53.2	7.72
32-38	5	73	33.1	80.6	11.7	48.0	6.96
32-39	5	81	38.4	92.8	13.5	49.6	7.19
32-40	5	90	36.8	88.9	12.9	50.5	7.32
Average				80.0	11.6	50.3	7.30
S.D.				13.6	1.98	1.89	0.[illegible]

TABLE A-4. DATA FOR 150°C ENVIRONMENT (CONTINUED)

Specimen No.	Exposure Time (hr)	Cooling Time (min)	P_{max} (kgf)	Flexural Strength (MPa)	Flexural Strength (ksi)	Flexural Modulus (GPa)	Flexural Modulus (x 10^6psi)
32-5	9	90	25.9	59.4	8.62	50.4	7.31
32-6	9	99	22.7	52.4	7.60	62.5	6.16
32-7	9	106	20.0	50.5	7.32	50.7	7.35
32-8	9	113	22.7	51.9	7.52	50.1	7.27
Average				53.5	7.76	48.4	7.02
S.D.				3.45	0.50	3.43	0.50
32-1	13	68	18.2	42.0	6.09	46.4	6.73
32-2	13	77	26.1	59.3	8.60	49.8	7.22
32-3	13	85	14.2	32.8	4.76	42.5	6.16
32-4	13	92	7.0	16.2	2.35	42.5	6.16
Average				37.6	5.45	45.3	6.57
S.D.				15.58	2.26	3.05	0.44
32-13	21	98	20.7	47.4	6.87	45.8	6.64
32-14	21	106	20.0	45.8	6.64	45.8	6.64
32-15	21	112	9.0	21.2	3.07	43.8	6.35
32-16	21	118	25.9	58.2	8.44	48.9	7.09
Average				43.2	6.27	46.1	6.69
S.D.				13.54	1.97	1.82	0.26
32-41	25	78	24.8	60.4	8.76	48.7	7.06
32-17	25	86	16.1	36.5	5.29	41.3	5.99
32-18	25	93	18.6	41.8	6.06	48.9	7.09
32-19	25	98	22.7	51.0	7.40	48.9	7.09
Average				47.4	6.87	47.0	6.82
S.D.				9.11	1.32	3.26	0.47
32-24	30	80	17.6	40.3	5.84	42.0	6.09
32-25	30	85	20.0	45.8	6.64	42.0	6.09
32-31	30	91	19.5	46.9	6.80	54.2	7.86
32-32	30	96	19.9	48.5	7.03	50.2	7.28
Average				45.4	6.58	47.1	6.83
S.D.				3.08	0.45	5.29	0.77

TABLE A-5. SHPB RESULTS FOR XS AND YS SPECIMENS

Specimen No.	Method	Spring Drawback (in)	Impact Speed (in/sec)	(m/s)	*Strain Rate at Max Stress (s^{-1})	*Maximum Stress (KSI)	(MPa)
YS-3	Direct	4.5	239	6.07	10	61.9	427
XS-7	Direct	4.5	239	6.07	14	61.5	424
YS-2	Direct	5	272	6.91	26	69.0*	476
XS-9	Direct	5	272	6.91	35	67.9	468
YS-7	SHPB	4.5	348	8.83	50	87.8	605
XS-6	SHPB	4.5	348	8.83	116	75.8	523
YS-10	SHPB	5	393	9.98	141	87.1	601
XS-5	SHPB	5	393	9.98	207	79.5	548
XS-8	SHPB	5.5	432	11.0	298	79.3	547
YS-8	SHPB	5.5	432	11.0	358	73.4	506
YS-5	SHPB	6	475	12.1	365	80.4	554
XS-1	SHPB	6	475	12.1	400	77.0	531
YS-9	SHPB	6.4	508	12.9	387	84.2	582
XS-10	SHPB	6.4	508	12.9	466	77.4	533

*not failed in the test, nor permanent deformation found after test.

TABLE A-6. SHPB RESULTS FOR XL AND YL 19 MM DIAMETER SPECIMENS PLATE 1850

Specimen No.	Gas Gun Pressure (psi)	Impact Speed (in/sec)	Impact Speed (m/s)	*Strain Rate at Max Stress	*Maximum Stress (KSI)	*Maximum Stress (MPa)
XL-5	120	69.6	1.77	58.3 sec^{-1} (33)	60.8 (60.5)	419 (417)
YL-10	120	69.9	1.78	13.5 sec^{-1} (4)	61.0 (60.6)	421 (418)
XL-6	135	133	3.38	164 sec^{-1}	57.9	399
YL-9	135	104	2.64	111 sec^{-1}	58.3	402
XL-4	150	117	2.97	102 sec^{-1}	94.9	654
YL-4	150	155	3.94	206 sec^{-1}	87.9	606
XL-7	175	219	5.56	395 sec^{-1}	61.8	426
YL-6	175	219	5.56	401 sec^{-1}	62.4	430
XL-10	200	260	6.60	446 sec^{-1} (452)	78.7 (82.5)	543 (569)
YL-3	200	263	6.68	416 sec^{-1} (425)	87.5 (91.3)	603 (630)
XL-8	250	338	8.59	664 sec^{-1}	78.9	544
YL-5	250	331	8.40	673 sec^{-1}	79.3	547
XL-1	300	398	10.1	916 sec^{-1}	71.7	494
YL-7	300	398	10.1	912 sec^{-1}	60.2	415
XL-9	400	506	12.9	1180 sec^{-1}	79.3	547
YL-8	400	505	12.8	1180 sec^{-1}	79.7	550

*Data in parentheses were based on the average method of Equations (8) and (14); other data in these columns is based on Equations (11) and (12); see Section IV.1.

TABLE A-7. SHPB RESULTS FROM 5 MM LONG SPECIMENS (PLATE 1912)

Specimen No.	Method	Spring Drawback (in)	Impact Speed (in/sec)	Impact Speed (m/s)	*Strain Rate at Max Stress (s^{-1})	*Maximum Stress (KSI)	*Maximum Stress (MPa)
Y8	Direct	4.5	238	6.05	46	60.3	416
Y1	Direct	5	264	6.71	122	63.5	438
X4	Direct	5	264	6.71	183	60.8	419
Y5	SHPB	3.5	263	6.68	13	65.7	453
C1	SHPB	4	300	7.62	134	77.7	536
Y7	SHPB	4	300	7.62	356	70.3	485
Y6	SHPB	4.25	327	8.31	117	78.9	544
Y8	SHPB	4.25	327	8.31	265	77.1	532
Y4	SHPB	4.5	348	8.84	483	66.0	455
X6	SHPB	4.5	348	8.84	551	62.5	431
X9	SHPB	4.75	369	9.37	710	66.3	457
X10	SHPB	5	393	9.98	757	66.5	459
Y11	SHPB	5	393	9.88	924	59.5	410

END

DTIC

9-86